Title
Hydrophobicity in a simple model of water

Author
Silverstein, Kevin Andrew Tang

Publication Date
1997

Peer reviewed|Thesis/dissertation

Hydrophobicity in a Simple Model of Water

by

Kevin Andrew Tang Silverstein

DISSERTATION

Submitted in partial satisfaction of the requirements for the degree of

DOCTOR OF PHILOSOPHY

in

Biophysics

in the

GRADUATE DIVISION

of the

UNIVERSITY OF CALIFORNIA

San Francisco

Date **University Librarian**

Degree Conferred: . . . . . .

To my wife, Karen,

and my son, Evan,

for making my life whole

Acknowledgements

I am deeply indebted to a number of individuals, without whom the completion of my degree would have been significantly more difficult.

First, I'd also like to thank my primary advisor and mentor, Ken Dill, for a very enjoyable and profitable working relationship. In particular, for: his willingness to let me work independently and discover things on my own, his astute advice and wisdom on projects and career choices, his unflagging optimism and genuine interest and excitement for my project throughout, and his dogged determination.

My close collaborator and really, my other advisor and mentor, Tony Haymet, deserves high recognition as well. I am thankful to Tony for his close correspondence and help along the way, even though separated by the vast Pacific Ocean; for going out of his way to help his students; for his helpful career advice; and his high level of excitement for our joint project.

Next, I thank my wife, Karen for her significant contributions: in addition to her companionship and being the source of a great improvement in the quality of my graduate years, she has been an important mentor for me. She helped me to realize that the lows and self-doubt which I experienced when projects failed, and during oral preparation, were simply normal experiences in a graduate student's life. And she really taught me to think; not the mere memorization of fact, or the surface-thinking that often obscures true enlightenment, but how to sit in the corner in a quiet room and really derive concepts from first principles. For these and many other gifts, I am very thankful.

One cannot forget Wilma Olson for getting me started in this business! Though I was only an undergraduate at the time, she really treated me like a graduate student, unselfishly offering me as much of her time as I needed. She has given many young students a start in the field, and should be applauded for her efforts. I am very greatful for her aid and advice in applying for fellowships and graduate programs, as well as for her training in my early, developing stage as a research scientist.

Special thanks are in order for Tack Kuntz and Julie Ransom. In addition to their role for bringing me here to UCSF, and to their support throughout my graduate career, I'm greatful that they convinced me to remain in the program when I had thoughts of leaving in my first year. At the time, I had considered going into science education. They suggested that with a Ph. D., I might be able to have wider impact and influence over science education and policy. Also, I might really find my rotation project with Ken very interesting. (Indeed they were right!) What impressed me the most was their unconditional support regardless of my decision. Tack and Julie, I have not forgotten about education, nor do I regret my decision.

My orals and thesis committees deserves particular acknowledgement: Peter Kollman, for taking on the responsibility of being my chair, and for informing me of the "dimensionally-challenged" nature of my water model; and to David Spellmeyer, Ron Siegel, and Robert Fletterick, who, with Peter managed to make my orals experience somewhat enjoyable (though I wish I could have said the same about the preparation phase...). Thanks also to David Agard and Tack Kuntz, and to members of the biophysics group and Pharm. Chem. students for stimulating discussions in preparing for my orals.

For financial support, I am greatful to the National Science Foundation for an NSF Graduate Fellowship. Subsequently, I received a UC Regents fellowship, for which I am also appreciative.

I cannot imagine what work in the lab would have been like without Danny Heap, our system administrator, and David Yee and Jack Schonbrun who served that role before and after him, respectively. Actually, I can vaguely imagine, based upon the short interval where we did not have a system administrator, and I am deeply appreciative! Thanks are also in order to Hue Sun Chan, Roland Dunbrack, Sarina Bromberg, Klaus Fiebig, and the rest of the Dill lab members, for many fun and educational years in the lab. Thanks particularly to Thomas Beutler for teaching me the tricks-of-the-trade in simulation, and to Claudia Johnson, for keeping the lab running smoothly.

My years in the Biophysics Group were greatly enlivened by my classmates, particularly my incoming year. Nalin Gupta, we're all thankful for organizing some of the best yearly-gatherings around!

Finally, special thanks to my parents, for sparking my interest in science at an early age; to my parents-in-law, for their helpful career decisions and support through grad school; and to all my close friends, particularly my roommates at Rutgers who migrated west with me. And of course, my dear son, Evan, for adding a silver lining even to those days that were clouded by the specter of a thesis not yet complete...

Authorship

Chapter 2 of this thesis is a reprint of the material as it was submitted to the *Journal of the American Chemical Society* and the coauthors, Prof. Dill and Prof. Haymet directed and supervised the research (as with all of the work reported here). Dr. Silverstein was the principal researcher for all of the studies reported in this thesis.

Ken Dill

Department of Pharmaceutical Chemistry

Hydrophobicity in a Simple Model of Water

Kevin Andrew Tang Silverstein

December 1997

Abstract

The molecular origins of hydrophobic effects are still under debate. The traditional view, in which apolar solutes induce clathrate-like structure in the surrounding solvent, has come under attack by those who contend that the large aversion of oil for water results mostly from the small size of the water molecule, and not from water structuring. Neither of these views directly addresses the large positive heat capacity of transfer, the defining feature of hydrophobicity.

To help to clarify the molecular origins of hydrophobicity, we have performed extensive simulations on a simple model of water. Water molecules are represented in the model by LJ disks with three hydrogen-bonding arms, arranged as in the Mercedes-Benz logo, hence the name "MB water". We show, using NPT Monte Carlo simulations, that the model, thermodynamically-speaking, looks a lot like water, in

the bulk and as a solvent. It qualitatively reproduces several of water's anomalous trends with temperature and has the correct transfer thermodynamics for small inert solutes.

Using the model we have investigated the microscopic origins of hydrophobicity. At low temperature, water molecules are ordered around small inert solutes and have strengthened hydrogen bonds relative to bulk water molecules. There is evidence for multiple modes of clathration. As temperature is increased, the shell water structure melts out faster than the bulk water structure. This hydrogen-bond breaking gives rise to the calculated heat capacity, as we have shown quantitatively using Muller's two-state model. Hydrogen bonds in the bulk and shell have roughly equal strength and numbers at T_S, when the transfer entropy is zero. Beyond this temperature, more structure is observed in the bulk than in the hydration shell.

Using an exhaustive enumeration scheme, and a formal expansion of the entropy with small systems of MB water molecules, we have determined that the entropic order in these systems is overestimated at the two-body level. Nevertheless, the ratio of intact and broken H-bonding states of two waters in the bulk, and the corresponding enthalpy difference, are reasonably close to the parameters for the two-state model. Explanation of the hydration shell parameters requires extrapolations to very large systems.

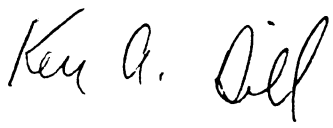

Contents

List of Tables

List of Figures

Chapter 1

Introduction

Investigations into the anomalous properties of water, and the phenomenon known as "hydrophobicity"[3, 7], have a long and rich history. This is not surprising considering the ubiquitous nature of water, which makes up some 65%-70% of human body mass and bathes the cells of all living creatures. Further, the mechanisms underlying transfers of hydrophobic solutes are believed to be involved in a diverse array of biochemical processes, such as protein folding, micellar aggregation, and ligand binding[2].

Water is also interesting because it has many anomalous or unusual thermodynamic properties which set it apart from simple liquids. These include, but are not limited to: a temperature of maximum density in the liquid phase over a wide range of pressures, an unusually high surface tension, a minimum in the isothermal compressibility as a function of temperature, and a large heat capacity throughout the liquid range. These properties are believed by many to arise from the ability of water to form tetrahedrally coordinated hydrogen bonds. However, the extent of the coordination of hydrogen bonds in liquid water, and the resulting structural features of this fluid, have been debated vigorously over the years[7, 34, 38].

Hydrophobic trends are equally striking. At all temperatures, transfers of nonpolar solutes are highly unfavorable from a free-energetic standpoint. Given the strong cohesive energy of water, one would expect that the introduction of an inert solute would be opposed enthalpically, due to the necessity of creating a cavity to accommodate the solute. However, at room temperature, such a transfer is actually enthalpically *favorable* from the gas phase, and at least neutral from the solute's own pure liquid phase. Instead, these processes are opposed by *entropy*. Even more re-

markably, the transfer is accompanied by a large heat capacity, often referred to as the signature of hydrophobicity[5]. This means that the low solubility of apolar solutes becomes less entropy-driven and more enthalpy-driven at higher temperatures. These properties should be contrasted with transfers to simple solvents (e.g., neopentane), where the solutes are only slightly insoluble, and the transfer is enthalpy-driven and not marked by an appreciable heat capacity.

It is not possible or relevant to thoroughly review here the large body of literature on these topics; comprehensive reviews on the theoretical and experimental studies of water[6, 7, 38, 47] and hydrophobicity[2, 3, 16, 39] have appeared. It is safe to say that the waters are still a bit murky despite the wealth of data gleaned over the last half of a century from solubility experiments[30, 46], microcalorimetry[11, 33], NMR[18, 25, 27, 36], x-ray[28] and neutron scattering experiments[37], and IR[1, 8, 17] and Raman spectroscopy[4, 10, 14, 15, 35, 43, 44, 45]. Theoretical work from simulations[1] [9, 12, 22, 23, 24], integral equation theory[19, 31, 32, 40], and scaled-particle theory[21, 29] have shed some light on the problem at hand. Yet, the field is lacking a unified picture of the physics behind hydrophobic effects. We seem to be stuck in a mass of details, with words like "structure makers" and "structure breakers" to characterize solutes in waters, which change depending on the experimental technique used[26]. Often it is not even clear what we mean by "structuring" on a microscopic level. It is not uncommon in the simulation literature, for example, to report a simple orientationlly-averaged pair correlation function and perhaps the

[1] For work in this area prior to 1993, see reviews [3] and [47], and references therein.

coordination numbers around solutes[13, 20, 41, 42]. Though informative, this leaves us yearning for a more complete picture.

I do not propose that we have all of the answers. However, in this work I have examined a model that can explore a more diverse array of properties of water and aqueous systems. It is a two-dimensional model of the physics of hydrogen bonding liquids, not an atomically-accurate model of water. Its limitations are that it gives up atomic detail, and 3-dimensionality, but it uses only few parameters, and is computationally simple enough to explore these broader-scale questions of physics. Its parameters are intuitive and conceptual, allowing us to directly observe the effects of removing or changing each one. Using direct comparisons to simple theoretical liquids with such subtle modifications we hope to identify the microscopic features that are necessary and sufficient for each of the anomalous properties of water. With this model, and comparisons to subtle modifications of it, our goal is to generate hypotheses that can be tested by experiments and molecular simulations, but cannot otherwise be generated by more realistic models of water.

In order to demonstrate that the essential details for a qualitative description of water and hydrophobicity have not been left out in this simplification, we make many comparisons of the model to experimental trends in Chapter 2 over a wide temperature range. The results are remarkably good. We present a wide array of microscopic structural evidence arising from the model to explain the observed thermodynamics.

Simply "observing" structural details in simulations which *might* determine the thermodynamics is not entirely satisfying. We endeavored to make a more quan-

titative connection between the microscopic and macroscopic pictures. Hence, in Chapter 3, we have used the two-state model of Muller[26] to quantitatively link the observed hydrogen-bond fraction in our simulations to the thermodynamics that we calculate exactly. The parameters of this two-state model are further justified by exhaustive enumerations of the states available to the model water molecules. The success of this two-state framework in our model system allows us to make some predictions and suggestions for real experimental analysis.

The exhaustive enumerations we have performed give indications that the "structuring" in water and hydrophobicity have a strong many-body component. In other words, a quantitative estimate of the entropy of these systems cannot be obtained from systems of two waters, or one water and a solute. In Chapter 4, we perform a rigorous multiple-body expansion of the entropy, using full angular correlation functions obtained from our simulations. This analysis gives us quantitative insight as to the sufficiency of two- and higher-body terms. Additionally, we are able to draw some conclusions about the relative contributions of translational and orientational order in these systems. The Appendices provide some formulae and derivations for work presented in Chapters 2 and 4.

Having focused in this work on simple systems of a single LJ particle in MB water, we have really only scratched the surface of what can be explored. Hence, in Chapter 5 we outline the scope of some of the areas that are amenable to study with the model. As the speed of computers increases at a dizzying rate, one thing will remain constant: this model will always be one to two orders of magnitude more computationally efficient than standard 3D models.

Bibliography

[1] G. Andaloro, M. Leone, and M. B. Palma-Vittorelli. Near-i.r. absorption of H_2O and D_2O in the liquid and supercooled range. *Nuovo Cimento*, 2 D(5):1239–1253, 1983.

[2] A. Ben-Naim. *Hydrophobic Interactions.* Plenum Press, New York, 1980.

[3] W. Blokzijl and J. B. F. N. Engberts. Hydrophobic effects. opinions and facts. *Angew. Chem. Int. Ed. Engl.*, 32:1545–1579, 1993.

[4] G. D'Arrigo, G. Maisano, F. Mallamace, P. Migliardo, and F. Wanderlingh. Raman scattering and structure of normal and supercooled water. *J. Chem. Phys.*, 75:4262–4270, 1981.

[5] K. A. Dill. Dominant forces in protein folding. *Biochemistry*, 29:7133–7155, 1990.

[6] D. Eisenberg and W. Kauzmann. *The structure and properties of water.* Oxford University Press, Oxford, 1969.

[7] F. Franks, editor. *Water, a Comprehensive Treatise*, volume 1-7. Plenum Press, New York, 1972-1982.

[8] Y. Fujita and S. Ikawa. Effect of temperature on the hydrogen bond distribution in water as studied by infrared spectra. *Chem. Phys. Lett.*, 159(2,3):184–188, 1989.

[9] S. Garde, G. Hummer, A. E. García, M. E. Paulaitis, and L. R. Pratt. Origin of entropy convergence in hydrophobic hydration and protein folding. *Phys. Rev. Lett.*, 77:4966–4968, 1996.

[10] P. A. Giguere and M. Pigeon-Gosselin. The nature of free OH groups in water. *Journal of Raman Spectroscopy*, 17:341–344, 1986.

[11] S. J. Gill, S. F. Dec, G. Olofsson, and I. Wadso. Anomalous heat capacity of hydrophobic solvation. *J. Phys. Chem.*, 89:3758–3761, 1985.

[12] B. Guillot and Y. Guissani. A computer simulation study of the temperature dependence of the hydrophobic hydration. *J. Chem. Phys.*, 99(10):8075–8094, 1993.

[13] B. Guillot, Y. Guissani, and S. Bratos. A computer-simulation study of hydrophobic hydration of rare gases and of methane. I. Thermodynamic and structural properties. *J. Chem. Phys.*, 95(5):3643–3648, 1991.

[14] D. E. Hare and C. M. Sorensen. Raman spectroscopic study of bulk water supercooled to -33 °C. *J. Chem. Phys.*, 93:25–33, 1990.

[15] D. E. Hare and C. M. Sorensen. Raman spectroscopic study of dilute HOD in liquid H_2O in the temperature range -31.5 to 160 °C. *J. Chem. Phys.*, 93:6954–6960, 1990.

[16] A. D. J. Haymet, K. A. T. Silverstein, and K. A. Dill. Hydrophobicity reinterpreted as "minimization of the entropy penalty of solvation". *Faraday Discuss.*, 103:117–124, 1996.

[17] D. Hecht, L. Tadesse, and L. Walters. Correlating hydration shell structure with amino acid hydrophobicity. *J. Am. Chem. Soc.*, 115:3336–3337, 1993.

[18] J. C. Hindman. Proton resonance shift of water in the gas and liquid state. *J. Chem. Phys.*, 44:4582–4592, 1966.

[19] F. Hirata, B. M. Pettitt, and P. J. Rossky. Application of an extended RISM equation to dipolar and quadrupolar fluids. *J. Chem. Phys.*, 77:509–520, 1982.

[20] W. L. Jorgensen and C. Ravimohan. Monte Carlo simulation of differences in free energies of hydration. *J. Chem. Phys.*, 83(6):3050–3054, 1985.

[21] B. Lee. Solvent reogranization contribution to the transfer thermodynamics of small nonpolar molecules. *Biopolymers*, 31(8):993–1008, 1991.

[22] R. L. Mancera and A. D. Buckingham. Temperature effects on the hydrophobic hydration of ethane. *J. Phys. Chem.*, 99:14632–14640, 1995.

[23] N. Matubayasi and R. M. Levy. Thermodynamics of the hydration shell. 2. Excess volume and compressibility of a hydrophobic solute. *J. Phys. Chem.*, 100:2681–2688, 1996.

[24] N. Matubayasi, L. H. Reed, and R. M. Levy. Thermodynamics of the hydration shell. 1. Excess energy of a hydrophobic solute. *J. Phys. Chem.*, 98:10640–10649, 1994.

[25] N. Muller. Concerning structural models for water and chemical-shift data. *J. Chem. Phys.*, 43:2555–2556, 1965.

[26] N. Muller. Does hydrophobic hydration destabilize protein native structures. *Trends in Biochemical Sciences*, 17(11):459–463, 1992.

[27] N. Muller and R. C. Reiter. Temperature dependence of chemical shifts of protons in hydrogen bonds. *J. Chem. Phys.*, 42(9):3265–3269, 1965.

[28] A. H. Narten, M. D. Danford, and H. A. Levy. X-ray diffraction study of liquid water in the temperature range 4-200 °C. *Discuss. Faraday Soc.*, 43:97–107, 1967.

[29] R. A. Pierotti. *Chem. Rev.*, 76:717, 1976.

[30] G. L. Pollack. Why gases dissolve in liquids. *Science*, 251:1323–1330, 1991.

[31] L. R. Pratt. Theory of hydrophobic effects. *Ann. Rev. Phys. Chem.*, 36:433–449, 1985.

[32] L. R. Pratt and D. Chandler. Theory of the hydrophobic effect. *J. Chem. Phys.*, 67:3683–3704, 1977.

[33] P. L. Privalov and S. J. Gill. Stability of protein structure and hydrophobic interaction. *Advances in Protein Chemistry*, 39:191–234, 1988.

[34] G. Robinson, S.-B. Zhu, S. Singh, and M. Evans. *Water in Biology, Chemistry and Physics: Experimental Overviews and Computational Methodologies.* World Scientific, Singapore, 1996.

[35] J. R. Scherer, M. K. Go, and S. Kint. Raman spectra and structure of water from -10 to 90 degrees. *J. Phys. Chem.*, 78:1304–1313, 1974.

[36] W. G. Schneider, H. J. Bernstein, and J. A. Pople. Proton magnetic resonance chemical shift of free (gaseous) and associated (liquid) hydride molecules. *J. Chem. Phys.*, 28:601–607, 1958.

[37] A. K. Soper and J. Turner. Impact of neutron scattering on the study of water and aqueous solutions. *International Journal of Modern Physics B*, 7(16):3049–3076, 1993.

[38] F. H. Stillinger. Water revisited. *Science*, 209:451–457, 1980.

[39] C. Tanford. *The Hydrophobic Effect: formation of micelles and biological membranes, 2nd Ed.* Wiley, New York, 1980.

[40] A. Tani. Nonpolar solute-water pair correlation functions-a comparison between computer simulation and theoretical results. *Molecular Physics*, 48:1229–1240, 1983.

[41] D. van Belle and S. J. Wodak. Molecular dynamics study of methane hydration and methane association in a polarizable water phase. *J. Am. Chem. Soc.*, 115:647–652, 1993.

[42] A. Wallqvist and B. J. Berne. Molecular dynamics study of the dependence of water solvation free energy on solute curvature and surface area. *J. Phys. Chem.*, 99:2885–2892, 1995.

[43] G. E. Walrafen. Raman spectral studies of the effects of temperature on water structure. *J. Chem. Phys.*, 47:114–126, 1967.

[44] G. E. Walrafen, M. R. Fisher, M. S. Hokmabadi, and W.-H. Yang. Temperature dependence of the low- and high-frequency raman scattering from liquid water. *J. Chem. Phys.*, 85(12):6970–6982, 1986.

[45] G. E. Walrafen, M. S. Hokmabadi, and W.-H. Yang. Raman isobestic points from liquid water. *J. Chem. Phys.*, 85(12):6964–6969, 1986.

[46] E. Wilhelm, R. Battino, and R. J. Wilcock. *Chem. Rev.*, 77:219, 1977.

[47] S.-B. Zhu, S. Singh, and G. W. Robinson. Field-perturbed water. *Adv. Chem. Phys.*, 85(3):627–731, 1994.

Chapter 2

The MB Model of Water and Nonpolar Solutions

Kevin A. T. Silverstein, A. D. J. Haymet, and Ken A. Dill

2.1 Abstract

We use a simple computational model, proposed originally by Ben-Naim, to study the anomalous properties of water and the hydrophobic effect. Waters are modeled as two-dimensional (2D) Lennard-Jones disks, with three orientation-dependent hydrogen-bonding arms, arranged as in the Mercedes Benz (MB) logo. Phase space is explored using NPT Monte Carlo simulations. For pure water, the MB model qualitatively predicts the density anomaly (and the related negative thermal expansion coefficient at low temperature), the minimum in the isothermal compressibility as a function of temperature, the large anomalous heat capacity, and freezing to the 2D model analog of ice, a low-density hexagonal crystal phase. For the solvation of nonpolar solutes (disks without H-bonds), the model predicts the experimental trends with temperature of the free energy, entropy, enthalpy, molar volume, and heat capacity. A unique feature of these simulations is that they provide well-converged heat capacities of transfer, an important fingerprint of hydrophobicity. This model gives an explanation for the temperature, T_S, at which the transfer entropy of nonpolar solutes is zero: below this temperature, shell water molecules have more hydrogen bonding than bulk water molecules; above T_S, the reverse is true.

2.2 Introduction

Water is regarded as an unusual and poorly understood liquid. Water properties have been reviewed extensively in the literature [29, 31, 60, 63, 66, 68]. Relative to simpler liquids, water has certain anomalous thermodynamic properties: a temperature of

maximum density in the liquid phase over a wide range of pressures, an unusually high surface tension, a minimum in the isothermal compressibility as a function of temperature, and a large heat capacity throughout the liquid range. These properties are thought to arise from the ability of water to form tetrahedrally-coordinated hydrogen bonds. There remains vigorous debate, however, over the role of hydrogen bonding in the properties of liquid water [31, 60, 63].

Water is also unusual as a solvent, particularly for nonpolar solute molecules [11, 17, 30, 58, 66]. Unlike simpler solvents, the insertion of nonpolar solutes into water is: (1) strongly unfavorable, (2) strongly opposed by entropy at room temperature, and (3) accompanied by a large positive heat capacity. These properties define the hydrophobic effect.

The physical basis for the hydrophobic effect has been the subject of debate. One group [17, 44, 45, 56, 57] holds that the large aversion of oil for water results mostly from the small size of the water molecule, and not from water structuring by the solute. Others believe that the large positive heat capacity of insertion of nonpolar solutes is a defining feature of hydrophobicity, and that it results from hydrogen bonding and the ordering of water molecules around the solute. Some of this difference of opinion may be semantic [37, 62].

In order to provide a physical explanation for the properties of water and the hydrophobic effect, many different computer simulations have been performed[1] [32, 34, 46, 48, 49]. These simulations usually aim for realism in representing the geometric

[1] For work in this area prior to 1993, see reviews [17] and [68], and references therein.

structure of water. But there are two intrinsic limitations of an atomistically-accurate, three-dimensional model of water. First, such models require large computational investments, and some properties — particularly those involving derivatives of the free energy — are computationally prohibitive to study, such as the molar volume and the heat capacity of transfer. Yet these are precisely the properties that are considered "signatures" of the hydrophobic interaction [27]. Second, simplified models can often address questions of principle that cannot be addressed in more realistic models. Realistic models tend to include many variables, geometric details, and types of interactions, including electrostatics, dipoles, hydrogen bonding and van der Waals interactions. In simpler models, with fewer parameters, it is easier to ascertain the dominant interactions, and to trace the connection from assumptions about driving forces to the observable properties.

Our aim here is to develop a simplified model, with the details stripped away. We want to see how much of the behavior of pure water, and of the hydrophobic effect, is simply due to a balance between Lennard-Jones interactions and orientation-dependent hydrogen bonding. No other electrostatic terms are included explicitly. Our aim is a simplest "toy" model of the physics, not a most-realistic model of the geometry. We use a two-dimensional model. Its limitations are that it gives up atomic structural detail, and three-dimensionality, but it uses only few parameters, and is computationally simple enough to explore properties that are difficult to study in more realistic models.

The two-dimensional model that we explore is one of a family of models first introduced by Ben-Naim [7] in 1971. He investigated the structure of the pure fluid

[7, 8], and a dilute hydrophobic solution [6, 9] using an integral equation formalism. Then, he explored several parameter sets using NVT Monte Carlo simulations at a single phase point for each parameterization, and obtained more accurate distributions of the pure fluid [10]. Concurrently, more realistic 3D models were being developed [64, 65]. Consequently, the Ben-Naim model was all but neglected until recently when Andaloro and Sperandeo-Mineo showed that it was simple enough to teach students about hydrophobicity without high-powered computers [3]. Andaloro and Sperandeo-Mineo explored a wider range of structural features of this model fluid around a fixed inert solute [3], and showed enhanced local structuring. Although their simulations were not well converged, they nonetheless showed that the model gives useful insights.

To date, what has *not* been explored in this model are effects of temperature and pressure, or thermal properties other than the internal energy. Many other 3D simulations are similarly limited. Pair correlation functions and counts of hydrogen bonds converge quickly; but the calculation of the transfer thermodynamics is quite expensive computationally. The computational requirements of the 3D models make systematic studies of solvation extremely difficult. With a simplified model, however, we can study systematically here the link between microscopic structures and the macroscopic thermodynamics.

The present paper shows that LJ and orientation-dependent hydrogen-bonding are sufficient, even in a 2D model, to capture a remarkably broad range of the experimentally-observed thermodynamic properties of pure water and the hydropho-

bic effect. Many of the results are consistent with more realistic simulations[2].

This paper is organized as follows. In Section 2.3, we define the MB model, briefly reviewing others of similar philosophy. Section 2.4 contains a description of the computational methods used. Then, in Sections 2.5 and 2.6, we compare our computed thermodynamic trends with those of experiments on bulk water and nonpolar solutions, respectively. Section 2.7 is a summary.

2.3 Model Description

Waters are represented in this model as two-dimensional disks with 3 symmetrically arranged arms, separated by an angle of 120°, as in the Mercedes Benz logo. Molecules interact pairwise through a Lennard-Jones (LJ) term and an explicit hydrogen bonding (HB) term,

$$U(\mathbf{X_i}, \mathbf{X_j}) = U_{LJ}(r_{ij}) + U_{HB}(\mathbf{X_i}, \mathbf{X_j}) \; . \tag{2.1}$$

We use Ben-Naim's notation, summarized in Figure 2.1: $\mathbf{X_i}$ denotes the vector representing both the coordinates and the orientation of the ith particle, and r_{ij} is the distance between the molecular centers of particles i and j. The LJ term is defined in the usual fashion

$$U_{LJ}(r_{ij}) = 4\,\epsilon_{LJ}\left[\left(\frac{\sigma_{LJ}}{r_{ij}}\right)^{12} - \left(\frac{\sigma_{LJ}}{r_{ij}}\right)^{6}\right] \; , \tag{2.2}$$

[2]Preliminary results from this work have been reported at the International Symposium on Molecular Thermodynamics and Molecular Simulation in Japan [38].

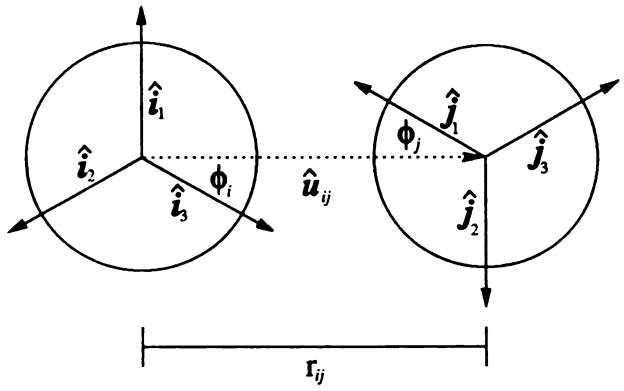

Figure 2.1: Two representative MB water molecules with indices i and j, separated by a distance r_{ij}. Each molecule has three hydrogen bonding arm vectors: $\hat{\mathbf{i}}_k$ and $\hat{\mathbf{j}}_l$ respectively $(k, l = 1, 2, 3)$. The intermolecular axis vector is denoted $\hat{\mathbf{u}}_{ij}$, and the angles that the closest arm of each molecule make with this vector are labeled ϕ_i and ϕ_j.

where ϵ_{LJ} and σ_{LJ} are the well-depth and contact parameters, respectively. Neighboring water molecules form explicit hydrogen bonds when the arm of one molecule aligns with the arm of another, with an energy that is a Gaussian function of separation and angle,

$$U_{HB}(\mathbf{X_i}, \mathbf{X_j}) = \epsilon_{HB}\, G(r_{ij} - r_{HB}) \sum_{k,l=1}^{3} G(\,\hat{\mathbf{i}}_k \cdot \hat{\mathbf{u}}_{ij} - 1)\, G(\,\hat{\mathbf{j}}_l \cdot \hat{\mathbf{u}}_{ij} + 1)\,, \qquad (2.3)$$

where $G(x)$ is an unnormalized Gaussian function,

$$G(x) = \exp[-x^2/2\sigma^2]\,. \qquad (2.4)$$

The unit vector $\hat{\mathbf{i}}_k$ represents the kth arm of the ith particle ($k = 1, 2, 3$) and $\hat{\mathbf{u}}_{ij}$ is the unit vector joining the center of molecule i to the center of molecule j. The parameters $\epsilon_{HB} = -1$ and $r_{HB} = 1$ define the optimal hydrogen bond energy and bond length respectively. By this definition, the strongest hydrogen bond occurs when one arm of one water is perfectly collinear with the arm of another water. We make no distinction between donors and acceptors; this contribution to the energy is just defined by the degree to which two arms line up. Angular deviations from this lowest-energy hydrogen bond have a Gaussian variation in energy, with a single width parameter used to attenuate the interaction. The same width parameter is used for both distance and angle deviations (although in principle, two separate width parameters could be used: one for hydrogen bond stretching; the other for bending). Figure 2.1 shows the definitions of the distances and angles between two model water molecules.

In total, there are 5 parameters. Ben-Naim explored several combinations of parameters, of which we chose one for this work. The interaction energy, ϵ_{LJ} is one-tenth of ϵ_{HB}, and the LJ contact distance is 0.7 that of r_{HB}. The width of the Gaussian $\sigma = 0.085$ was chosen to be small enough that a direct H-bond is more favorable than a bifurcated H-bond. All energies and temperatures will be reported in reduced units, normalized to the strength of the optimal hydrogen bond (e.g., $T^* = k_B T/|\epsilon_{HB}|$, $H^* = H/|\epsilon_{HB}|$). Similarly, all distances are scaled by the length of an idealized hydrogen bond separation (e.g., $V^* = V/r_{HB}^2$).

2.3.1 Comparison with other simple models

A completely different two-dimensional model has been investigated by Okazaki, Nosé, Kataoka and Yamamoto [55], who subsequently studied a three dimensional model that was related to it [42]. The model of Okazaki *et al.* displays four anomalous behaviors of water: a temperature of maximum density, a minimum in the isothermal compressibility, a shift in the temperature dependence between isobars of the thermal expansion coefficient, and the singular properties of supercooled water. Our model differs from theirs in the H-bond geometry, and ours is simpler insofar as it lacks any long-range electrostatics. No analysis of the solvation properties of their model has been published, to our knowledge. The success of the MB model indicates that explicit electrostatics and the distinction between donors and acceptors are not the central components of the physics of hydrophobic hydration.

Yet another primitive model was explored by Dahl and Andersen [24, 25]; it too

captures several anomalous properties of liquid water. Their three-dimensional model used a hard-sphere reference with a double square-well hydrogen bond potential that is tetrahedrally coordinated. The thermodynamics were computed by a cluster expansion approximation. More recently, Nezbeda *et al.* have investigated the structural properties of related models [43, 51, 53], comparing the solutions of several approximations with Monte Carlo simulations. These authors used the model to investigate the phase behavior of inert gases and n-alkanes with some qualitative success [52, 54]. These models, like the one we explore, neglect the long-range Coulombic interactions, and model the H-bonding explicitly. Simulations of these three-dimensional models are still reasonably intensive; hence the thermodynamics are only accessible through the approximate theories.

Among other recent, simplified 3D models of water are those based on an orientational octupole-octupole interaction [18, 19, 20, 26]. These octupolar models, which have been developed by Blum and co-workers, have few parameters, and can be solved analytically, but are more or less still in the development stage. Lattice models of water have been studied by various researchers [13, 14, 21, 28, 59], based upon the model of Bell [5]. In these models, waters are configured on a bcc lattice with a discrete number of orientational states, and the thermodynamics is often solved by a zeroth- or first-order approximation. These models have also been able to capture numerous anomalous properties of water, but the confines of the lattice may be too restrictive to correctly model the qualitative trends of hydrophobicity [28].

2.4 Simulation Methods

2.4.1 General Procedure

To obtain thermodynamic and structural properties of MB water, we performed Monte Carlo simulations in the NPT ensemble [2]. At each successive step, a move for one molecule is chosen randomly among the following three options:

$$x \to x + \xi_1 \Delta x,\ y \to y + \xi_2 \Delta y,\ \phi \to \phi + \xi_3 \Delta \phi \tag{2.5}$$

where the ξ_i's are random numbers generated over the interval $-1 \leq \xi_i \leq 1$, and Δx, Δy, and $\Delta \phi$ are fixed maximum displacements in the coordinates and angle of the chosen molecule. These increments are automatically adjusted during an initial equilibration simulation to achieve approximately a 50% acceptance ratio. To hold the pressure constant, every 5 passes [41] (1 pass = N molecules), an attempt is made to scale the dimensions of the box, and all of its component particles, according to

$$q_i \to q_i(1 + \xi \Delta q), \tag{2.6}$$

where the q_i's represent the particle coordinates and box length, and the random number ξ and maximum volume increment Δq are defined as above.

Unless otherwise indicated, all simulations in this study were performed on systems of 60 water molecules (covering the same area as a cross-section of a 3D system having about 500 particles), using standard periodic boundary conditions and the minimum image convention. The starting configuration of each phase point was selected at random, and the first 2×10^4 passes were discarded as the system equilibrated. Statistics were gathered over the next 1×10^7 passes. Simulations with solutes were carried out

under the same procedures with 60 water molecules and a single LJ solute (with the same well-depth and contact parameters as the water molecules) fixed in the center of the simulation box.

2.4.2 Computational Speed Enhancements

To speed up the hydrogen bond calculation, two computational enhancements were implemented; they have virtually no effect on the Markov chain of states generated. First, an interparticle distance cutoff is chosen, beyond which hydrogen bond energies are assumed to equal zero. The cutoff was chosen such that the energy of neglected interactions does not exceed 1×10^{-10}, corresponding to a distance of ≈ 0.577. We did not use a cutoff for the LJ interaction, other than that implied by the minimum image convention. The second speed-up involves the form of the hydrogen bond calculation. Since the Gaussian-width parameter is so narrow, two arms of one molecule can never make an appreciable interaction with the same neighboring molecule (of course, one arm *can* interact with arms of *different* neighbors, forming a bifurcated hydrogen bond). Therefore, it is unnecessary to calculate all 9 arm-arm interactions for two water molecules. Instead, we pre-determine which arm of each molecule is nearest to the intermolecular axis vector, and then calculate only the hydrogen bond between the appropriate two arms. This is accomplished with the following simple formula, and speeds up the total simulation time by roughly a factor of 2:

$$U_{HB}(\mathbf{X_i}, \mathbf{X_j}) \;=\; \epsilon_{HB}\, G(r_{ij} - r_{HB})\, G(u(i,\ \hat{\mathbf{u}}_{ij}) - 1)\, G(v(j,\ \hat{\mathbf{u}}_{ij}) + 1)\,, \quad (2.7)$$

where the expressions,

$$
\begin{aligned}
u(i,\ \hat{\mathbf{u}}_{ij}) &= MAX(\ \hat{\mathbf{i}}_1 \cdot\ \hat{\mathbf{u}}_{ij},\ \hat{\mathbf{i}}_2 \cdot\ \hat{\mathbf{u}}_{ij},\ \hat{\mathbf{i}}_3 \cdot\ \hat{\mathbf{u}}_{ij}) \\
v(j,\ \hat{\mathbf{u}}_{ij}) &= MIN(\ \hat{\mathbf{j}}_1 \cdot\ \hat{\mathbf{u}}_{ij},\ \hat{\mathbf{j}}_2 \cdot\ \hat{\mathbf{u}}_{ij},\ \hat{\mathbf{j}}_3 \cdot\ \hat{\mathbf{u}}_{ij})\ ,
\end{aligned}
\tag{2.8}
$$

select out the appropriate arm of the ith and jth molecule, respectively, and the Gaussian function, $G(x)$, again has the form defined in Eq. 2.4.

Most of the simulation runs were performed on the farm of DEC Alphas at the University of Sydney, requiring approximately 30 hours of CPU time per phase point. A comparable study on a 3D model would take approximately two orders of magnitude longer, due to the number of particles that would be needed.

2.4.3 Calculations of Thermodynamic Quantities

Mechanical averages such as the enthalpy and volume are computed in the standard way, as the average of those quantities over the course of the simulation. The heat capacity, C_p^*, the isothermal compressibility, κ^*, and the thermal expansion coefficient, α^*, are computed from the fluctuations:

$$C_p^* = \frac{C_p}{k_B} = \frac{< H^{*2} > - < H^* >^2}{NT^{*2}}\ , \tag{2.9}$$

$$\kappa^* = \frac{< V^{*2} > - < V^* >^2}{T^* < V^* >}\ , \tag{2.10}$$

$$\alpha^* = \frac{< V^* H^* > - < V^* >< H^* >}{T^{*2} < V^* >}\ , \tag{2.11}$$

where k_B is the Boltzmann constant.

For the insertion of a model solute into water, all thermodynamic averages were computed using the Widom test-particle method [67] and related fluctuation formulae.

The Widom method is a specific case of the free energy perturbation technique. A ghost particle is placed at random among the N molecules of the pure fluid, but not allowed to interact. Instead, an appropriately-weighted scaling of the solute's hypothetical interaction with the fluid is computed. In this manner, the free energy change, and appropriate thermodynamic derivatives can be computed in terms of the configurations generated in the reference pure fluid. In principle, the configurations which contribute strongly to the solution (i.e., the ensemble of $N + 1$ particles) will arise in the reference fluid through fluctuations, and make a significant contribution to the computed thermodynamic values, if the simulation is run long enough. However, in practice, such configurations are never fully explored if the reference ensemble differs greatly from that of the solution (e.g., as in the case of a large solute, where a cavity large enough to accommodate it would never be found in reasonable simulation time [15]). Guillot and Guissani used the Widom method to compute free energies, enthalpies, and entropies at several temperatures for methane and various noble gases [34, 35]. Although this was a pioneering study, showing the wide utility of the test-particle method, the transfer entropies and enthalpies were poorly converged. Also, the criticism of Beutler *et al.* suggests that the higher noble gases in the simulation by Guillot and Guissani were probably too large.

The advantage of the test-particle method is that the thermodynamics of transfer can be calculated accurately for small solutes using only a single simulation; free energy perturbation (FEP) and thermodynamic integration (TI) methods require multiple-step transformations. Also in the Widom method, there are multiple insertion sites in each *snapshot* of the fluid, so several attempted insertions can be made

per frame. These two features make the insertion method far superior to both FEP and TI, so long as the solutes inserted are small. As a check, we compared our test-particle results with those calculated using FEP and TI at a few temperatures, and obtained nearly-perfect agreement. In Appendix A, we collect together the appropriate test-particle equations for computing transfer free energies, enthalpies, entropies, molar volumes, and heat capacities.

As an additional check, we determined that our simulations are not limited by artifacts of box size. We found no dependence of the thermodynamic properties on the size or shape of the simulation box. For a few state points, simulations were carried out with 120 water molecules, to compare with the usual 60. Figure 2.2 shows a typical comparison of the pair correlation function for the two box sizes. All thermodynamic values are identical within the error bars.

2.5 Results for Bulk Water

MB Water Captures Some Experimentally Observed Properties of Real Water. Constant-pressure simulations of pure MB water at a reduced pressure of 0.19 reveal several similarities to pure water. Trends at a lower pressure of 0.12 were also explored, and had all of the same qualitative trends, except for a more poorly defined minimum in the isothermal compressibility. A limitation of our study, as with many others, is that we do not know the full phase diagram[3], but the part we have

[3]We believe the liquid range of MB water is probably small and it is possible that the pressure we have chosen to show for the calculations here may be above the critical pressure [61]. But even if this is the case, this does not limit the value of the model for the properties we study here.

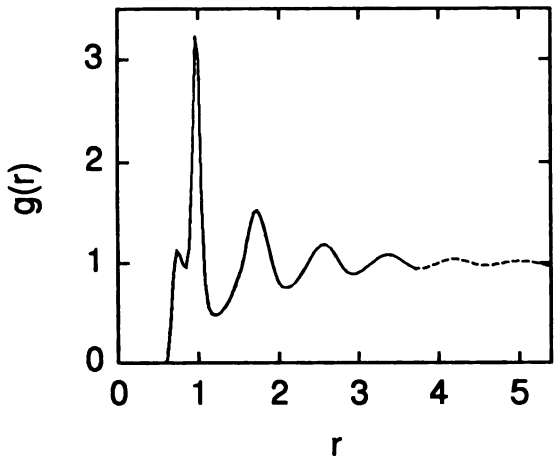

Figure 2.2: Pair correlation function at $T^* = 0.20, P^* = 0.19$ for boxes containing 60 (solid line) and 120 (dashed line) particles overlap exactly. This observed box size insensitivity is representative of other temperatures and pressures studied.

explored is sketched in Figure 1 of reference [61].

MB Water Freezes into an Ice-like Structure at Low Temperatures. At low temperatures, MB water has a non-close packed ice-like ground state, having low density and crystalline ordering. The hexagonal symmetry is the same as would be observed in real 3D ice, viewed down the c-axis. MB ice forms spontaneously from a random initial state in constant pressure MC simulations[4]. An ice configuration

[4]Note, however, that the "ice" that forms in a square box is *not* of the lowest-energy possible in the model. A perfect honeycomb lattice of $a \times b$ molecules fits in a rectangular unit cell of sides $\frac{3a}{2} \times \frac{b\sqrt{3}}{2}$ where a and b are both even; so a square will stretch the hydrogen bonds along one of the coordinate axes, in order to retain the periodicity through the boundaries. Hence in representing ice in this model accurately, one should begin with a rectangular box of the proper dimensions. But the shape of the box has absolutely no effect on the converged properties of the simulations for disordered fluid states, which is the state of interest here.

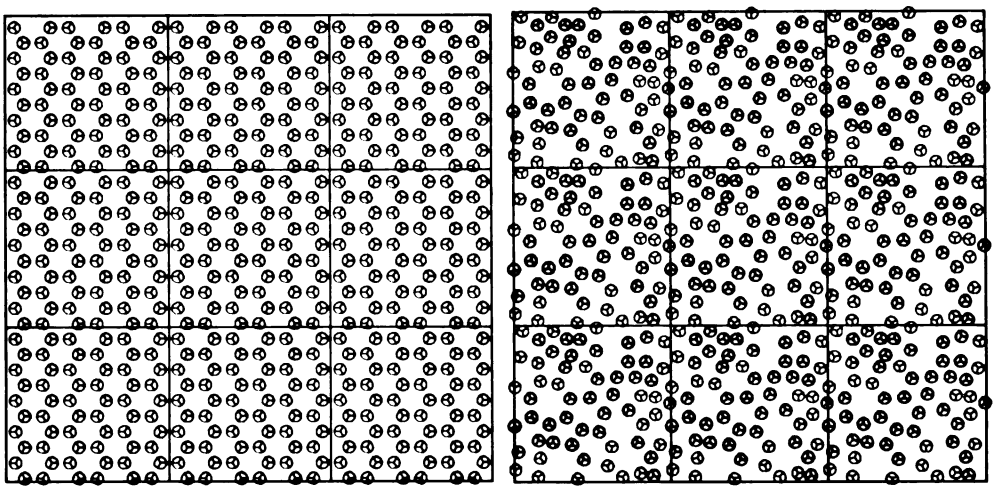

Figure 2.3: Two snapshots a system of 60 MB water molecules. On the left, the ground-state "ice" configuration forms a perfect hexagonal honeycomb lattice; and on the right, a typical liquid configuration at $T^* = 0.20, \rho = 0.9$.

is shown in Figure 2.3, along with a typical fluid configuration, for which there is considerably less regularity. As with real water, MB ice has lower density than MB liquid water. In the MB model, the lower density of ice arises because the hydrogen bonding interactions that favor low-density ordered packing are stronger than the van der Waals interactions that favor random higher-density packing.

The liquid is denser than the ice phase. As noted above, MB ice has an open, low-density structure. The ice structure is a result of the optimization of hydrogen bonding. Heating melts the ice, leading to a liquid of higher density than the solid, indicating that MB ice would float on its liquid, just as real water does. Moreover, it follows from the Clapeyron equation, $dp/dT = \Delta S/\Delta V$, that since the molar volume is lower in the phase of higher entropy (assumed to be the liquid), the liquid/solid phase boundary will have the typical "backward" slope that water has, $dp/dT < 0$,

whereby the melting pressure decreases with temperature. The thermal expansion coefficient, $\alpha = \frac{1}{V}\left(\frac{\partial V}{\partial T}\right)_P$ shown in Figure 2.4 (c), is just the derivative of the function in Figure 2.4 (a). As in real water, the thermal expansion coefficient becomes negative at low temperature, and equals zero at the density anomaly temperature.

The density anomaly. If liquid water is heated above its melting temperature, a remarkable behavior is observed: the density at first *increases*, then ultimately decreases as in more normal liquids. The temperature at which the density trend changes from increasing to decreasing is the density anomaly, or temperature of maximum density (TMD). Figure 2.4 shows that MB water has a density anomaly similar to that of real water.

What is the physical basis for these properties? The MB model gives the following interpretation. The structure and thermodynamics of the ice phase is dominated by hydrogen bonding. The relatively low density of ice is due to the fact that hydrogen bonding is stronger than the van der Waals interactions. Optimal hydrogen bonding is incommensurate with the tighter packing that would be favored by the van der Waals interactions. Ice melts when the thermal energy is sufficient to disrupt and disorder the hydrogen bonds, broadening the distribution of H-bond angles and lengths. Now among this broadened H-bond distribution, the van der Waals interactions favor those conformations of the system that have higher density. Hence liquid water is denser than ice. Heating liquid water continues to further deform hydrogen bonds and increase the density up to the density anomaly temperature. Further increase of temperature beyond the density anomaly weakens both H-bonds and van der Waals bonds, thus reducing the density, as in simpler liquids.

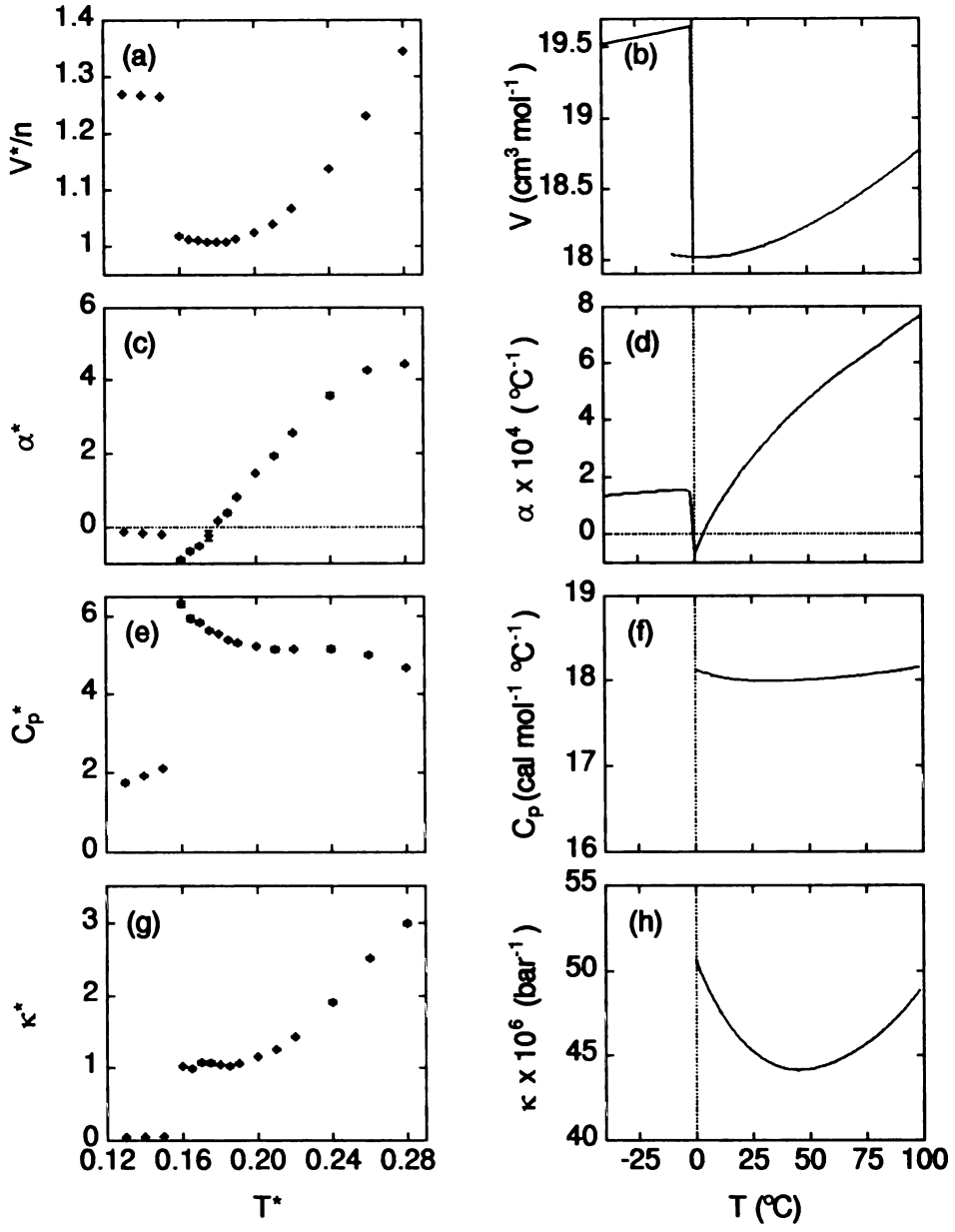

Figure 2.4: Comparison of various simulated temperature trends in pure MB water (a, c, e, and g) and experiment (b, d, f, and h). Experimental data is replotted from [29]: Molar volumes, (a) and (b); thermal expansion coefficient, (c) and (d); heat capacity (e) and (f); and isothermal compressibility, (g) and (h). Simulated quantities are in reduced units, as described in the text ($T^* = k_B T/\epsilon_{HB}$, $V^* = V/r_{HB}^2$, and pressure is defined so that $P^*V^* = PV/\epsilon_{HB}$). Error bars reported throughout this work are one standard deviation about the mean.

The compressibility correlates loosely with density. As the density increases, the molecules are better packed and the compressibility decreases. As bonds break (both hydrogen bonds and van der Waals interactions) with increasing temperature, the fluid density decreases and compressibility increases. Hence just as there is a maximum in the density, there is also a minimum in compressibility.

An alternative explanation of the density anomaly is due to Stillinger [63]. He explains the density anomaly in terms of the shift from ice-like six-membered H-bonded rings towards more strained H-bonded ring networks. Robinson and coworkers [22, 60] gave a related explanation: hydrogen-bond bending promotes the crowding of second- and more distant neighbors. These may all be different perspectives on the same physics. It may be that different diagnostics report consequences of the same shifted balance between H-bonds and van der Waals interactions.

Pure Water has a High Heat Capacity. Water has an unusually high heat capacity. MB water also has a high heat capacity, of approximately the correct magnitude ($\approx 12\,\mathrm{cal\ mol^{-1}{}^{\circ}C^{-1}}$ at its peak, for the configurational component). Moreover, the temperature dependence of the heat capacity of MB water is similar to that found experimentally (see Figure 2.4 (e)). MB water has a minimum in the isothermal compressibility vs. temperature, but it is not as pronounced as in experiments (see Figure 2.4 (g)).

What accounts for the heat capacity of pure water? Since the heat capacity is defined as $C_p = (\partial H/\partial T)_P$, the heat capacity describes the extent to which some kind of bonds are broken (increasing H) with increasing temperature. Breaking bonds is an energy storage mechanism. The heat capacity is low in the ice phase because

thermal energy at those temperatures is too small to disrupt the H-bonds. The heat capacity peaks at the melting temperature where the solid-like H-bonds of ice are weakened to become the liquid-like H-bonds of liquid water. The reason liquid water has a higher heat capacity than van der Waals liquids have is because water has an additional energy storage mechanism, namely the H-bonds, that can also be disrupted by thermal energies.

2.6 Results for a Single Solute Molecule in Water

The Thermal Anomalies of the Hydrophobic Effect are also Found in MB Water. To study the transfer of hydrophobic solutes into MB water, we performed separate MC simulations for the pure fluid and the fluid with a single fixed nonpolar LJ solute (with the same parameters as their water counterparts) under various external conditions. Thermodynamic quantities were obtained from the Widom test-particle method, as described earlier and in Appendix A. Structural distributions were obtained directly from the simulated dilute solutions.

We find that MB water as a solvent is much like real water in its thermal behavior. Figure 2.5 shows a comparison of the model thermodynamics to the corresponding experimental values for the transfer of gaseous argon into water. The experimental data was obtained from Crovetto *et al.* [23], using the Ben-Naim standard state [12], and from Biggerstaff and Wood [16]. The correct temperature trends of the free energy, enthalpy, and entropy of transfer are given by the model, as shown in Figure 2.5 (a) and (b). Hence the defining features of the hydrophobic effect are captured by

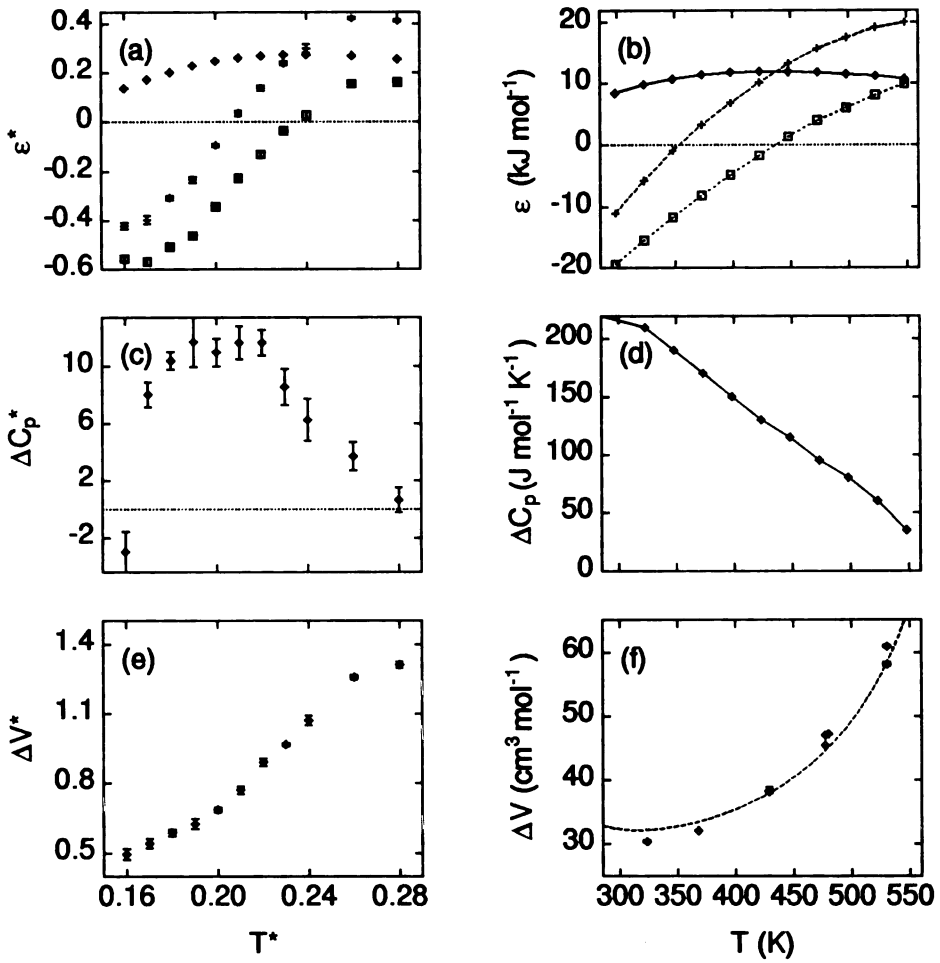

Figure 2.5: Temperature trends in the transfer thermodynamics of a simple LJ solute in MB water (a, c, e), as compared to the experimental transfer of gaseous Ar into water (b, d, f). (a) simulation data (this work) for ΔG_{tr} (diamonds), ΔH_{tr} (plus signs), and $T\Delta S_{tr}$ (squares) and for (b) experiments (originally reported in [23], and adjusted for the Ben-Naim standard state in [12]) for the same quantities. The large positive heat capacities of transfer are shown in (c) for this work and (d) from the same experimental source. Also shown are the apparent molar volumes of transfer for (e) simulations and (f) the experiments of Biggerstaff and Wood [16] (symbols) replotted along with the analytical infinite-dilution expression of Harvey, *et al.* [36] (line).

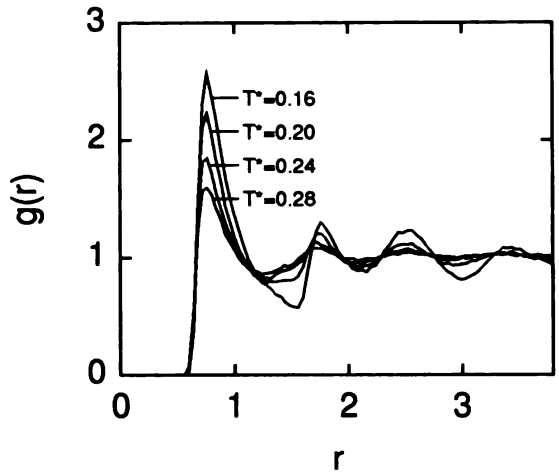

Figure 2.6: Solute-water pair correlation function at the four temperatures indicated in the figure.

the MB model: The large temperature dependence of the transfer enthalpy and entropy (and the curvature in the free energy) all indicate that the heat capacity is quite large. Indeed, we have calculated the heat capacity of transfer, shown in (c) alongside its experimental counterpart in (d), and it is large and positive, declining with increasing temperature. Finally, the molar volume of transfer is also plotted in Figure 2.5. It is interesting to note that, consistent with experiments, the slope of this curve is considerably steeper than that in Figure 2.4 (a) for pure water. That is, increasing temperature opens up more space around the solute than around water molecules.

The solute-water pair correlation function $g_{SW}(r)$ is shown in Figure 2.6. It flattens out with increasing temperature. However, it is unclear how much of this effect is actually induced by the solute *per se*, and how much is merely a reflection of the natural breakdown of bulk water structure with temperature.

To analyze the water behavior in the shells around the solute, we define the first and second shells of water molecules as those within the first and second minima of $g_{SW}(r)$ respectively. We analyze the angular distributions of water molecules in each shell. Figure 2.7 (a) shows that at low temperature, the water molecules "straddle" the solute, in order to avoid wasting hydrogen bonds, consistent with observations of other simulation models [33, 46]. We also observe that this angular order diminishes rapidly with temperature, particularly for those water molecules in the second shell (see Figure 2.7 (b)).

Now we consider the water-water relationship. The first and second neighbors of bulk and shell water molecules are defined as those molecules that are within the first and second minima of $g_{WW}(r)$, the water-water pair correlation function. At low temperature, $g_{WW}(r)$ for the first-shell water molecules is remarkably similar to that of bulk water, despite the excluded volume of the nearby solute (see Figure 6 in [61]). The significance of this observation was discussed by Hirata and Rossky [40], where references to several 3D studies making the same observation can also be found. We also find that the orientational ordering of water molecules surrounding the solute is *more* pronounced than that observed around bulk water molecules (see Figure 2.7 (c) and (d) in contrast to (a) and (b)). Furthermore, Figure 2.7 shows that the angular ordering around the solute is more temperature sensitive than around a bulk water molecule.

The Entropy Convergence Temperature, T_S, is the point at which Shell and Bulk Waters around a Solute Reverse Roles in Hydrogen Bonding.

As in real water, the MB model has a temperature T_S at which the entropy of

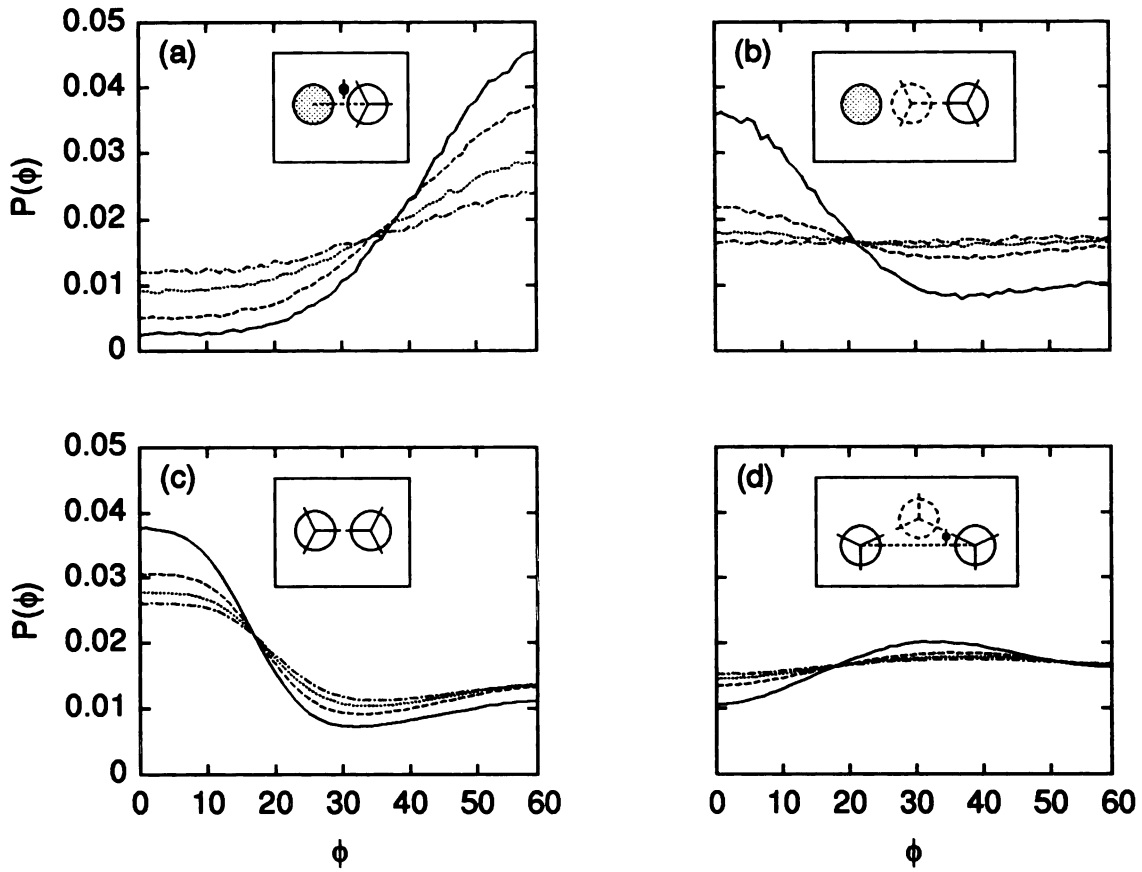

Figure 2.7: Angular distributions of (a) 1st shell and (b) 2nd shell water molecules about the solute, in comparison to the (c) 1st and (d) 2nd shell neighbors of bulk water molecules at four temperatures: $T^* = 0.16$ (solid), $T^* = 0.20$ (dashed), $T^* = 0.24$ (dotted), and $T^* = 0.28$ (dot-dashed). The most-probable orientations are shown in the insets. The angle ϕ, measured in degrees, is the angle that the closest arm of the neighboring (rightmost) water molecule makes with line connecting its center to the center of the reference (leftmost) molecule. $P(\phi)$ indicates the fraction of molecules observed in 1° bins about ϕ.

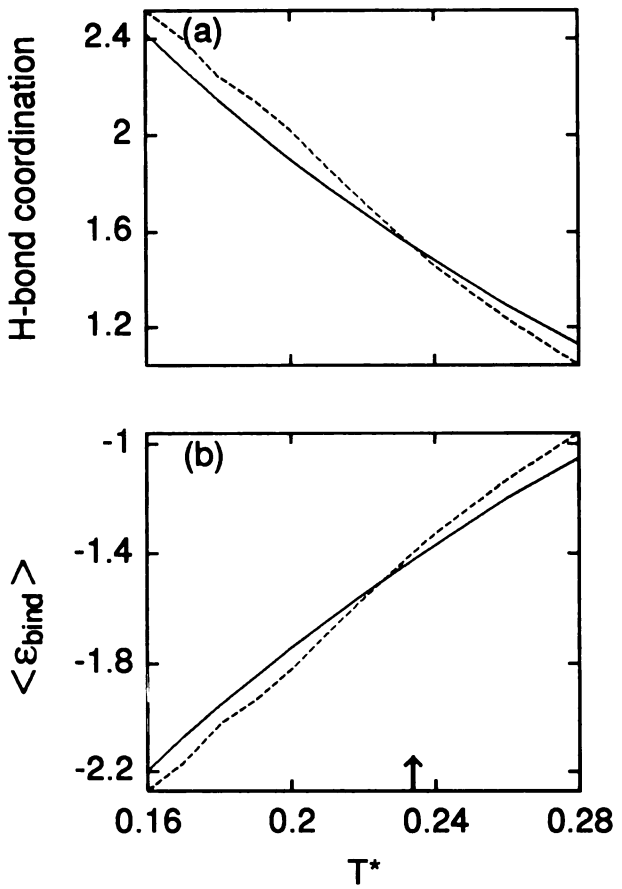

Figure 2.8: (a) Average hydrogen-bond coordination and (b) binding energy of shell (dashed) and bulk (solid) water molecules. The arrow indicates T_S in the model.

transfer of the nonpolar solute is zero [4, 50, 58], i.e. $T_S \Delta S_{tr} = 0$. What is the physical basis for T_S? In the MB model, this temperature delineates two different behaviors of shell water molecules around a solute. Below T_S, shell water molecules have more and tighter H-bonds than bulk water molecules have (see Figure 2.8). Above T_S, this behavior reverses: bulk water molecules have more and tighter H-bonds than shell water molecules have.

In Figure 2.8, hydrogen bond coordination around a given molecule was calculated

by summing all of its pairwise hydrogen bond interactions that are below an energetic cutoff. Several cutoffs (in the range from -0.5 to -0.25) were explored yielding the same crossing temperature and qualitative temperature trends. The binding energy is defined to be sum of the energetic interactions of a given water with all other water molecules in the simulation. (To be fair in making conclusions about relative structuring, the interaction with the solute is left out.) From either measure, it is clear that the shell molecules have more favorable energies and higher hydrogen bond coordination than bulk water molecules below T_S. Beyond this temperature, the roles reverse. The widths of both coordination number and binding energy distributions are tighter at all temperatures for shell molecules (not shown).

At all temperatures we studied, the water molecules directly surrounding shell molecules have more orientational order than those around bulk water molecules. Second-neighbor water molecules around shell-water molecules have only slight ordering up to T_S (Figure 7 in [61]).

Why should shell water molecules be more ordered and have better H-bond coordination than bulk water molecules? Matubayasi has proposed a geometric explanation [47]. He showed that a solute adjacent to two shell molecules occupies a region of space that is inconsistent with local solvent tetrahedrality (i.e. in reference to the angle a third solvent molecule might make with the pair). Thus, inserting the solute increases the probability of local tetrahedrality among the water molecules (since solvent molecules won't be in the occluded "mismatching" zone). Better tetrahedrality correlates with better hydrogen bonding arrangements. This explanation, invoking 3- and 4- body correlations, may be important, but it is insufficient to explain T_S

and the reversal of shell and bulk H-bonding we observe at higher temperatures. We believe such geometric arguments may be part of the explanation for hydrophobicity, but not all of it.

Inserting a Nonpolar Solute Also Inserts Local Free Volume. To study molar volumes of transfer and ideas of clathration, we use Voronoi polygons. A Voronoi polygon defines the region of space that is closer to a given molecule than to any other molecule in the system. Thus, the volume of the polygon is a direct measure of the local "space" attributable to each molecule. The number of edges in these polygons gives a geometric measure of coordination.

The distributions in Voronoi volumes and surfaces (actually perimeters in 2D) around the shell water molecules, bulk water molecules, and solute are shown in Figures 2.9 and 2.10, respectively. The average volume, surface and coordination are shown in Figure 2.11 as functions of temperature. The model shows that the molar volume of the solute increases with temperature. This increased volume is largely localized around the solute, consistent with the findings of Guillot and Guissani [34]. The average number of water neighbors around a solute increases with temperature, while the average number of water neighbors around a shell water molecule decreases with temperature. This information, taken together with the breadth of the distributions around the solute, suggest that well-ordered small collections of water molecules at low temperature are replaced by highly variable fluctuating larger structures at higher temperatures. The difference between shell and bulk local volumes remains fairly constant over the temperature range.

The Voronoi volumes and surfaces surrounding the solute give some indication of

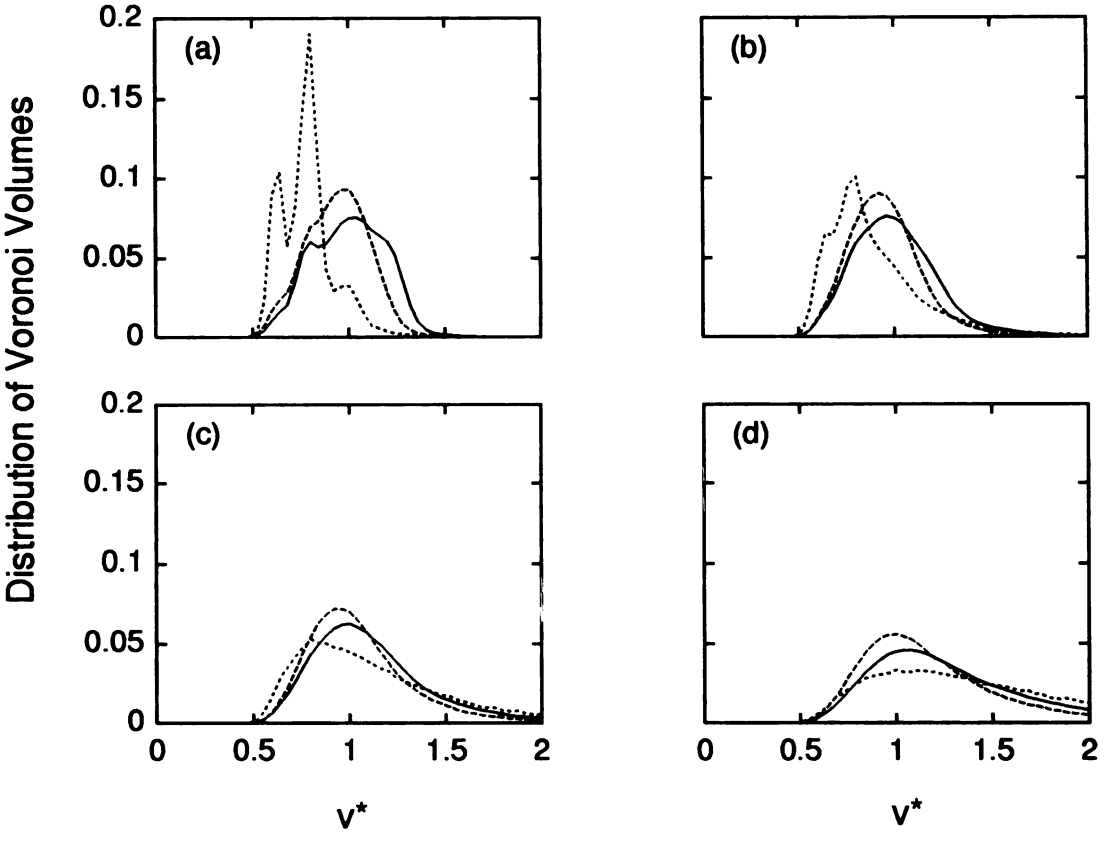

Figure 2.9: Voronoi volume distributions around bulk water molecules (solid), shell water molecules (dashed), and the solute (dotted) for (a) $T^* = 0.16$, (b) $T^* = 0.20$, (c) $T^* = 0.24$, and (d) $T^* = 0.28$. Here, v^* denotes the reduced volume ($v^* = v/r_{HB}^2$) of a Voronoi polygon, and the y-axis measures the relative distributions of Voronoi volumes using a binwidth of 0.04.

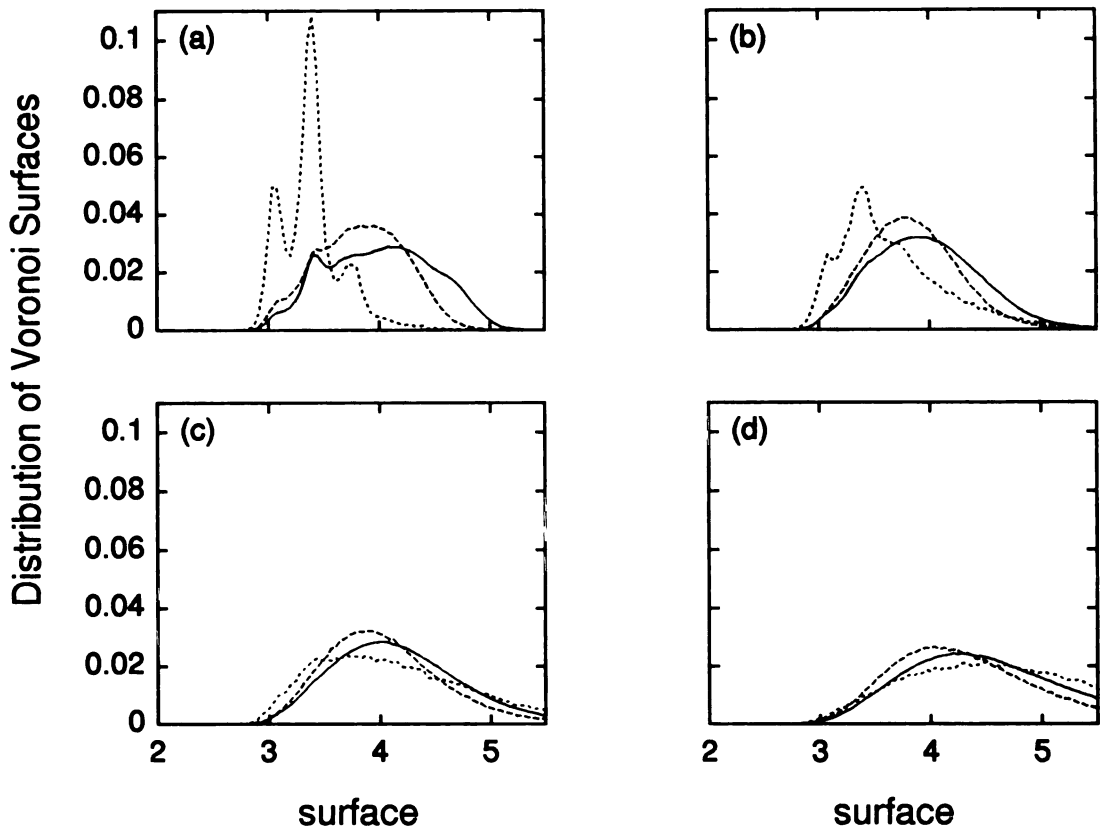

Figure 2.10: Voronoi surface (perimeter) distributions around bulk water molecules (solid), shell water molecules (dashed), and the solute (dotted) for (a) $T^* = 0.16$, (b) $T^* = 0.20$, (c) $T^* = 0.24$, and (d) $T^* = 0.28$. Voronoi surfaces are in units of r_{HB}, and the y-axis measures their relative distributions using a binwidth of 0.04.

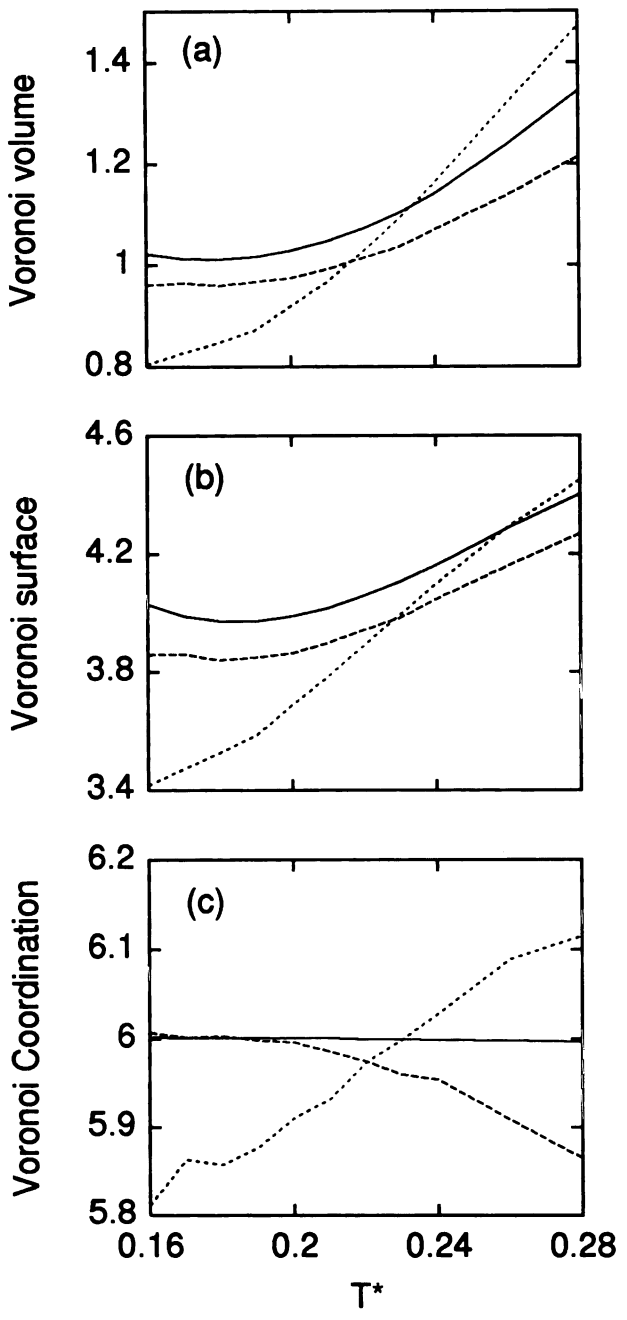

Figure 2.11: Average Voronoi (a) volume, (b) surface, and (c) coordination for bulk water molecules (solid), shell water molecules (dashed), and the solute (dotted).

Table 2.1: Computed Voronoi volumes and surfaces (perimeters) of idealized rings of water molecules surrounding a solute.

Ring size	Volume	Surface
5	0.657	3.09
6	0.866	3.46
7	1.12	3.88

clathrate-like populations. We calculated the volumes and surfaces for idealized 5-, 6-, and 7-membered rings of H-bonded water molecules around a solute (see Table 2.1). The three peaks in the Voronoi distribution curves at the lowest temperature coincide with these idealized values, indicating multiple modes of clathration around the solute, as has been found in 3D studies [1, 39]. These peaks weaken with temperature.

2.7 Conclusions

Our aim has been to model the thermodynamic properties of pure water and the hydrophobic effect. We use a simple two-dimensional model of water that describes a competition between Lennard Jones interactions that favor random dense states and hydrogen bonding that favors ordered open states. At low temperature, MB model water freezes to a low density crystal, like ice. The anomalous properties of the volume of water with temperature are reproduced: (1) that the liquid state is more dense, and (2) that there is a temperature of maximum density in the liquid range, also known as the density anomaly.

The MB model reproduces the thermal anomalies of nonpolar solvation, including a large free energy that opposes the insertion of oil into water, a large entropic component at low temperatures, and a large heat capacity. The MB model supports the classical picture of hydrophobic hydration, in which the orientations of shell water molecules that are restricted at low temperature become accessible upon heating, as summarized by Dill [27]. At low temperature, first-shell water molecules are ordered around small inert solutes and have strengthened hydrogen bonds relative to bulk water molecules. There are multiple interchanging modes of clathration. This excess ordering of the shell causes the transfer enthalpies and entropies to be negative. As temperature is increased, shell water structure melts out at a lower temperature than bulk water structure, consistent with the assumptions of the two-state model of Muller [50]. The MB model has a temperature T_S at which the transfer entropy changes sign. T_S coincides with the point where the hydrogen bonds in shell and bulk molecules reverse their relative strengths and numbers. Mancera and Buckingham [46] found similar changes in hydrogen bonding coordination as temperature is increased.

Finally, the steady increase in the molar volume of transfer with temperature is linked to an increase in the local volume surrounding the solute. This occurs as a relatively small number of ordered shell-water motifs give way to more-varied and larger fluctuating structural arrangements.

2.8 Acknowledgements

KATS greatfully acknowledges support under a U.S. National Science Foundation Graduate Research Fellowship and a UCSF Regent's Fellowship. In Australia, this research was supported by the Australian Research Council (ARC) (Grant No. A29530010), and SydCom, the USyd/UTS Distributed Computing Facility funded by an ARC infrastructure grant. In addition, we would like to thank Karen Tang for her continuous support to KATS and helpful suggestions; Mike Laskowski, for his enthusiasm in the early stages of the project; Thomas Beutler, for his advice and simulation tips; and David Agard, Robert Fletterick, Peter Kahn, Peter Kollman, I. D. Kuntz, Ron Siegel, and David Spellmeyer for helpful discussions on the model.

Bibliography

[1] G. Alagona and A. Tani. Structure of a dilute aqueous solution of argon. A Monte Carlo simulation. *J. Chem. Phys.*, 72(1):580–588, 1980.

[2] M. P. Allen and D. J. Tildesley. *Computer simulation of liquids.* Oxford University Press, Oxford, 1987.

[3] G. Andaloro and R. M. Sperandeo-Mineo. Monte carlo simulation of hydrophobic hydration for pedagogical purposes. *Eur. J. Phys.*, 11:275–282, 1990.

[4] R. L. Baldwin. Temperature dependence of the hydrophobic interaction in protein folding. *Proc. Natl. Acad. Sci. USA*, 83:8069–8072, 1986.

[5] G. M. Bell. Statistical mechanics of water: lattice model with directed bonding. *J. Phys. C.: Solid State Phys.*, 5:889–905, 1972.

[6] A. Ben-Naim. Simulation of hydrophobic interaction in a two-dimensional system. *Chem. Phys. Lett.*, 11:389–392, 1971.

[7] A. Ben-Naim. Statistical mechanics of 'waterlike' particles in two dimensions. I. Physical model and application of the Percus-Yevick equation. *J. Chem. Phys.*, 54(9):3682–3695, 1971.

[8] A. Ben-Naim. Statistical mechanics of water-like particles in two-dimensions. II. One component system. *Molecular Physics*, 24:705–721, 1972.

[9] A. Ben-Naim. Statistical mechanics of water-like particles in two-dimensions. III. Two component system, hydrophobic interaction. *Molecular Physics*, 24:723–733, 1972.

[10] A. Ben-Naim. Generalized molecular distribution functions. *J. Chem. Phys.*, 59(12):6535–6555, 1973.

[11] A. Ben-Naim. *Hydrophobic Interactions.* Plenum Press, New York, 1980.

[12] A. Ben-Naim. *Solvation Thermodynamics.* Plenum Press, New York, 1987.

[13] N. A. M. Besseling and J. Lyklema. Equilibrium properties of water and its liquid-vapor interface. *J. Phys. Chem.*, 98:11610–11622, 1994.

[14] N. A. M. Besseling and J. M. H. M. Scheutjens. Statistical thermodynamics of molecules with orientation-dependent interactions in homogeneous and inhomogeneous systems. *J. Phys. Chem.*, 98:11597–11609, 1994.

[15] T. C. Beutler, D. R. Béguelin, and W. F. van Gunsteren. Free energy of cavity formation in solvent: computational, methodological and physical aspects. *J. Chem. Phys.*, 102(9):3787–3793, 1995.

[16] D. R. Biggerstaff and R. H. Wood. Apparent molar volumes of aqueous argon, ethylene, and xenon from 300 to 716 K. *J. Phys. Chem.*, 92:1988–1994, 1988.

[17] W. Blokzijl and J. B. F. N. Engberts. Hydrophobic effects. opinions and facts. *Angew. Chem. Int. Ed. Engl.*, 32:1545–1579, 1993.

[18] L. Blum and L. Degreve. Monte Carlo study of an octupolar potential for water. *Molecular Physics*, 88:585–590, 1996.

[19] L. Blum and F. Vericat. Solution of the Ornstein-Zernike equation for spheres with octupolar surface adhesion - toward a simple model of water. *J. Phys. Chem.*, 100:1197–1205, 1996.

[20] L. Blum, F. Vericat, and D. Bratko. Towards and analytical model of water: the octupolar model. *J. Chem. Phys.*, 102:1461–1462, 1995.

[21] S. S. Borick, P. G. Debenedetti, and S. Sastry. A lattice model of network-forming fluids with orientation-dependent bonding: Equilibrium, stability, and implications for the phase behavior of supercooled water. *J. Phys. Chem.*, pages 3781–3792, 1995.

[22] C. H. Cho, Singh, and G. W. Robinson. An explanation of the density maximum in water. *Phys. Rev. Lett.*, 76:1651–1654, 1996.

[23] R. Crovetto, R. Fernández Prini, and M. L. Japas. Solubilities of inert gases and methane in H_2O and in D_2O in the temperature range of 300 to 600 K. *J. Chem. Phys.*, 76(2):1077–1086, 1982.

[24] L. W. Dahl and H. C. Andersen. Cluster expansions for hydrogen-bonded fluids. III. Water. *J. Chem. Phys.*, 78(4):1962–1979, 1983.

[25] L. W. Dahl and H. C. Andersen. A theory of the anomalous thermodynamic properties of liquid water. *J. Chem. Phys.*, 78(4):1980–1993, 1983.

[26] L. Degrève and L. Blum. Analytic potential for water: a Monte Carlo study. *Physica A*, 224:550–557, 1996.

[27] K. A. Dill. Dominant forces in protein folding. *Biochemistry*, 29:7133–7155, 1990.

[28] R. L. Dunbrack, K. A. Silverstein, K. A. Dill, and A. D. J. Haymet. Lattice model of water: comparison of the quasi-chemical approximation with exact Monte Carlo simulation. unpublished data, 1995.

[29] D. Eisenberg and W. Kauzmann. *The structure and properties of water.* Oxford University Press, Oxford, 1969.

[30] H. S. Frank and M. W. Evans. *J. Chem. Phys.*, 13:507, 1945.

[31] F. Franks, editor. *Water, a Comprehensive Treatise*, volume 1-7. Plenum Press, New York, 1972-1982.

[32] S. Garde, G. Hummer, A. E. García, M. E. Paulaitis, and L. R. Pratt. Origin of entropy convergence in hydrophobic hydration and protein folding. *Phys. Rev. Lett.*, 77:4966–4968, 1996.

[33] A. Geiger, A. Rahman, and F. H. Stillinger. Molecular dynamics study of the hydration of Lennard-Jones solutes. *J. Chem. Phys.*, 70(1):263–276, 1979.

[34] B. Guillot and Y. Guissani. A computer simulation study of the temperature dependence of the hydrophobic hydration. *J. Chem. Phys.*, 99(10):8075–8094, 1993.

[35] B. Guillot, Y. Guissani, and S. Bratos. A computer-simulation study of hydrophobic hydration of rare gases and of methane. I. Thermodynamic and structural properties. *J. Chem. Phys.*, 95(5):3643–3648, 1991.

[36] A. H. Harvey, J. M. H. L. Sengers, and J. C. Tanger IV. Unified description of infinite-dilution thermodynamic properties for aqueous solutes. *J. Phys. Chem.*, 95:932–937, 1991.

[37] A. D. J. Haymet, K. A. T. Silverstein, and K. A. Dill. Hydrophobicity reinterpreted as "minimization of the entropy penalty of solvation". *Faraday Discuss.*, 103:117–124, 1996.

[38] A. D. J. Haymet, K. A. T. Silverstein, and K. A. Dill. Hydrophobicity. In *International Symposium on Molecular Thermodynamics and Molecular Simulation*, pages 143–152, Tokyo, Japan, Jan 12-15 1997. Hosei University.

[39] T. Head-Gordon. Is water structure around hydrophobic groups clathrate-like? *Proc. Natl. Acad. Sci USA*, 92:8308–8312, August 1995.

[40] F. Hirata and P. J. Rossky. On the interpretation of solute induced solvent structure. *J. Chem. Phys.*, 74(9):5324–5326, 1981.

[41] W. L. Jorgensen. Convergence of Monte Carlo simulations of liquid water in the NPT ensemble. *Chem. Phys. Lett.*, 92(4):405–410, 1982.

[42] Y. Kataoka, H. Hamada, S. Nosé, and T. Yamamoto. Studies of liquid water by computer simulations. II. Static properties of a 3D model. *J. Chem. Phys.*, 77(11):5699–5709, 1982.

[43] J. Kolafa and I. Nezbeda. Monte Carlo simulations on primitive models of water and methanol. *Mol. Phys.*, 61(1):161–175, 1987.

[44] B. Lee. The physical origin of the low solubility of nonpolar solutes in water. *Biopolymers*, 24:813–823, 1985.

[45] B. Lee. Solvent reogranization contribution to the transfer thermodynamics of small nonpolar molecules. *Biopolymers*, 31(8):993–1008, 1991.

[46] R. L. Mancera and A. D. Buckingham. Temperature effects on the hydrophobic hydration of ethane. *J. Phys. Chem.*, 99:14632–14640, 1995.

[47] N. Matubayasi. Matching-mismatching of water geometry and hydrophobic hydration. *J. Am. Chem. Soc.*, 116:1450–1456, 1994.

[48] N. Matubayasi and R. M. Levy. Thermodynamics of the hydration shell. 2. Excess volume and compressibility of a hydrophobic solute. *J. Phys. Chem.*, 100:2681–2688, 1996.

[49] N. Matubayasi, L. H. Reed, and R. M. Levy. Thermodynamics of the hydration shell. 1. Excess energy of a hydrophobic solute. *J. Phys. Chem.*, 98:10640–10649, 1994.

[50] N. Muller. Search for a realistic view of hydrophobic effects. *Acc. Chem. Res.*, 23:23–28, 1990.

[51] I. Nezbeda and G. A. Iglesias-Silva. Primitive model of water III. Analytic theoretical results with anomalies for the thermodynamic properties. *Molecular Physics*, 69(4):767–774, 1990.

[52] I. Nezbeda, J. Kolafa, J. Pavlíček, and W. R. Smith. Molecular theory of phase equilibria in model and real associated mixtures. II. Binary aqueous mixtures of inert gases and n-alkanes. *J. Chem. Phys.*, 102(24):9638–9646, 1995.

[53] I. Nezbeda and J. Slovák. A family of primitive models of water: three-, four and five-site models. *Mol. Phys.*, 90(3):353–372, 1997.

[54] I. Nezbeda, W. R. Smith, and J. Kolafa. Molecular theory of phase equilibria in model and real associated mixtures. I. Binary mixtures of water and a simple fluid. *J. Chem. Phys.*, 100:2191–2201, 1994.

[55] K. Okazaki, S. Nosé, Y. Kataoka, and T. Yamamoto. Study of liquid water by computer simulations. I. Static properties of a 2D model. *J. Chem. Phys.*, 75(12):5864–5874, 1981.

[56] A. Pohorille and L. R. Pratt. Cavities in molecular liquids and the theory of hydrophobic solubilities. *J. Am. Chem. Soc.*, 112:5066–5074, 1990.

[57] L. R. Pratt and A. Pohorille. Theory of hydrophobicity: Transient cavities in molecular liquids. *Proc. Natl. Acad. Sci. USA*, 89:2995–2999, April 1992.

[58] P. L. Privalov and S. J. Gill. Stability of protein structure and hydrophobic interaction. *Advances in Protein Chemistry*, 39:191–234, 1988.

[59] C. J. Roberts and P. G. Debenedetti. Polyamorphism and density anomalies in network-forming fluids: zeroth- and first-order approximations. *J. Chem. Phys.*, 105:658–672, 1996.

[60] G. Robinson, S.-B. Zhu, S. Singh, and M. Evans. *Water in Biology, Chemistry and Physics: Experimental Overviews and Computational Methodologies.* World Scientific, Singapore, 1996.

[61] K. A. T. Silverstein, K. A. Dill, and A. D. J. Haymet. Hydrophobicity in a simple model of water: solvation and hydrogen bond energies. In *Thirteenth Symposium on Thermophysical properties*, Boulder, Colorado, June 22-27 1997. National Institute of Standards and Technology.

[62] D. E. Smith and A. D. J. Haymet. Free energy, entropy, and internal energy of hydrophobic interactions: computer simulations. *J. Chem. Phys.*, 98(8):6445–6454, 1993.

[63] F. H. Stillinger. Water revisited. *Science*, 209:451–457, 1980.

[64] F. H. Stillinger and A. Rahman. Molecular dynamics study of temperature effects on water structure and kinetics. *J. Chem. Phys.*, 57(3):1281–1292, 1972.

[65] F. H. Stillinger and A. Rahman. Improved simulation of liquid water by molecular dynamics. *J. Chem. Phys.*, 60(4):1545–1557, 1974.

[66] C. Tanford. *The Hydrophobic Effect: formation of micelles and biological membranes, 2nd Ed.* Wiley, New York, 1980.

[67] B. Widom. Some topics in the theory of fluids. *J. Chem. Phys.*, 39(11):2808–2812, 1963.

[68] S.-B. Zhu, S. Singh, and G. W. Robinson. Field-perturbed water. *Adv. Chem. Phys.*, 85(3):627–731, 1994.

Chapter 3

A Two-state Model of Hydrophobicity: Microscopic Connection to the MB model

Kevin A. T. Silverstein, A. D. J. Haymet, and Ken A. Dill

3.1 Abstract

Oil and water don't mix. Why not? Thermodynamic experiments characterize this disaffinity, but not the molecular mechanism. Few all-atom simulations yet have the capacity to explore the main fingerprint of hydrophobicity, the large positive heat capacity of insertion of a nonpolar solute into water. Muller has devised a simple double-two-state model to explain hydrophobic solvation, but it involves several parameters that are not yet derivable from traditional structural models of water. Here we use a statistical mechanical model of water, the MB model, to give physical meaning to the quantities in the Muller model. We find that inserting a nonpolar solute into water strengthens hydrogen bonding in the first solvation shell by making the poorer, higher-energetic hydrogen bonds thermally less accessible than good ones. H-bonds in the solute shell are "more broken" than H-bonds in the bulk. We find that hydrophobic solvation enthalpies and entropies are not accurately approximated by pair interactions, or triplets, or even first-shell polyhedra: solvation appears to be more subtle than properties of pure water. We suggest a recipe for interpreting spectroscopic experiments to bring them into consistency with thermodynamics for determining the fraction of hydrogen bonds that are made or broken as a function of temperature.

3.2 Introduction

The hydrophobic effect is poorly understood. Hydrophobic solvation refers to the anomalous thermodynamics: a large positive free energy of transfer of nonpolar so-

lutes into water, dominated by a large negative entropy around room temperature, and large positive heat capacity. For understanding the physics, the heat capacity is the most fundamental of these properties, because the others can be derived from it. Considerable insight into the nature of hydrophobicity comes from simulations[1] [8, 11, 29, 32, 33], integral equation theory [20, 41, 42, 52] and scaled-particle theory [23, 40], NMR experiments [19, 34, 36, 47] and neutron diffraction [51]. But such studies have not yet shed much light on the key quantity, the heat capacity. The closest attempt to achieve this goal is the recent work by Madan and Sharp [28, 48], who used the Random Network Model [18, 44, 45, 46] to calculate heat capacities, and separate simulations to obtain structural detail. However, what is needed is an approach which yields *both* microscopic structural data *and* macroscopic heat capacity measurements *from the same model.*

What is the physical basis for the large positive heat capacity? If, in addition, we also knew the physical basis for the temperatures, T_H and T_S where the enthalpy and entropy of transfer equal zero [2, 35, 43], we would then understand the full thermodynamics of the hydrophobic solvation. This is because the thermodynamics can be expressed as

$$\begin{aligned} \Delta G(T) &= \Delta H - T\Delta S \qquad (3.1) \\ &= \Delta H(T_H) - T\Delta S(T_S) + \int_{T_H}^{T} \Delta C_p dT + \int_{T_S}^{T} \Delta C_p/T dT\,, \end{aligned}$$

where T is the absolute temperature.

We develop here a model of the hydrophobic effect. Until now, there have been

[1] For work in this area prior to 1993, see reviews [4] and [61], and references therein.

two main classes of models, but each has its problems. First, all-atom simulations have been an important source of insight into water properties. But due to limitations of current computational power, it has been notoriously difficult to achieve numerical convergence for properties as subtle as the heat capacity. Second, there have been thermodynamic models, such as "mixture models", which assume that water has discrete states, with hydrogen bonds that are either made or broken, for example [6]. These too have provided very useful insights, but such models [6, 35, 37] have many adjustable parameters, so their physical bases are not always clear.

Here we take a third approach. We use a model of water for which the statistical mechanics can be explored completely, and which has been shown to have the interesting and anomalous properties of water [50], but is simple enough that we can obtain complete convergence on subtle properties, including the heat capacity. We use the model to obtain the parameters for one of the most useful of the thermodynamic models, due to Muller [35], to provide a microscopic interpretation for the anomalous thermodynamics of nonpolar solvation. We also derive from the model a recipe for interpreting experiments to give the fraction of water molecules that are hydrogen bonded in the bulk, and in the first neighbor shell around the solute.

3.3 The Model of Water and Nonpolar Solvation

We model water using the MB model [50], so-named because of the resemblance of each model water molecule to the Mercedes-Benz logo. Waters are 2-dimensional Lennard-Jones disks with 3 hydrogen bonding arms that can align with arms of neigh-

boring water molecules. Constant-pressure Monte Carlo sampling has shown that this model predicts the volumetric anomalies of water and the temperature dependence of transfer of nonpolar solutes. Hence the balance of hydrogen bonding and Lennard-Jones interactions in the MB model are sufficient to capture the thermodynamics of the hydrophobic effect.

Our aim here is to derive the parameters for the Muller double-two-state model [35] from our MB model simulations, hence providing a physical basis for interpreting the large heat capacity of solvation. Muller's model focuses on the hydrogen bonds among water molecules. They occur in four possible states: hydrogen bonds that are intact in bulk water (BI), hydrogen bonds that are broken in bulk water (BB), hydrogen bonds that are intact in the first-neighbor shell of a nonpolar solute (SI), and hydrogen bonds that are broken in the first-neighbor shell around the solute (SB). Muller treats the transfer of a solute into water as a process in which n hydrogens that participated in hydrogen bonds in the bulk now become a part of the hydration shell of the solute. The resulting heat capacity change is:

$$\Delta C_p = n \left[C_{p,s} - C_{p,b} \right] . \tag{3.2}$$

In Muller's model, the hydrogen bond breakage for either bulk or shell waters can be described as a two-state equilibrium

$$\text{H-bond}(\textit{intact}) \Rightarrow \text{H-bond}(\textit{broken}) , \tag{3.3}$$

with equilibrium constant, K_b:

$$K_b = f_b/(1 - f_b) = \exp(-\Delta H_b^\circ/kT + \Delta S_b^\circ/k) , \tag{3.4}$$

where f_b is the fraction of bonds broken, and the subscript b indicates the bulk phase (to distinguish it from the hydration shell). The two states have a free energy difference $\Delta G_b^\circ \equiv \Delta H_b^\circ - T\Delta S_b^\circ$, where ΔH_b° is the enthalpy of breaking a hydrogen bond in bulk water, and $\exp(\Delta S_b^\circ/k)$ is the change in the degeneracy, i.e., the number of configurations that have a broken bond, relative to the intact form. The constants k and T are the Boltzmann constant and absolute temperature, respectively. In the Muller model, ΔH_b° and ΔS_b° are *assumed* to be independent of temperature. Hence, bond breaking contributes to the heat capacity $\Delta C_{p,b}$, in the classical two-state fashion [10]:

$$\Delta C_{p,b} = (\Delta H_b^\circ)^2 f_b(1 - f_b)/kT^2 \,. \tag{3.5}$$

A similar hydrogen-bond-breaking equilibrium applies to waters in the hydration shell of the solute:

$$K_s = f_s/(1 - f_s) = \exp(-\Delta H_s^\circ/kT + \Delta S_s^\circ/k) \tag{3.6}$$

and

$$\Delta C_{p,s} = (\Delta H_s^\circ)^2 f_s(1 - f_s)/kT^2 \,. \tag{3.7}$$

In addition to its effect on the heat capacity change, the transfer of the nonpolar solute into water will also change the enthalpy and entropy. Muller's original model assumed, for simplicity, that the "upper" (broken) state is identical in the bulk and in the hydration shell. But there is little reason to believe these states should be the same. Lee and Graziano [25] have generalized the Muller model by assigning two additional parameters, ΔH_U and ΔS_U, to reflect the offsets in the enthalpy and entropy of the two upper levels. With these definitions, the contribution that the

reorganizations of hydrogen bonds make to the enthalpy and entropy of transfer are, respectively,

$$\Delta H_r = n\left[\Delta H_U - (1 - f_s)\Delta H_s^\circ + (1 - f_b)\Delta H_b^\circ\right] \tag{3.8}$$

and

$$\Delta S_r = n\left[\Delta S_U - (1 - f_s)\Delta S_s^\circ + (1 - f_b)\Delta S_b^\circ - k\Delta F\right] , \tag{3.9}$$

where $\Delta F \equiv F_s - F_b$ is the mixing entropy with F_b defined as

$$F_b = f_b \ln f_b + (1 - f_b)\ln(1 - f_b) \tag{3.10}$$

and F_s is defined similarly in terms of f_s.

The generalized Muller model has a total of seven independent parameters (n, ΔH_b°, ΔS_b°, ΔH_s°, and ΔS_s° determine the transfer heat capacity change; and the remaining two ΔH_U and ΔS_U complete the determination of the transfer enthalpy and entropy, respectively). The first one, n, the number of waters in the hydration shell, can be estimated on geometric grounds based on the surface area of the solute [43]. In the past [25, 35], the quantities ΔH_b° and ΔS_b° have been estimated using the difference in heat capacity between steam and liquid water, and the estimate of Pauling [39] for f_b at 0 $^\circ C$. Since the values for $C_{p,s}$ and f_s are unknown, the remaining parameters in the original model, ΔH_s° and ΔS_s°, have previously been estimated using a best fit to the hydration enthalpy, entropy, and heat capacities of nonpolar transfer. Lee and Graziano introduced ΔH_U and ΔS_U (which were assumed to be zero in Muller's treatment) to show that relatively small values for each could support their view of enthalpy-entropy compensation [21, 23, 24, 27]. Hence, the main limitation of this model is the many parameters that are freely adjustable. Lee

and Graziano have noted that [25] "Many different models can be made to reproduce the observed thermodynamic properties by only a small adjustment of the model parameters because of the built-in amplification by the size of the hydration shell."

The overabundance of free parameters can be circumvented if the hydrogen bonded fraction of bulk and shell waters were known as a function of temperature. The MB model gives such information [50]. So the MB model can both test the two-state assumption and produce a consistent set of parameters for the Muller model. Least-squares fitting of the Monte Carlo simulations of the MB model to Eq. 3.4 separately for the bulk and hydration shell yields the energy gaps and relative degeneracies directly. If the two-state approximation is adequate, then these four parameters should be sufficient to fit the hydrogen-bond-breaking contribution to the heat capacity change. The enthalpy offset could then be determined from a direct fit to the reorganizational contribution to the total hydration enthalpy [12, 21]. The reorganizational contribution is defined to be the portion of the transfer enthalpy which is due to the change in water structure induced by the solute (i.e., the direct attraction of the solute for the solvent molecules must be subtracted from the full transfer enthalpy) :

$$\Delta H_r = \Delta H_{tr} - E_a \,. \tag{3.11}$$

Here, ΔH_{tr} is the total enthalpy of transfer, E_a is the solute-solvent interaction energy, and, ΔH_r corresponds to the enthalpy change predicted by the double-2-state model. The one remaining parameter, ΔS_U, determines the degeneracies of the bulk states relative to the shell states. Since the entropy is not formally separable [60] into

reorganizational and direct contributions, a fit to the transfer entropy yields a value for this parameter that may only be approximate. This is because the Muller model only includes information about the reorganizations of hydrogen bonds, and the actual counting of configurations may be affected by the direct solute-water interaction.

3.4 Exhaustive Grid Enumerations of Few-Body Systems

What is the minimal number of water molecules needed to understand the essential physics of hydrophobic solvation? Hydrophobic solvation has been modeled by pair interactions. Or sometimes hydrophobic solvation is regarded as a property of "tetrahedrality" of water, implying the importance of 3-body or 4-body arrangements of waters [31]. And sometimes hydrophobicity is considered to result from polyhedral clathrate cages [1, 16], implying 6-body or 7-body effects might be important. Such polyhedra are also found in the MB model [50].

Our aim in this section is to perform few-body exhaustive grid enumerations to find out how many water molecules in the MB model adequately predict the MB Monte Carlo results. We enumerate all relative orientations and separations of two model water molecules on a grid. We then systematically add additional waters one-at-a-time and enumerate their contributions to the partition function by similar exhaustive grid enumeration.

To do this, we fix a first MB water molecule in space. A second water molecule

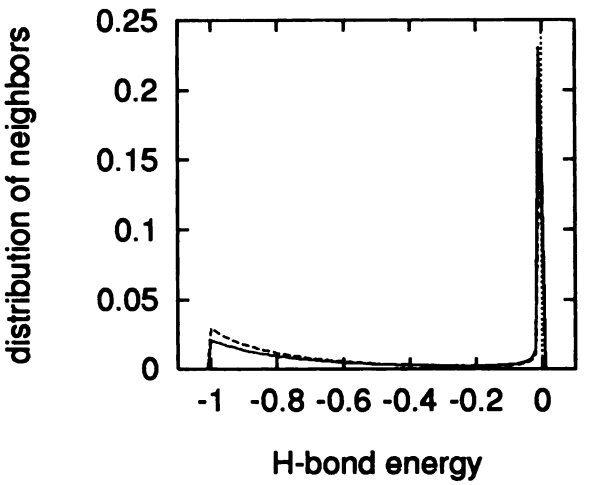

Figure 3.1: Distribution of the hydrogen bond energies (in units of $|\epsilon_{HB}|$) of neighboring water molecules in the bulk (solid) and shell (dashed) is bimodal for the MB model at all temperatures studied. The temperature shown ($T^* = 0.18$) is below T_S.

is added to the system and moved in fixed increments in the xy coordinate system. Water number two is constrained to be within a neighbor distance from the first (i.e., within the first minimum of the water-water pair correlation function, $g_{WW}(r)$, as determined from previous full Monte Carlo simulations). At each relative position, the angles of each molecule are sampled in fixed increments (the grid size is made small enough so that subsequent reductions cause no changes in the relative distributions obtained) from 0° to 120° (this upper limit is dictated by the molecular symmetry).

Our Monte Carlo simulations of the MB model show that water configurations fall into two distinct classes, which can reasonably be defined as having intact or broken hydrogen bonds. Figure 3.1 shows the distribution of energies for water neighbors in

the shell and the bulk. This distribution is clearly bimodal, indicating that the two-state approximation is valid, and that it is meaningful in the MB model to refer to "intact" and "broken" bonds, even though the hydrogen-bond energy function for the MB model is continuous and unimodal. The minimum in this bimodal function is very broad, so there is little sensitivity to how we choose the cutoff that delineates intact from broken bonds. We explored several cutoffs from 0.5 to 0.25, each yielding similar results for the Muller model parameters, and show results for a cutoff of 0.33. To be consistent, we chose the same cutoff for the grid enumeration as for the Monte Carlo simulations. For comparison with the double-two-state model, we bin the total energy of a configuration into two classes (one entry for each pair of water neighbors). Each distribution, for "intact" or "broken" H-bonded waters, is then Boltzmann-weighted to yield the average energy and entropy. For example, the average values for the distribution corresponding to the bulk-intact (BI) state are:

$$< E_{BI} > = \sum_{\epsilon} \epsilon\, \Omega(\epsilon) \exp[-\epsilon/kT] / \sum_{\epsilon} \Omega(\epsilon) \exp[-\epsilon/kT] \tag{3.12}$$

$$< S_{BI}/k > = < E_{BI} > /kT + \ln(\sum_{\epsilon} \Omega(\epsilon) \exp[-\epsilon/kT]) \,, \tag{3.13}$$

where the sums are performed over the energy bins or levels, ϵ, and $\Omega(\epsilon)$ is the density of states obtained from the enumeration. Similar calculations are performed for states BB, SI, and SB. Taking differences of these quantities gives the parameters relevant for the Muller model:

$$\begin{aligned} \Delta E_b(T) &= < E_{BB} > - < E_{BI} > \\ \Delta E_s(T) &= < E_{SB} > - < E_{SI} > \\ \Delta S_b/k(T) &= < S_{BB}/k > - < S_{BI}/k > \end{aligned} \tag{3.14}$$

$$\Delta S_s/k(T) \;=\; < S_{SB}/k > - < S_{SI}/k > \;. \qquad (3.15)$$

corresponding to the ΔH_b° and ΔS_b° (or ΔH_s° and ΔS_s° for the shell) of the Muller model, Whereas the Muller model assumes that these quantities don't depend on temperature, they do in the MB model, but only weakly.

We follow the same general procedure when additional water molecules are included in the enumeration. When a solute is present, the fixed reference water is always within its hydration shell (i.e., the solute and fixed water are separated by a distance within the first minimum in the solute-water pair correlation function, $g_{SW}(r)$). Each water molecule that is added to the system must be a neighbor of an existing water, so the system remains contiguous (i.e., if water molecules are the nodes of a graph, and if edges indicate joined neighbors, the graph is connected).

In practice, the exhaustive-grid enumeration scheme described above could only be carried out with at most 4 molecules. Hence Boltzmann-weighted sampling (i.e., Metropolis Monte Carlo) was performed as well on systems of 2-12 water molecules (with and without a solute), without periodic boundary conditions, but with the same connectivity requirements around a fixed reference water as above.

In order to attempt to use the MB model to determine the physical basis of the remaining two parameters, ΔH_U and ΔS_U, of the Muller model, we use two methods. The first is purely geometric. We simply take each of the pure-water configurations obtained in the enumerations described above, and determine what percentage of the volume would be occluded by the systematic placement of a solute in fixed-space increments. By its nature, this geometric approximation predicts that broken

and intact states are occluded with equal frequency. In the second, more rigorous approach, we performed the equivalent of the Widom test-particle method [58] to obtain energy distributions for the intact and broken bonds in the hydration shell, while sampling only pure water configurations. This method allows us to compare the bulk and shell distributions on the *same relative scale.* In practice, this is achieved by randomly placing a ghost-solute particle in the shell of the reference water, and calculating the solute's hypothetical interaction, $\mathcal{E}$, with the system. Each of the neighboring water molecules of the hypothetical solute may be participating in some broken and intact hydrogen bonds with other water molecules also in the hydration shell. If we define some quantity m_{BI} to represent the number of intact H-bonds among the bulk-water configurations that are in the shell of an arbitrarily-placed ghost solute:

$$m_{BI} = \#\text{ intact H-bonds in pure sample}\,,$$

then the reweighted ratio of intact H-bonds in the shell would be:

$$m_{SI} = \frac{\langle m_{BI} \exp(-\beta\mathcal{E})\rangle_N}{\langle \exp(-\beta\mathcal{E})\rangle_N}\,, \tag{3.16}$$

where the ensemble averages are computed over the N-water system. For each system configuration recorded, an increment of m_{BI} is made for the bulk-intact energy bin that corresponds to the total system energy. The distribution obtained in this manner will reflect the likelihood of having a bulk-intact bond present with a given total system energy. A corresponding increment of m_{SI} is added to the (total-system-energy + $\mathcal{E}$) bin for the shell. The proper Boltzmann-reweighting of Eq. 3.16 ensures that this SI distribution is on the same relative scale as the BI distribution. Analogous

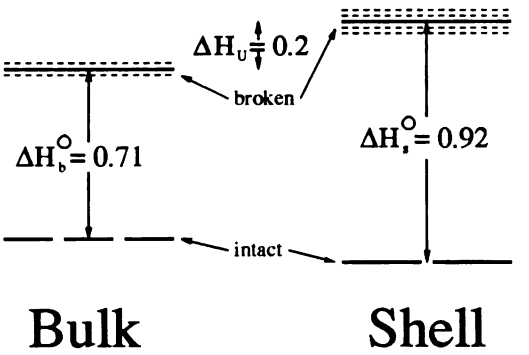

Figure 3.2: Schematic diagram of the two-state model which best fits the simulation data. Enthalpy gaps are normalized by the strength of the hydrogen-bond (i.e., ΔH_b°, ΔH_s°, and ΔH_U are all in units of $|\epsilon_{HB}|$).

definitions relate BB and SB. As a check, we determined that the shell distributions obtained this way are indeed the same as those obtained directly with the solute-water system sampling (apart from an arbitrary multiplicative constant that is dependent on the simulation time).

3.5 Results

3.5.1 Parameters for the Muller Model

Figure 3.2 shows an energy diagram for the best Muller parameters derived from the MB simulations. We find that hydrogen bonds in the solvation shell are stronger than hydrogen bonds in the bulk, a result that has also been observed in all-atom

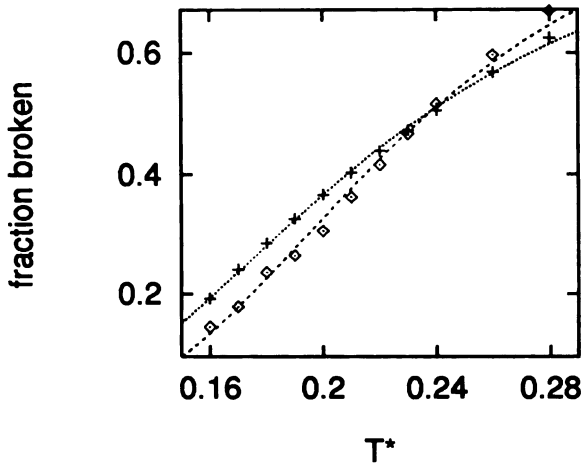

Figure 3.3: Fraction of broken hydrogen bonds in the hydration shell ($\diamond$), and bulk (+). The least-squares fit to a separate two-state formalism for each is shown. Parameters for these fits are in the text.

simulations [9, 38]. Here, this arises because the solute effectively increases the energy gap between intact and broken H-bonded states, making poorer H-bonded configurations thermally less-accessible than good H-bonds. Moreover, a broken H-bond in the solvation shell is "more broken" than a broken H-bond in bulk water.

The temperature dependence of f_b and f_s are shown in Figure 3.3, along with the least-squares fit to the two-state model. The fit yields the following four parameter values: $\Delta H_b^\circ = 0.71$, $\Delta S_b^\circ/k = 2.99$, $\Delta H_s^\circ = 0.92$, and $\Delta S_s^\circ/k = 3.88$. The errors in fitting are quite small, due to the excellent convergence of the simulations.

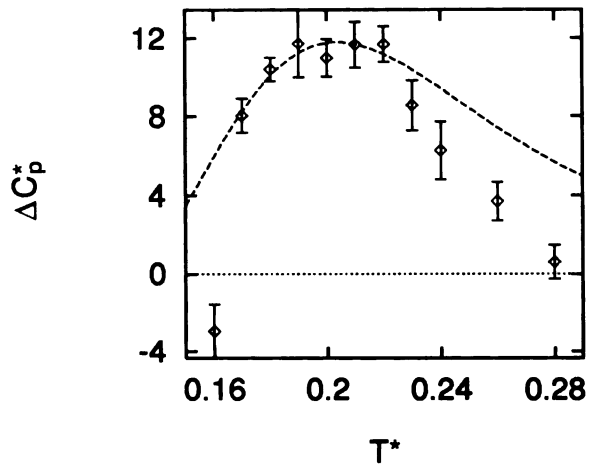

Figure 3.4: The heat capacity as a function of temperature. Along with the simulation points ($\diamond$), the theoretical two-state prediction is shown (dotted line). Only the four parameters directly obtained from the hydrogen-bond fractions are used for the water-reorganization contribution to the heat capacity. The mild contribution from the solute-water interaction $\frac{\partial E_a}{\partial T^*} = 1.23$ has been added.

3.5.2 The Muller Double-2-State Model Predicts Well the Monte Carlo Simulations

We now test whether the simple Muller model, with its assumption of only four states, adequately captures the essence of the hydrophobic heat capacity in our continuum-energy model. In specific, we now determine whether the four parameters obtained from fitting to our Monte Carlo simulations are sufficient to give back the configurational contribution to the transfer heat capacity change. Figure 3.4 shows that the double-2-state model works extremely well. This is particularly remarkable since

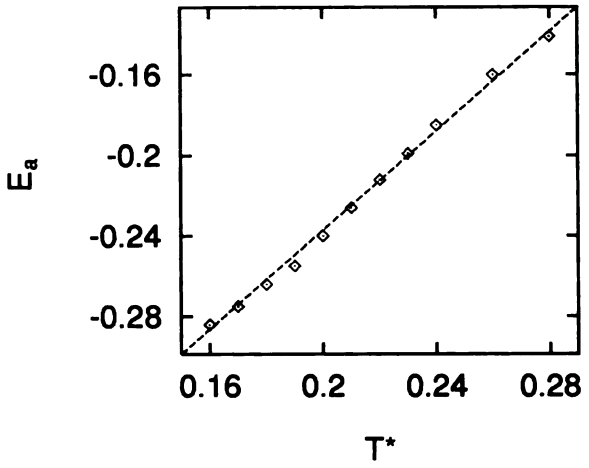

Figure 3.5: The mild temperature dependence of the solute-water binding energy is fit to a line with slope 1.23.

the heat capacity is a very sensitive function of such parameters. The double-2-state model is not quantitatively accurate at very high or low temperatures, however. Adding additional states, above the two upper states in the Muller model, would act in the right direction to reduce these errors.

3.5.3 Interpreting T_H and T_S

In past thermodynamic modeling of hydrophobic solvation, it has been common to assume that solute-water interactions are simple, and that the nonidealities of hydrophobicity arise in the water-water interactions. In particular, it is assumed that the enthalpy of the solute-water interaction is independent of temperature. But Figure 3.5 makes an interesting point to the contrary. Even though the solute-water pair energy in the MB model *is independent* of temperature, the *average* solute-water

enthalpy is not. This means that the solute-water interaction contributes to the hydrophobic heat capacity. Why? This arises because the observable enthalpy is the integral of (the solute-water energy) $\times$ (the solute-water pair correlation function), and the latter quantity changes with temperature. That is, the average separation and angle of a water molecule relative to the solute changes with temperature, so even though the pair energy is a constant, the mean energy is temperature dependent. The key point is that hydrophobic hydration cannot be deconvoluted into two simple components, a classical part and an "abnormal" part.

The model allows us to interpret T_H, the temperature at which the enthalpy of solute transfer is zero. We define the *reorganization enthalpy* as the total enthalpy of transfer minus the solute-water binding energy, as in Eq. 3.11. Once the binding energy is subtracted from the transfer enthalpy obtained in the simulations, the resulting reorganizational enthalpy can be fit to Eq. 3.8 to yield the value of ΔH_U, since all the other parameters are already determined. The fit, with a value $\Delta H_U = 0.195$, is shown in Figure 3.6. The quantity ΔH_U determines only where the transfer enthalpy crosses zero, but otherwise has no effect on the shape of the temperature dependence. Hence, the crossing temperature, T_H reflects the shift of the two fixed-gap bulk states relative to the two fixed-gap shell states.

The model also gives an interpretation for T_S, the temperature at which the entropy equals zero. The remaining parameter, ΔS_U, plays a similar role for T_S that ΔH_U plays for T_H. If water reorganization accounted for all of the transfer entropy, then a value of $\Delta S_U/k = 0.46$ would fit the data well (see Figure 3.7). The parameters

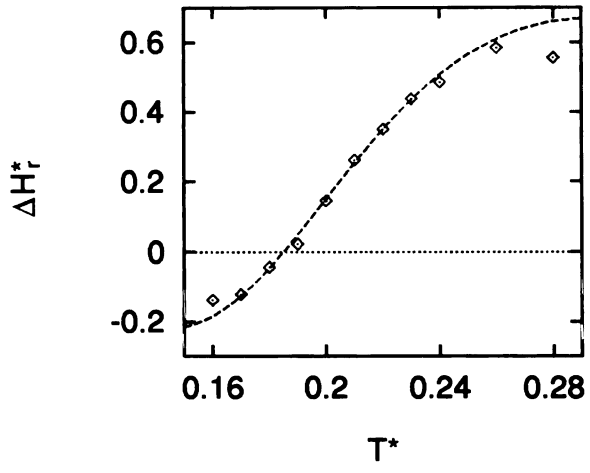

Figure 3.6: The reorganization enthalpy is plotted along with the two-state result. The slope and shape of this curve are predetermined by the original 4 parameters. The additional parameter which describes the offset between the two sets of energy levels determines the intersection of the curve with the x-axis.

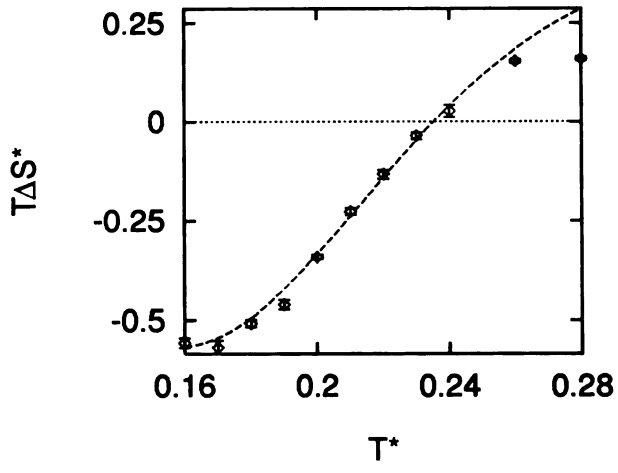

Figure 3.7: The transfer entropy ($T\Delta S^*$) is plotted along with the two-state result. The slope and shape of this curve are predetermined by the original 4 parameters. The additional parameter which describes the relative degeneracies of the upper energy levels in each set determines the intersection of the curve with the x-axis.

described here and above provide a self-consistent set[2] and indicates that for every three intact hydrogen bonds in the bulk, there are only two in the hydration shell (i.e., $\exp(\Delta S_{BI\rightarrow SI}/k) = 2/3$, where $\Delta S_{BI\rightarrow SI} = \Delta S_{SI} - \Delta S_{BI}$).

Lee [21, 22, 25] and others [33, 59] have argued that the reorganizational entropy should nearly exactly compensate the corresponding enthalpic term. The value of ΔS_U which would realize this expectation ($0.88k$) would indicate that there is a

[2]The 3 entropy parameters that we have determined are all fully satisfied if the 4 energy levels have the following *relative* number of states: Beginning with the least degenerate state, the intact hydration shell level, and moving clockwise in Figure 3.2, the relative number of states at the four levels is some multiple of 1:1.5:30:48.

roughly one-to-one correspondence[3] of hydrogen-bonding degenerate states in the bulk and hydration shell. Unfortunately, the results we obtained for our exhaustive enumerations disagree with both values for ΔS_U (see Section 3.5.5), leaving this issue, as yet unresolved.

3.5.4 Subtle Consequences of the Hydrophobic Effect

The "structuring" of water that results from nonpolar solvation is very subtle. It manifests differently for the different types of experiment used to measure it. For example, the temperature at which the enthalpy becomes zero is not the same as the temperature at which the entropy becomes zero. Other properties too change signs at different temperatures. An example is the NMR chemical shift.

Muller noted that his motivation for developing the double-2-state model was to account for puzzling NMR chemical shifts upon nonpolar solvation. A downfield shift is believed to indicate enhanced hydrogen bonding. But while downfield shifts are observed at low temperatures, upfield shifts are observed at higher temperatures. The implication is that solvation shell hydrogen bonds are not stronger than bulk hydrogen bonds at all temperatures. Muller described the relationship between chemical shift, $\Delta\delta$ and the fraction of broken hydrogen bonds with the expression

$$\Delta\delta/m = (n/111.1)[B(1 - f_s) - A(1 - f_b)]\,, \tag{3.17}$$

where m is the molality of the solute in water and A and B are the downfield chemical

[3]Following the same convention described in the previous footnote, the relative number of states at the four levels would be 1:1:20:48 to satisfy a nearly-complete compensation criterion.

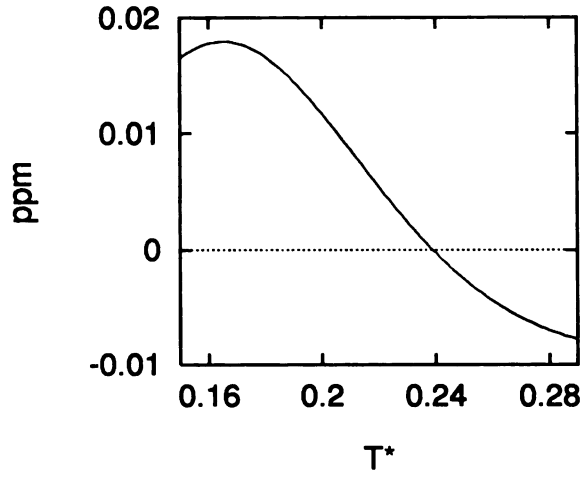

Figure 3.8: Predicted NMR chemical shift with assumptions from the text.

shifts that result from hydrogen bonds in the bulk and shell respectively. Although our parameters our quite different than Muller's, Figure 3.8 shows that our model also suitably accounts for this behavior. For simplicity, we've assumed that $A = B$, and that they are both given the value of 5.5 ppm that Muller estimated from the literature. Increasing the value of B relative to A merely shifts the crossing temperature to the right.

Our parameters are different than those estimated by Muller. Our model shows that there is a crossing temperature: shell H-bonds are more populated at low temperatures and bulk H-bonds are more populated at high temperatures (see Figure 3.3). In contrast, Muller's parameters predict that bulk H-bonds are more populated at all temperatures. We believe this particular result from the original Muller parameters is nonphysical, and is also inconsistent with results of all-atom simulations [9, 29, 38]. The problem arises from choosing parameters only to fit the heat capacity of hydration, as Muller did (see Figure 3.9, where we have performed a least-squares fit to the

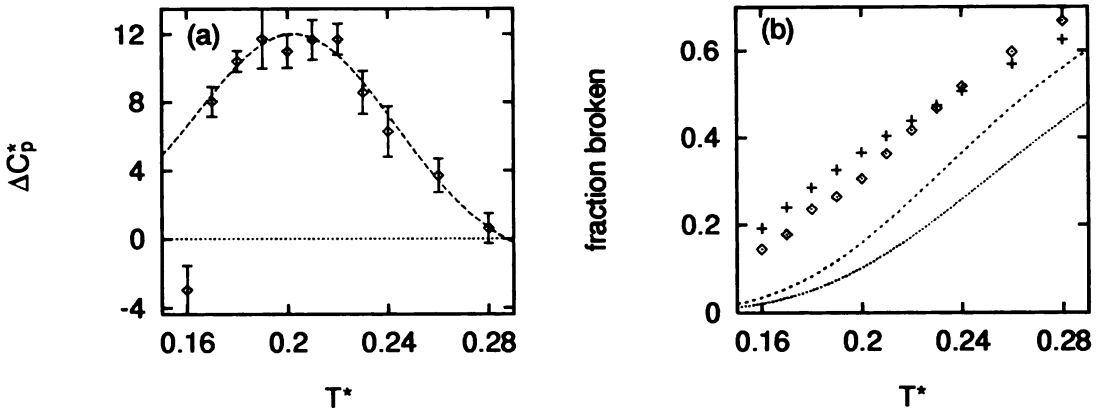

Figure 3.9: Demonstration that (a) overfitting the heat capacity leads to (b) the very same qualitatively-incorrect assumptions about hydrogen bonds of Muller's original parameterization. Labels for curves and points in (b) are the same as Figure 3.3.

heat capacity to derive the parameters, rather than fitting f_b and f_s directly).

3.5.5 Microscopic picture

Is there a simple two-body or three-body explanation for these parameters? We first focus on the bulk-water case. The full enumeration of only two water molecules is sufficient to give a remarkably good estimate of the bulk-water parameters. The two-body approximation gives $\Delta H_b^\circ = 0.71$ and $\Delta S_b^\circ/k = 2.7$ (from both the semi-exhaustive enumeration and the Boltzmann-weighted sampling), to be compared with $\Delta H_b^\circ = 0.71$ and $\Delta S_b^\circ/k = 2.99$ from the full many-body Monte Carlo simulation. The unweighted distribution of states is shown in Figure 3.10. The underestimate at the two-body level in the relative entropy of broken to intact H-bonded states implies

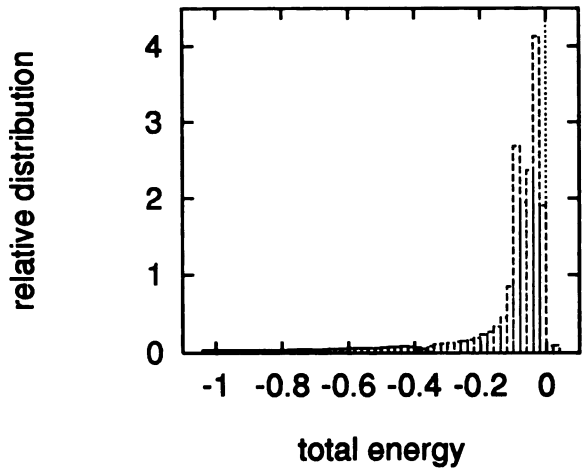

Figure 3.10: The relative distribution of intact (solid) and broken (dashed) H-bonded states for the enumeration of two MB waters.

that there are more intact states than in many-body systems. The presence of more intact states leads to an *overestimate* in the H-bonded order (see Figure 3.11) relative to the full simulation, which is most pronounced at low temperatures, due to the effects of the Boltzmann weighting. This trend has been shown elsewhere in a formal theoretical expansion of the entropy of MB water [49].

While the two-body partition function gives a reasonable model for bulk water, it is not sufficient for nonpolar solvation. For nonpolar solvation, the minimum number of waters needed *even to begin to get the correct trends* is 5 water molecules – the smallest number that can make a ring or clathrate around the solute. But even a single solvation shell is not sufficient to predict the solvation thermodynamics adequately. Figure 3.12 shows this trend, where the values are plotted versus the reciprocal of the system size. For systems of 4 or more waters, these plots are linear, and an

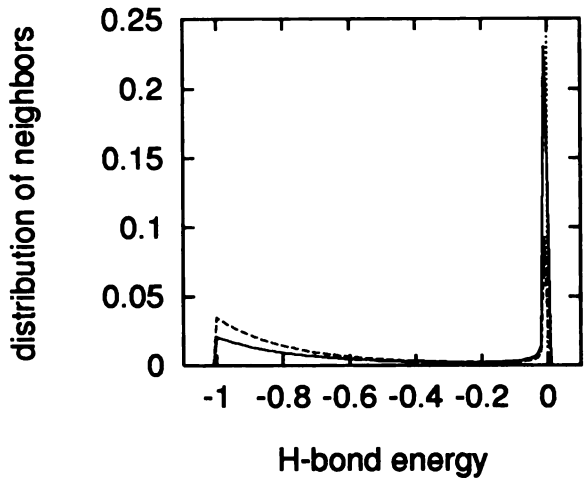

Figure 3.11: The distribution of hydrogen-bond energies at a low temperature ($T^* = 0.18$) for the full simulation (solid) and the 2-water system (dashed).

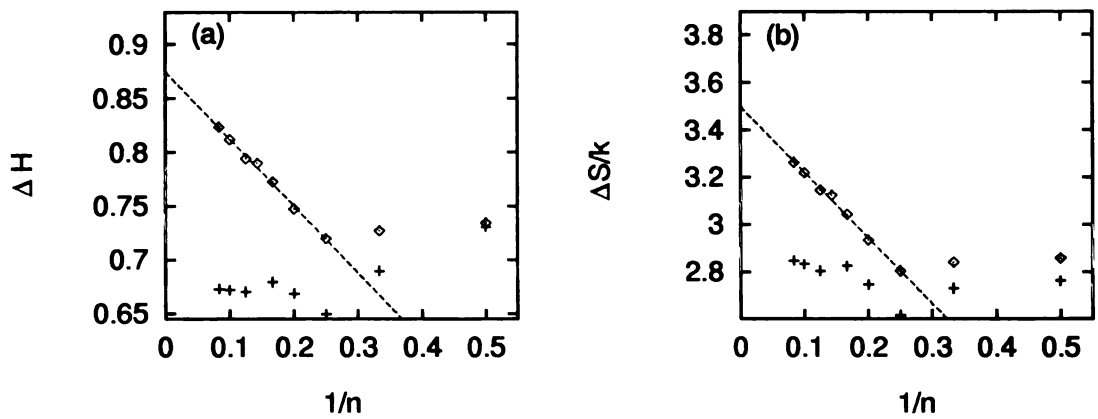

Figure 3.12: The progression of (a) ΔH° and (b) $\Delta S^\circ/k$ as a function of the reciprocal number of waters (1/n) for the hydration shell ($\diamond$) and the bulk (+), all at $T^* = 0.18$.

extrapolation to $1/n \to 0$ (infinite system size) yields the parameters $\Delta H_s^\circ = 0.88$ and $\Delta S_s^\circ/k = 3.5$, which are close to the expected values ($\Delta H_s^\circ = 0.92$ and $\Delta S_s^\circ/k = 3.88$). As a control, the bulk water values, also shown in Figure 3.12, show little change with system size.

Enumerations for the remaining two parameters ΔH_U and ΔS_U did not yield values in agreement with those obtained from macroscopic fitting of the MB data. The first, purely geometric method yielded a 39% reduction in states with the introduction of the solute, occluding both intact and broken states with equal proportions. Though this agrees well with the expected 33% reduction of intact H-bonded states, it is in disagreement with the expected *increase* in broken states suggested by the expected value ($exp(\Delta S_U/k) = exp(0.46) = 1.58$). The more rigorous Widom protocol also yielded poor agreement, even when extrapolated to infinite system size in the same manner as the other two shell parameters. These extrapolations suggest the values $\Delta H_U = -0.14$ and $\Delta S_U/k = -1.6$, which not even the same sign as the parameters that fit the macroscopic MB data. It is possible that the total energy of the system is not the distribution variable we should be looking at. However, the total H-bond energy (i.e., neglecting the LJ terms) in the system does not yield the expected values for ΔH_U and ΔS_U either (and that distribution variable even fails to give the correct values for the other 4 crucial parameters).

3.5.6 Analysis of Spectroscopic Measurements

Numerous spectroscopic techniques have been applied, using a two-state assumption, to obtain estimates of the H-bond fraction. Among these are Raman [5, 14, 15, 54, 56, 57], IR [26], and NMR spectroscopy [19, 34, 36, 47]. Additionally, viscosity measurements have also been used [55]. Unfortunately, these estimates are all very different, predicting, for example, a value of f_b anywhere from 7% to 62% at 0 °C. The thermodynamic predictions of the two-state model can be used to test the consistency of each of these estimates. Assuming that the predominant contribution to the configurational heat capacity of pure water can be attributed to making and breaking (or deforming) hydrogen bonds, any hydrogen bond fraction estimate should produce heat capacities in reasonable agreement with experimental values.

We have taken various estimates for bulk water from the literature, and fit them to Eq. 3.4 (see Figure 3.13) to obtain the corresponding enthalpy gap and relative degeneracy for each, which we have compiled in Table 3.1. Then we computed the resulting heat capacity contribution using these parameters and Eq. 3.5. Finally we compare these curves with the configurational part[4] of the heat capacity from the

[4]Eisenberg and Kauzmann [7] have estimated the contribution of rotations, translations, and vibrations to C_v throughout the liquid range, based on known spectral frequencies. This value we denote C_v'. The corresponding value for C_p' may be obtained from the thermodynamic relation, $C_p' = C_v' + TV\alpha^2/\kappa$, where T is the temperature, V is the molar volume, α is the thermal expansion coefficient, and κ is the isothermal compressibility. This value of C_p' is then simply subtracted off the total heat capacity of bulk water from the steam tables to obtain the configurational portion of the heat capacity.

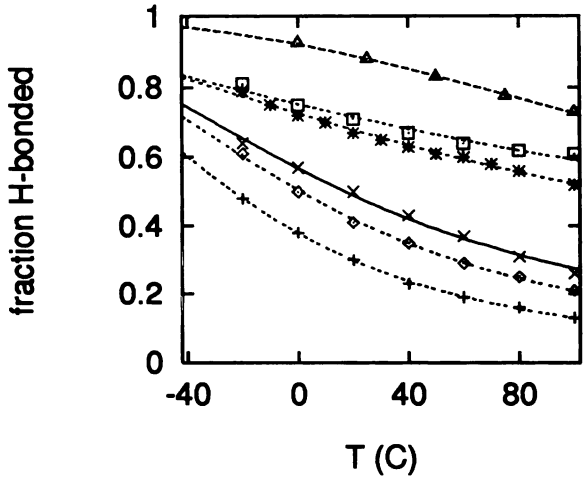

Figure 3.13: Various experimental estimates in the literature for the fraction of intact bonds in the bulk ($1 - f_b$), fit to the two-state formalism. ($\diamond$, $+$, $\square$): Hare and Sorensen [14], with three different methods used to deconvolute their data, as described in their work; ($\times$): D'Arrigo, *et al.* [5]; ($\triangle$): Walrafen [54] (where $1 - f_b = \sum_{i=0}^{4} i f_i / 4$); ($*$): Hare and Sorensen [15].

Table 3.1: Enthalpy and entropy parameters obtained from H-bond fraction estimates in the literature.

Source	Experiment used	ΔH_b°	$\Delta S_b^\circ/k$
		$kJ\ mol^{-1}$	
[5]	Raman	10.5	4.36
[14]	Raman	11.4	5.02
[14]	Raman	12.0	5.76
[14]	Raman	6.3	1.65
[15]	Raman	7.5	2.33
[19]	NMR	6.5	1.16
[54]	Raman	12.5	3.07
[55]	Viscosity	10.2	3.34
[56, 57]	Raman	10.9	3.13

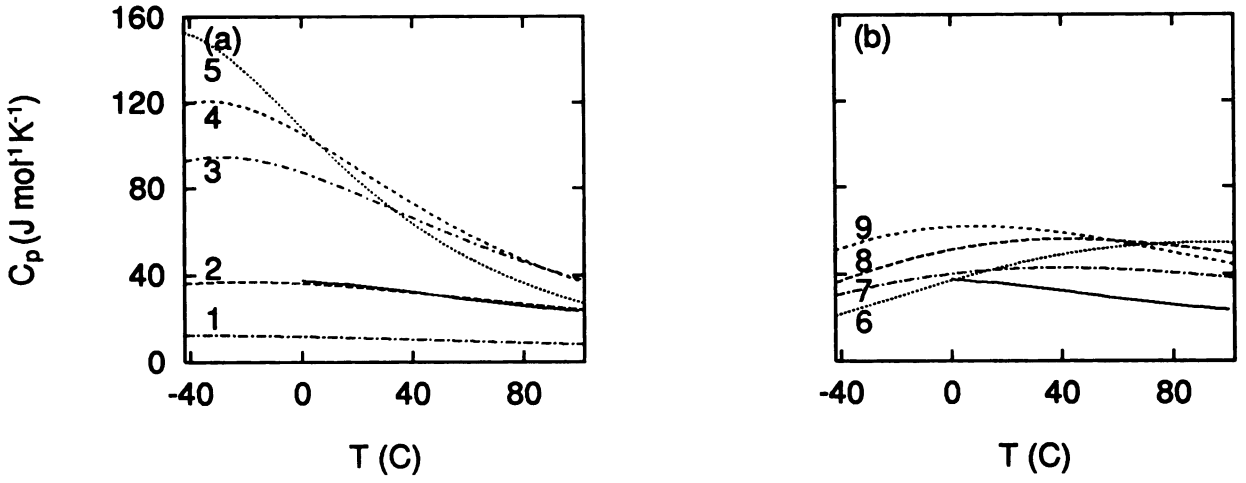

Figure 3.14: Bulk water heat capacity derived from the various estimates for the fraction of intact H-bonds, as compared with the configurational part of the heat capacity in the steam tables (solid line). (a) (1, 4, 5): Hare and Sorensen [14] corresponding to □, ◇, and +, respectively in Figure 3.13; (2): Hare and Sorensen [15]; (3): D'Arrigo, *et al.* [5]; (b) (6): Walrafen [54] (7): Muller [35]; (8): Walrafen *et al.* [56, 57]; (9): Walrafen and Chu [55].

steam tables [13] in Figure 3.14. The results are striking. Nearly all experimental estimates of f_b give widely inconsistent values for C_p, with the exception of the careful Raman estimate of Hare and Sorensen [15]. Their data shows excellent agreement over the whole temperature range. Note that Muller's original parameters give considerably poorer agreement (though they are reasonable at 0 °C, the temperature at which they were parameterized).

The analysis that Hare and Sorensen used to deconvolute their spectra does not require any a priori assumptions about the energy gap or spectral frequency of the

pure broken and intact species. They merely assumed a one-to-one correspondence between the Raman frequency shift and the energy state of the OD oscillator[5]. By plotting the relative intensities of the signal at each frequency separately over the temperature range in a van't Hoff plot, they were able to obtain the average deuterium hydrogen bond energy as a function of the Raman shift. In this plot, there was a clear minimum in energy at the same frequency as the hydrogen bond in the ice. Moreover, in moving to higher frequencies, the energy increased steeply before reaching a plateau region at a much higher energy ($\approx$ 3.2 kcal/mol). They attributed this region to the non-hydrogen bonded species. In their subsequent two-state analysis, they determined the average hydrogen bond strength to be about 1.9 kcal/mol, or about 60% of the value obtained as the energy to completely break the bond. This is similar to our observation of an average H-bond energy gap that is considerably smaller than the maximum value (compare 0.71 to the maximum H-bond energy gap of 1.0 in the MB model).

Given the success of their analysis, we believe it would be profitable for other spectroscopic techniques to be deconvoluted in a similar manner. This may lead to estimates of $f_b(T)$ across experiments in far better agreement than currently exists, and consequently a consistent value for the strength of a hydrogen bond in liquid water.

Estimates of f_s are far more difficult to obtain experimentally. This is largely due to the fact that hydrophobic solutes are sparingly soluble in water, and thus don't

[5]They used 10 mol % HOD in H_2O in order to remove the coupling of the dilute OD oscillator to other oscillators in solution, thus simplifying the spectral analysis.

provide a strong enough signal to noise ratio. In the past, systematic studies have been made on dilute alkane-substituted alcohol [30] ammonium [3, 53] and sulfonate [17] solutions. Although the effects of the hydrogen-bonding groups of these compounds complicates the interpretation, a consistent analysis similar to the work of Hare and Sorensen might yield reliable estimates of $f_s(T)$. The systematic variation with increasing number of methylene groups recently observed by Hecht *et. al.* [17] is suggestive that their spectral peaks do indeed correspond to changes in the water structure attributable to the hydrophobic moieties. Analysis of difference spectra similar to theirs over a wide temperature range, and the resulting hydrogen bond fractions are eagerly awaited.

3.6 Conclusions

We have used the MB model, a statistical mechanical model of water, to explore the principles of hydrophobic solvation. We have found that the Muller Model, as modified by Lee and Graziano, which approximates solvation using two states – hydrogen bonds are made or broken – in the bulk and solvation shell, accounts well for the thermodynamic temperature trends of hydrophobic transfers in the MB model of water. The Muller model has as its primary parameters, an enthalpy gap and relative degeneracy of states for both the hydration shell and the bulk. Our simulation allows us to obtain these parameters from a microscopic model, from the fraction of broken bonds. The heat capacity, enthalpy, and entropy which are calculated as a function of temperature are in reasonable quantitative agreement with the corresponding values

from the same set of simulations.

By systematic exhaustive enumerations of multiple water conformations on a grid, we find that the thermodynamics of pure water is reasonably well approximated by two waters, but solvation requires more waters than fill a first shell.

In its most general form, the two state model has an additional parameter to describe the relative shift in the two sets of intact-broken energy levels. This enthalpy shift parameter is found to directly affect the crossing temperature of the transfer enthalpy, T_H. Analogously, a parameter to describe the relative degeneracies of the two sets of energy levels is found to affect the temperature, T_S, at which the transfer entropy crosses zero.

We have used the Muller formalism to screen experimental spectroscopic estimates of the hydrogen bond fraction in the literature. We have fit these estimates to the model in the same manner as the MB data, and have calculated the predicted contribution to the heat capacity of pure water. We have found that only the estimate of Hare and Sorensen [15] is consistent with the experimental value for the configurational heat capacity obtained from the steam tables. Their data suggest that breaking a hydrogen bond in bulk water costs approximately 1.9 kcal/mol, and results in an entropy change of $\Delta S^\circ/k = 2.33$. If an analysis similar to that advocated by these two authors is used on difference spectra of alkane-substituted solutes, it is hoped that hydration shell parameters may be obtained in an analogous fashion. The current study suggests that the heat capacity arising from these four parameters should be in reasonable agreement with calorimetric measurements.

3.7 Acknowledgements

KATS greatfully acknowledges support under a U.S. National Science Foundation Graduate Research Fellowship and a UCSF Regent's Fellowship. We thank NIH for support. In Australia, this research was supported by the Australian Research Council (ARC) (Grant No. A29530010), and SydCom, the USyd/UTS Distributed Computing Facility funded by an ARC infrastructure grant. In addition, KATS would like to thank Karen Tang for many pertinent and lengthy discussions.

Bibliography

[1] G. Alagona and A. Tani. Structure of a dilute aqueous solution of argon. A Monte Carlo simulation. *J. Chem. Phys.*, 72(1):580–588, 1980.

[2] R. L. Baldwin. Temperature dependence of the hydrophobic interaction in protein folding. *Proc. Natl. Acad. Sci. USA*, 83:8069–8072, 1986.

[3] R. Bhanumathi and S. K. Vijayalakshamma. ^{1}H NMR chemical shifts of solvent water in aqueous solutions of monusubstituted ammonium compounds. *J. Phys. Chem.*, 90:4666–4669, 1986.

[4] W. Blokzijl and J. B. F. N. Engberts. Hydrophobic effects. opinions and facts. *Angew. Chem. Int. Ed. Engl.*, 32:1545–1579, 1993.

[5] G. D'Arrigo, G. Maisano, F. Mallamace, P. Migliardo, and F. Wanderlingh. Raman scattering and structure of normal and supercooled water. *J. Chem. Phys.*, 75:4262–4270, 1981.

[6] D. Eisenberg and W. Kauzmann. *The structure and properties of water*, pages 256–265. Oxford University Press, Oxford, 1969.

[7] D. Eisenberg and W. Kauzmann. *The structure and properties of water.* Oxford University Press, Oxford, 1969.

[8] S. Garde, G. Hummer, A. E. García, M. E. Paulaitis, and L. R. Pratt. Origin of entropy convergence in hydrophobic hydration and protein folding. *Phys. Rev. Lett.*, 77:4966–4968, 1996.

[9] A. Geiger, A. Rahman, and F. H. Stillinger. Molecular dynamics study of the hydration of Lennard-Jones solutes. *J. Chem. Phys.*, 70(1):263–276, 1979.

[10] S. J. Gill, S. F. Dec, G. Olofsson, and I. Wadso. Anomalous heat capacity of hydrophobic solvation. *J. Phys. Chem.*, 89:3758–3761, 1985.

[11] B. Guillot and Y. Guissani. A computer simulation study of the temperature dependence of the hydrophobic hydration. *J. Chem. Phys.*, 99(10):8075–8094, 1993.

[12] B. Guillot, Y. Guissani, and S. Bratos. A computer-simulation study of hydrophobic hydration of rare gases and of methane. I. Thermodynamic and structural properties. *J. Chem. Phys.*, 95(5):3643–3648, 1991.

[13] L. Haar, J. S. Gallagher, and G. S. Kell. *NBS/NRC Steam Tables.* Hemisphere Publishing, Washington, DC, 1984.

[14] D. E. Hare and C. M. Sorensen. Raman spectroscopic study of bulk water supercooled to -33 °C. *J. Chem. Phys.*, 93:25–33, 1990.

[15] D. E. Hare and C. M. Sorensen. Raman spectroscopic study of dilute HOD in liquid H_2O in the temperature range -31.5 to 160 °C. *J. Chem. Phys.*, 93:6954–6960, 1990.

[16] T. Head-Gordon, J. M. Sorenson, A. Pertsemlidis, and R. M. Glaeser. Differences in hydration structure near hydrophobic and hydrophilic amino acids. Preprint, 1997.

[17] D. Hecht, L. Tadesse, and L. Walters. Defining hydrophobicity: Probing the structure of solute-induced hydration shells by Fourier transfor infrared spectroscopy. *J. Am. Chem. Soc.*, 114:4336–4339, 1992.

[18] A. R. Henn and W. Kauzmann. *J. Chem. Phys.*, 93:3770–3783, 1989.

[19] J. C. Hindman. Proton resonance shift of water in the gas and liquid state. *J. Chem. Phys.*, 44:4582–4592, 1966.

[20] F. Hirata, B. M. Pettitt, and P. J. Rossky. Application of an extended RISM equation to dipolar and quadrupolar fluids. *J. Chem. Phys.*, 77:509–520, 1982.

[21] B. Lee. The physical origin of the low solubility of nonpolar solutes in water. *Biopolymers*, 24:813–823, 1985.

[22] B. Lee. Isoenthalpic and isoentropic temperatures and the thermodynamics of protein denaturation. *Proc. Natl. Acad. Sci. USA*, 88:5154–5158, 1991.

[23] B. Lee. Solvent reogranization contribution to the transfer thermodynamics of small nonpolar molecules. *Biopolymers*, 31(8):993–1008, 1991.

[24] B. Lee. Enthalpy-entropy compensation in the thermodynamics of hydrophobicity. *Biophysical Chemistry*, 51:271–278, 1994.

[25] B. Lee and G. Graziano. A two-state model of hydrophobic hydration that produces compensating enthalpy and entropy changes. *J. Am. Chem. Soc.*, 118:5163–5168, 1996.

[26] W. A. P. Luck. Spectroscopic studies concerning the structure and the thermodynamic behavior of H_2O, CH_3OH and C_2H_5OH. *Disc. Faraday Soc.*, 43:115–147, 1967.

[27] R. Lumry, E. Battistel, and C. Jolicoeur. Geometric relaxation in water: it's role in hydrophobic hydration. *Faraday Symp. Chem. Soc.*, 17:93–108, 1982.

[28] B. Madan and K. Sharp. Heat capacity changes accompanying hydrophobic and ionic solvation: A Monte Carlo and Random Network Model study. *J. Phys. Chem.*, 100:7713–7721, 1996.

[29] R. L. Mancera and A. D. Buckingham. Temperature effects on the hydrophobic hydration of ethane. *J. Phys. Chem.*, 99:14632–14640, 1995.

[30] M.-M. Marciacq-Rousselot and M. Lucas. Nuclear magnetic resonance chemical shift of the water proton in aqueous alcoholic solutions at various temperatures. Some thermodynamic properties of these solutions. *J. Phys. Chem.*, 77(8):1056–1060, 1973.

[31] N. Matubayasi. Matching-mismatching of water geometry and hydrophobic hydration. *J. Am. Chem. Soc.*, 116:1450–1456, 1994.

[32] N. Matubayasi and R. M. Levy. Thermodynamics of the hydration shell. 2. Excess volume and compressibility of a hydrophobic solute. *J. Phys. Chem.*, 100:2681–2688, 1996.

[33] N. Matubayasi, L. H. Reed, and R. M. Levy. Thermodynamics of the hydration shell. 1. Excess energy of a hydrophobic solute. *J. Phys. Chem.*, 98:10640–10649, 1994.

[34] N. Muller. Concerning structural models for water and chemical-shift data. *J. Chem. Phys.*, 43:2555–2556, 1965.

[35] N. Muller. Search for a realistic view of hydrophobic effects. *Acc. Chem. Res.*, 23:23–28, 1990.

[36] N. Muller and R. C. Reiter. Temperature dependence of chemical shifts of protons in hydrogen bonds. *J. Chem. Phys.*, 42(9):3265–3269, 1965.

[37] G. Nemethy and H. A. Scheraga. Structure of water and hydrophobic bonding in proteins. II. Model for the thermodynamic properties of aqueous solutions of hydrocarbons. *J. Chem. Phys.*, 36(12):3401–3417, 1962.

[38] S. Okazaki, K. Nakanishi, H. Touhara, N. Watanabe, and Y. Adachi. A Monte Carlo study on the size dependence in hydrophobic hydration. *J. Chem. Phys.*, 74(10):5863–5871, 1981.

[39] L. Pauling. *The nature of the chemical bond, 3rd ed.*, page 468. Cornell University Press, Ithaca, NY, 1960.

[40] R. A. Pierotti. *Chem. Rev.*, 76:717, 1976.

[41] L. R. Pratt. Theory of hydrophobic effects. *Ann. Rev. Phys. Chem.*, 36:433–449, 1985.

[42] L. R. Pratt and D. Chandler. Theory of the hydrophobic effect. *J. Chem. Phys.*, 67:3683–3704, 1977.

[43] P. L. Privalov and S. J. Gill. Stability of protein structure and hydrophobic interaction. *Advances in Protein Chemistry*, 39:191–234, 1988.

[44] S. A. Rice and M. G. Sceats. A random network model for water. *J. Phys. Chem.*, 85:1108–1119, 1981.

[45] M. G. Sceats and S. A. Rice. A random network model calculation of the free energy of liquid water. *J. Chem. Phys.*, 72(11):6183–6191, 1980.

[46] M. G. Sceats, M. Stavola, and S. A. Rice. A zeroth order random network model of liquid water. *J. Chem. Phys.*, 70(8):3927–3938, 1979.

[47] W. G. Schneider, H. J. Bernstein, and J. A. Pople. Proton magnetic resonance chemical shift of free (gaseous) and associated (liquid) hydride molecules. *J. Chem. Phys.*, 28:601–607, 1958.

[48] K. A. Sharp and B. Madan. The hydrophobic effect, water structure, and heat capacity changes. *Journal of Physical Chemistry B*, 101:4343–4348, 1997.

[49] K. A. T. Silverstein, K. A. Dill, and A. D. J. Haymet. Entropy of hydrophobic hydration: A full angular multiparticle expansion. To be submitted to the *Journal of Physical Chemistry*, Dec 1997.

[50] K. A. T. Silverstein, A. D. J. Haymet, and K. A. Dill. A simple model of water and the hydrophobic effect. Submitted to the *Journal of the American Chemical Society*, 1997.

[51] A. K. Soper and J. Turner. Impact of neutron scattering on the study of water and aqueous solutions. *International Journal of Modern Physics B*, 7(16):3049–3076, 1993.

[52] A. Tani. Nonpolar solute-water pair correlation functions-a comparison between computer simulation and theoretical results. *Molecular Physics*, 48:1229–1240, 1983.

[53] J. Z. Turner, A. K. Soper, and J. L. Finney. Ionic versus apolar behavior of the tetramethylammonium ion in water. *J. Chem. Phys.*, 102(13):5438–5443, 1995.

[54] G. E. Walrafen. *Water, a Comprehensive Treatise*, volume 1, chapter 5. Plenum Press, New York, 1972.

[55] G. E. Walrafen and Y. C. Chu. Shear viscosity, heat capacity, and fluctuations of liquid water, all at constant molal volume. *J. Phys. Chem.*, 95:8909–8921, 1991.

[56] G. E. Walrafen, M. R. Fisher, M. S. Hokmabadi, and W.-H. Yang. Temperature dependence of the low- and high-frequency raman scattering from liquid water. *J. Chem. Phys.*, 85(12):6970–6982, 1986.

[57] G. E. Walrafen, M. S. Hokmabadi, and W.-H. Yang. Raman isobestic points from liquid water. *J. Chem. Phys.*, 85(12):6964–6969, 1986.

[58] B. Widom. Some topics in the theory of fluids. *J. Chem. Phys.*, 39(11):2808–2812, 1963.

[59] H.-A. Yu and M. Karplus. A thermodynamic analysis of solvation. *J. Chem. Phys.*, 89(4):2366–2378, 1988.

[60] Y. yu Shi, A. E. Mark, W. Cun-xin, H. F. a nd Herman J. C. Berendsen, and W. F. van Gunsteren. Can the stability of protein mutants be predicted by free energy calculations? *Prot. Eng.*, 6(3):289–295, 1993.

[61] S.-B. Zhu, S. Singh, and G. W. Robinson. Field-perturbed water. *Adv. Chem. Phys.*, 85(3):627–731, 1994.

Chapter 4

Entropy of Hydrophobic Hydration: A Full, Angular Multiparticle Expansion

Kevin A. T. Silverstein, Ken A. Dill, and A. D. J. Haymet

4.1 Abstract

We study the entropy of water, and the entropy of a nonpolar solute in water. Such entropies are often approximated using pair correlation functions. Are such two-body approximations sufficient? Or are multi-body terms required? In this paper, we first develop the appropriate multi-particle correlation functions, with the full angle dependence included, in the NVT ensemble. This type of formalism goes beyond the current capabilities of all-atom simulations, however, because collecting sufficient statistics for such high-order functions is not computationally feasible. To remedy this problem, we test the formalism on a simpler model instead. We use the MB model of water, which is a simple two-dimensional model of water, in which molecules are represented as Lennard-Jones disks with 3 hydrogen-bonding arms arranged as in the Mercedes Benz logo. The MB model captures the volumetric anomalies of water and the temperature dependence of hydrophobic solvation. We find that at high temperatures, the two-body approximation is sufficient for both pure water and a nonpolar solute in water. However, we find that for liquid water and nonpolar solutions at moderate and low temperatures, the two-body approximation strongly overestimates the degree of water ordering. This means that at ambient and low temperature, higher order terms in the entropy expansion cause a *reduction* of the entropy in order for the sum of pair terms and higher order terms to yield the correct entropy of water and of nonpolar solvation.

4.2 Introduction

A fingerprint of hydrophobic solvation is the large negative entropy associated with inserting a nonpolar solute into water. This entropy penalty, which has been ascribed[4] to order induced by the solute in the surrounding solvent, leads to the low solubility of inert molecules in water at room temperature. What is the nature of this solvation entropy? Since the same hydration thermodynamics, including the entropy, is observed for a disk solute in a simple, two dimensional model of water, recently studied by us[10, 11, 25, 26], called the Mercedes-Benz (MB) model, we have exploited the reduced dimensionality of the simple model to calculate the magnitude and sign of certain terms in the full angular expansion of the entropy.

Notably, we find that (the ensemble invariant analogue of) the simple " $g \ln g$ " term greatly *over*estimates the true entropy penalty at the temperatures of interest. (i.e., The two-body term overestimates the order induced in the model water.) Therefore, higher-order terms must describe additional *dis*order in the liquid, and the sum of the terms yields the correct, observed, thermodynamic entropy penalty.

This paper is organized as follows. In Section 4.3 we summarize briefly the history of calculating entropy via multi-particle correlation functions, and the explicit formulae used in this work for both pure water and the solution. In Section 4.4 we describe the method by which a Fourier series expansion can be used to greatly speed up the convergence of the angular correlation functions, after briefly reviewing the model and computational procedures used. In Sections 4.5.1 and 4.5.2, the results of our calculations for bulk water and a dilute nonpolar solution, respectively, are

presented. Some of these results were presented in preliminary form at a conference [11]. Finally, Section 4.6 is a summary.

4.3 Entropy Expansions

4.3.1 The Kirkwood - Green Expansion

For liquids with only pairwise-additive interactions between particles, many thermodynamic quantities, such as the average potential energy and the pressure, may be calculated directly from the pair correlation functions. However, for important statistical quantities, such as the entropy and free energy, an analogous direct and exact calculation is not possible. Typically, such quantities have been calculated indirectly using the techniques of thermodynamic integration and histogram-reweighting methods, which involve the calculation of the properties of the solution over an entire range of thermodynamic states between a reference (ideal) state and the state of interest. Not surprisingly, these methods require significant computer resources.

A direct, but approximate, method for calculating the entropy (and hence the free energy) from the pair correlations alone has been explored for a variety of liquids [2, 12, 13, 15, 16, 22, 30]. This method is based on truncation of an exact, but infinite-order, expansion for the entropy in terms of multiparticle correlation functions. Even for pairwise-additive systems, the expansion of the entropy in terms of multiparticle correlation functions does not truncate at the pair level, but instead has contributions from all orders [6, 23]. At present the calculation of multiparticle correlation functions

is at best an extremely difficult task, and recent work has focused on manipulating the entropy expansion in order to obtain the best possible estimate of the entropy from the pair correlation functions alone [15].

Building upon the work of Kirkwood [14], H.S. Green [6], Nettleton and M.S. Green [23] and Raveché [24], Hernando [12, 13] recast the entropy expansion into a particularly useful form, via a partial resummation of the higher-order terms. This expression has been generalized to a mixture of any number, μ, components by Laird, Wang and Haymet [18], and applied to electrolytes systems by Laird and Haymet [17].

The resulting expansion may be written as the sum of four terms:

$$S[g^{(n)}]/Nk \;=\; s^{IG} + s^{(2)} + s_{ring} + \sum_{i=3}^{\infty} s'_{mix}(i)[g^{(m)}_{\alpha\beta\ldots};\, m \leq i]. \tag{4.1}$$

The functions $g^{(m)}_{\alpha\beta\ldots}(\mathbf{r}_\alpha, \mathbf{r}_\beta, \ldots)$ are the m-particle (multicomponent) correlation functions of the liquid. In the ensemble invariant form [2], the first term

$$s^{IG} \equiv \frac{5}{2} - \sum_{\alpha=1}^{\mu} x_\alpha \ln \rho_\alpha \Lambda_\alpha^3 \tag{4.2}$$

is the ideal gas contribution, where α is the species label, Λ_α is the de Broglie thermal wavelength, ρ_α is the number density of component α, $\rho \;=\; \sum_{\alpha=1}^{\mu} \rho_\alpha$ is the total number density, and $x_\alpha = \rho_\alpha/\rho$ is the mole fraction. The second term,

$$s^{(2)} \equiv -\frac{\rho}{2} \sum_{\alpha=1}^{\mu} \sum_{\beta=1}^{\mu} x_\alpha x_\beta \int d\mathbf{r}_{\alpha\beta}\, [g^{(2)}_{\alpha\beta}(r_{\alpha\beta}) \ln g^{(2)}_{\alpha\beta}(r_{\alpha\beta}) - g^{(2)}_{\alpha\beta}(r_{\alpha\beta}) + 1]\,, \tag{4.3}$$

results from the usual second-order truncation of the entropy expansion, and contains the familiar "$g \ln g$" term. The next term is the so-called "ring" contribution,

$$s_{ring} \equiv \frac{1}{2(2\pi\rho)^3} \int d\mathbf{k} [\ln |\, \mathbf{I} + \tilde{\mathbf{H}}(k)\, | + \frac{1}{2} \mathrm{Tr}\tilde{\mathbf{H}}^2(k) - \mathrm{Tr}\tilde{\mathbf{H}}(k)]\,, \tag{4.4}$$

where $\mathbf{I}$ is the $\mu \times \mu$ identity matrix and

$$\tilde{\mathbf{H}}(k)_{\alpha\beta} \equiv \rho_\alpha^{1/2} \tilde{h}_{\alpha\beta}(k) \rho_\beta^{1/2} \,. \tag{4.5}$$

Hernando derived this term by extracting the leading contribution ("ring" diagram) from each individual order of the expansion hierarchy, and summing these contributions to infinite order. The function $\tilde{h}_{\alpha\beta}(k)$ is the Fourier transform of the total correlation function $h_{\alpha\beta}(r) \equiv g_{\alpha\beta}(r) - 1$. When pair correlation functions obtained from the HNC approximation are inserted into this expansion, the sum of the first three terms is exactly equal to the well-known HNC entropy. Since the first three terms require structural information only up to pair correlation functions, they form a particularly useful approximation to the total entropy.

Applications of formulae analogous to Eqns. 4.1–4.5 to aqueous systems initially used the canonical (i.e., "$g \ln g$") formulae [19, 30]. However, canonical formulae should not be used with correlation functions determined from simulations [28], due to their nonlocal nature [2] (i.e., they would require unattainably-large system sizes for reliable convergence). More recent publications use the correct formulae [1] but introduce additional approximations.

4.3.2 Entropy Expansion for Pure Water

To adequately describe the correlations among particles of a *molecular* fluid such as water, we need to go beyond the traditional centers-averaged n-body correlation functions. Water contains a high degree of angular ordering, and this information is lost in these orientationally-averaged functions. Site-site correlation functions (e.g.,

$g^{(2)}_{OO}(r)$, $g^{(2)}_{OH}(r)$, $g^{(2)}_{HH}(r)$, $g^{(3)}_{OOO}(r,s,t)$, ...) have been used extensively in the literature. However, even these functions do not contain a full angular description. It is necessary to establish the distributions of the relative orientations between molecules in addition to their relative separation. The resulting full angular correlation function can be used to re-construct all of the site-site functions; but the reverse is not possible. Different angular descriptions can be consistent with a single site-site correlation function [5].

The entropy of a molecular liquid can be expressed in terms of these and higher-order angular correlation functions[1]. The exact expression for the general case of a mixture of molecular components is:

$$\frac{S}{Nk} = s^{IG} + s^{(2)} + s^{(3)} + ... \tag{4.6}$$

for N total particles at temperature T and volume V, and k is the Boltzmann constant. The first term, which is analogous to the ideal gas term for atomic species in Eq. 4.2, but has additional angle-dependent variables, is derived in Appendix B:

$$s^{IG} = 1 + \sum_{\alpha=1}^{\mu} x_\alpha \left[\frac{\nu_\alpha}{2} - \ln\left(\rho_\alpha \sigma_\alpha \Lambda_{t,\alpha}^d \Lambda_{r,\alpha}\right) \right] , \tag{4.7}$$

where α is an index over μ particle species, x_α, ν_α, ρ_α, σ_α, $\Lambda_{t,\alpha}$, and $\Lambda_{r,\alpha}$ are the mole fraction, number of degrees of freedom, number density, symmetry number, translational thermal wavelength, and rotational wavelength, respectively, of species α, and d is the spatial dimension. Since the first term is an ideal-gas contribution,

[1] An expansion which includes the orientational degrees of freedom needed for a molecular fluid was presented by Lazaridis and Paulaitis [19] in the *canonical* ensemble. As described earlier, however, the canonical formulae is nonlocal. To obtain the correct, ensemble-invariant formulae, we have applied the procedure of Baranyai and Evans [2].

the two- and higher-body correlations account for the excess order in the liquid. The 2-body term is of the form

$$s^{(2)} = -\frac{\rho}{2\Omega^2}\sum_{\alpha,\beta}^{\mu} x_\alpha x_\beta \int_V d\mathbf{r}d\omega_\alpha d\omega_\beta \left[g^{(2)}_{\alpha\beta}(\mathbf{r},\omega_\alpha,\omega_\beta)\ln g^{(2)}_{\alpha\beta}(\mathbf{r},\omega_\alpha,\omega_\beta) - g^{(2)}_{\alpha\beta}(\mathbf{r},\omega_\alpha,\omega_\beta)+1\right], \tag{4.8}$$

where $\rho = \sum_{\alpha=1}^{\mu}\rho_\alpha$ is the total number density, Ω is the total angular volume of integration, β is another molecular species index, $\mathbf{r}$ is the center-of-mass interparticle separation, ω_α represents the Euler angles of species α, and $g^{(2)}_{\alpha\beta}(\mathbf{r},\omega_\alpha,\omega_\beta)$ is the two-body angular correlation function. Likewise, the 3-body expression is

$$\begin{aligned} s^{(3)} = & -\frac{\rho^2}{3!V\Omega^3}\sum_{\alpha,\beta,\gamma}^{\mu} x_\alpha x_\beta x_\gamma \\ & \times \int_V\int_V\int_V d\mathbf{r}_\alpha d\mathbf{r}_\beta d\mathbf{r}_\gamma d\omega_\alpha d\omega_\beta d\omega_\gamma \left[g^{(3)}_{\alpha\beta\gamma}(\mathbf{r}_{\alpha\beta},\mathbf{r}_{\beta\gamma},\mathbf{r}_{\alpha\gamma},\omega_\alpha,\omega_\beta,\omega_\gamma)\right. \\ & \times \ln\left(\frac{g^{(3)}_{\alpha\beta\gamma}(\mathbf{r}_{\alpha\beta},\mathbf{r}_{\beta\gamma},\mathbf{r}_{\alpha\gamma},\omega_\alpha,\omega_\beta,\omega_\gamma)}{g^{(2)}_{\alpha\beta}(\mathbf{r}_{\alpha\beta},\omega_\alpha,\omega_\beta)g^{(2)}_{\beta\gamma}(\mathbf{r}_{\beta\gamma},\omega_\beta,\omega_\gamma)g^{(2)}_{\alpha\gamma}(\mathbf{r}_{\alpha\gamma},\omega_\alpha,\omega_\gamma)}\right) \\ & - g^{(3)}_{\alpha\beta\gamma}(\mathbf{r}_{\alpha\beta},\mathbf{r}_{\beta\gamma},\mathbf{r}_{\alpha\gamma},\omega_\alpha,\omega_\beta,\omega_\gamma) + 3g^{(2)}_{\alpha\beta}(\mathbf{r}_{\alpha\beta},\omega_\alpha,\omega_\beta)g^{(2)}_{\beta\gamma}(\mathbf{r}_{\beta\gamma},\omega_\beta,\omega_\gamma) \\ & \left. - 3g^{(2)}_{\alpha\beta}(\mathbf{r}_{\alpha\beta},\omega_\alpha,\omega_\beta)+1\right] \end{aligned} \tag{4.9}$$

where γ is a third index over molecular species.

4.3.3 Entropy Expansion for a Solution

An expansion can also be written to describe the entropy of the solute-transfer process [1]. Using the above general expression for a mixture of waters and solutes, the derivative with respect to solute number (at constant T, V, and N_W) is extrapolated to infinite dilution. After subtracting off the so-called "liberation entropy", we obtain

the Ben-Naim standard state entropy:

$$\frac{\Delta S^*}{k} = \Delta s^{(2)} + \Delta s^{(3)} + ... \tag{4.10}$$

where the 2-body term is

$$\begin{aligned} \Delta s^{(2)} = & - \frac{\rho_W}{\Omega^2} \int_V d\mathbf{r}_{SW} d\omega_S d\omega_W \left[g^{(2)}_{SW} \ln g^{(2)}_{SW} - g^{(2)}_{SW} + 1 \right] \\ & - \frac{\rho_W}{2\Omega^2} \int_V d\mathbf{r}_{WW} d\omega_{W_1} d\omega_{W_2} \left[\left(\frac{\partial g^{(2)}_{WW}}{\partial \rho_S} \right)^{\infty}_{T,V,N_W} \ln g^{(2)}_{WW} \right] , \end{aligned} \tag{4.11}$$

and the subscripts W and S denote water and solute respectively, and we have used a simplified notation for the correlation functions. The partial derivative in the second term is taken at the limit of infinite dilution of the solute. In the case of an isotropic solute, the integration over the Euler angles of the solute is omitted, and we are left only with the angular degrees of freedom of the waters. From this expression, it is clear that the only two terms that contribute to the 2-body transfer entropy is one for the orientational and translational restrictions of the waters about the solute, and a second term for the water-water reorganization in the presence of the solute. At the moment, we neglect the contribution of the second term, as some others have done [19, 20, 21] because of the computational expense involved.

The 3-body term is comprised of two similar components:

$$\begin{aligned} \Delta s^{(3)} = & - \frac{\rho_W^2}{3! V \Omega^3} \int_V d\mathbf{r}_{W_1 W_2} d\mathbf{r}_{SW_1} d\mathbf{r}_{SW_2} d\omega_S d\omega_{W_1} d\omega_{W_2} \left[g^{(3)}_{SWW} \ln \left(\frac{g^{(3)}_{SWW}}{g^{(2)}_{WW} g^{(2)}_{SW_1} g^{(2)}_{SW_2}} \right) \right. \\ & \left. - g^{(3)}_{SWW} + 2 g^{(2)}_{WW} g^{(2)}_{SW} + g^{(2)}_{SW_1} g^{(2)}_{SW_2} - 2 g^{(2)}_{SW} - g^{(2)}_{WW} + 1 \right] \\ & - \frac{\rho_W^3}{3! V \Omega^3} \int_V d\mathbf{r}^3_{WW} d\omega^3_W \left\{ \left(\frac{\partial g^{(3)}_{WWW}}{\partial \rho_S} \right)^{\infty}_{T,V,N_W} \ln \left(\frac{g^{(3)}_{WWW}}{g^{(2)}_{W_1 W_2} g^{(2)}_{W_2 W_3} g^{(2)}_{W_1 W_3}} \right) \right. \\ & \left. + 3 \left(\frac{\partial g^{(2)}_{WW}}{\partial \rho_S} \right)^{\infty}_{T,V,N_W} \left[2 g^{(2)}_{WW} - 1 - \frac{g^{(3)}_{WWW}}{g^{(2)}_{WW}} \right] \right\} . \end{aligned} \tag{4.12}$$

This time, the first term describes the correlations of *pairs* of water about the solute, and the second term represents water reorganizations at the 3-body level.

4.4 Model and Computational Details

To study the multiple-body correlations of a molecular liquid such as water, it is necessary to track not only the intermolecular separations of particles, but their relative orientations as well. For two-body interactions of real water, this would amount to accumulating a correlation function that is a function of six variables in 3 dimensions (one center-of-mass separation variable, and five Euler angles). This is not computationally feasible. Instead, we use a simplified, two-dimensional model of water, the MB model [3, 26], which has recently been shown to have the anomalous thermodynamic trends of water and the hydrophobic effect [26, 27]. Fortunately in d=2 there are only three variables (center-of-mass separation, and a single angular variable for each molecule). This allows us to get well-converged correlation functions that can be integrated accurately. The convergence of these correlation function can be further enhanced by accumulating the angular information as a Fourier series (see Section 4.4.2). Coefficients as a function of r are accumulated as ensemble averages in the simulation in a manner similar to that of Streett and Tildesley [29].

4.4.1 MB model

In this subsection we review the properties of the MB model of water [3, 26]. In the model, water molecules are represented as disks in two dimensions, with 3 arms

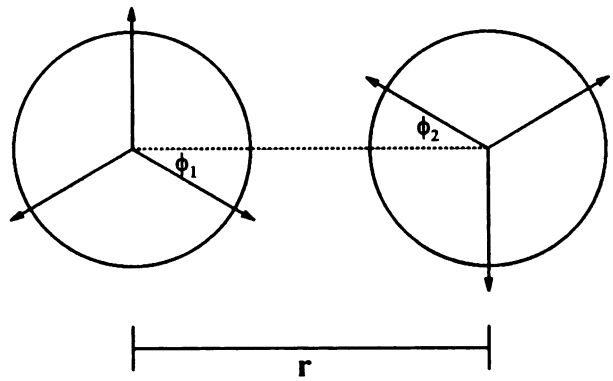

Figure 4.1: Two representative MB "water" molecules, separated by a distance r. The angle, ϕ, that each molecule makes with the intermolecular axis is shown.

arranged as in the Mercedes-Benz logo. Molecules interact pairwise through a standard Lennard-Jones term (2 parameters), and an explicit hydrogen-bond interaction between arms of nearby molecules. There are no charges. The hydrogen bond has a defined optimal distance $r_{HB} = 1$ and optimal angle for each molecule's bonding arm ($\phi = 0$) with the vector that joins their centers (see Figure 4.1). Deviations from this lowest-energy hydrogen bond are described by a Gaussian expression with a single width parameter used to attenuate the interaction. The same width parameter is used for both separation and angle deviations.

In total, there are 5 parameters. These are the same as those studied extensively in our earlier work [26], where more details are provided. The LJ well-depth parameter is one-tenth of ϵ_{HB}, the minimum value of the hydrogen bond function, and the LJ contact distance is 0.7 of r_{HB}. The width in the Gaussian $\sigma = 0.085$ was chosen to be small enough that the direct h-bond contact is more favorable than a bifurcated

h-bond. All energies and temperatures are reported in reduced units (i.e., normalized by $|\epsilon_{HB}|$). Likewise all distances are scaled by r_{HB}.

Monte Carlo simulations performed in this work were similar to those described earlier, but were carried out here in the canonical ensemble. Boxes containing 60 molecules at two densities (the ice density, $\rho \approx 0.7698$, and $\rho = 0.9$) were studied using standard periodic boundary conditions and the minimum image convention. Dilute nonpolar solutions contained 60 water molecules and one LJ solute (with the same well depth and contact parameters as the water molecules) fixed at the center of the simulation box. Starting configurations at each temperature were selected at random.

The model has been shown, using NPT Monte Carlo simulation, to have the correct qualitative temperature dependence of a variety of pure water properties, including the existence of a density anomaly and related negative thermal expansion coefficient at low temperature, a minimum in the isothermal compressibility, a large anomalous heat capacity, and spontaneous freezing to the d=2 model analog of ice, a low-density hexagonal crystal phase. Also, for the transfer of nonpolar solutes, the MB model predicts the correct temperature trends of the free energy, entropy, enthalpy, molar volume and heat capacity.

4.4.2 Fourier Expansion of the Angular Correlation Function

In principle, the two-body angular correlation function for d=2, $g^{(2)}_{WW}(r, \phi_1, \phi_2)$, can be accumulated in a simple 3-dimensional histogram. The histogram can then be

accurately numerically integrated, provided that the binsize is sufficiently small. We have gathered such histograms using a binsize for r and ϕ of 0.02 and 2° respectively. Reasonable convergence is achieved in 1×10^7 passes (1 pass = N molecules).

It is far more efficient, however, to expand the angular correlation function in a Fourier series. Streett and Tildesley have shown, in the analogous case for d=3 using spherical harmonics, that the coefficients of the series may be accumulated as a function of r as ensemble averages in the simulation [29]. Using this method for our system, excellent convergence of the correlation functions is attained in fewer than 5×10^5 passes, or about 1 to 2 orders of magnitude faster than the histogram. Such an expansion is crucial to the three-body case, rather than just convenient as it is here, since the three interparticle distances will already comprise a 3-dimensional histogram.

In Appendix C, we have shown that the two-body water-water angular correlation function can be expanded as the Fourier series

$$g^{(2)}_{WW}(r,\phi_1,\phi_2) = \sum_{m_1}\sum_{m_2} c(m_1,m_2;r)e^{im_1\phi_1}e^{im_2\phi_2},\ \ m_1,m_2 = 0,\pm3,\pm6,\ldots \qquad (4.13)$$

where i is the imaginary number, m_1 and m_2 are indices of the coefficients, and each of the coefficients themselves, $c(m_1,m_2;r)$ a function of r. Only indices that are multiples of 3 contribute to the series due to the $2\pi/3$ symmetry of the MB water molecule.

The coefficients of this series may be determined as a product of angle- and r-dependent terms which are accumulated as ensemble averages in the simulation:

$$c(m_1,m_2;r) = g^{(2)}_{WW}(r)\left\langle e^{-im_1\phi_1}e^{-im_2\phi_2}\right\rangle_{r+\Delta r}. \qquad (4.14)$$

The first term of the product is simply the centers-averaged pair correlation function. The second term is the ensemble average accumulated only over a shell about r of thickness Δr.

The expansion for the solute-water angular correlation function, $g^{(2)}_{SW}(r,\phi)$ is simpler, since the solute is isotropic. In this case, there is only one angular degree of freedom, ϕ, at the two-body level – that of the water molecule. Histograms of this function are slow to converge because there are statistically fewer water molecules around the solute than there are water-water pairs. Again, in this case, a corresponding Fourier series can greatly speed up convergence. Since this function is always symmetric about 0°, and there is only one angle, a much simpler Fourier cosine series expansion (which derived in a manner similar to the water-water series in Appendix C) may be used in the solute-water case:

$$g^{(2)}_{SW}(r,\phi) = \sum_m c_m(r) cos(m\phi), \quad m = 0,3,6,\ldots \tag{4.15}$$

In this case, the coefficients may be obtained from

$$c_m(r) = \begin{cases} g^{(2)}_{SW}(r) & m = 0 \\ 2g^{(2)}_{SW}(r)\left\langle cos(m\phi)\right\rangle_{r+\Delta r} & m = 3,6,9,\ldots \end{cases} \tag{4.16}$$

where $g^{(2)}_{SW}(r)$ is the centers-averaged solute-water pair correlation function, and the indicated ensemble average is defined as above.

4.4.3 Calculation of the Exact Entropy

The exact excess (xs) entropy (i.e., the sum of all terms beyond the ideal gas term) was computed for bulk water using thermodynamic integration by two independent

pathways: one at constant density, from the chosen temperature out to the infinite temperature regime; the other at constant temperature, from zero density up to the desired density. In principle, only one pathway is necessary, but both were done for verification of accuracy.

The entropy along the constant-ρ pathway is obtained from the thermodynamic relation

$$\frac{S^{xs}}{nk} = \int_{T_0}^{\infty} dT[C_v/T] \tag{4.17}$$

where T_0 is the temperature of interest, and C_v is the heat capacity, which is also a function of the temperature, T. This procedure yields the excess entropy for *any* temperature above T_0 at that fixed density. In practice, simulations can only be done at regular intervals up to some finite temperature. To overcome this obstacle, we performed more than a dozen simulations beyond a chosen temperature spanning 6 orders of magnitude in T, and fit the curve of C_v/T vs. T to an expression of the form $C_v/T = (c/T)^{\alpha}$ which went through all of the points within the error bars.

Along the constant-T pathway, the expression used by Hansen and Verlet [9] may be used to obtain the free energy:

$$\frac{F^{xs}}{nkT} = \int_0^{\rho_0} d\rho \left[\frac{\beta p/\rho - 1}{\rho}\right] . \tag{4.18}$$

Here, ρ_0 is the density of interest, p is the calculated pressure at each density ρ along the pathway, and $\beta p/\rho$ is the compressibility factor with $\beta \equiv 1/kT$. In practice, the compressibility factor is plotted as a function of density, and fit to a 5th or 6th order polynomial, which is forced to have a 0th order term of 1. In this manner, the above integral can easily be performed analytically. The excess entropy can then

be obtained from the usual relationship, $S^{xs}/nk = \beta U/n - \beta F^{xs}/n$, where U is the system energy at the given density and temperature.

For the case of the nonpolar solution, exact transfer entropies were computed using a fluctuation formula derived from the Widom method. This is the same approach used by Guillot and Guissani [7, 8] and us [26] in earlier works.

4.5 Results

4.5.1 Entropy of Bulk Water

The full two-body angular correlation function itself still comprises a four-dimensional plot, and hence cannot be visualized in its entirety. Thus we display cross sections of the full curve. Two such cross sections of the pure water distribution curve, $g_{WW}(r, \phi_1, \phi_2)$, are shown in Figure 4.2. The first surface plot shows the distributions of a second water molecule, when the first one is fixed to point one of its arms directly along the intermolecular axis (i.e., $\phi_1 = 0°$). It is clear that the second water molecule has a pronounced preference to be situated one H-bonding unit away, pointing its arm toward the first molecule. The large peak has been cut away in order to better visualize the undulations marking the subsequent shells of water. In the second plot of Figure 4.2, the first molecule is fixed at an angle of 30° relative to the intermolecular axis of a given pair. This angle is just the right angle for an intervening molecule to form a bridge with a second-shell water. In an ideal arrangement, such a second-shell molecule would also have an angle of 30° relative to the fixed molecule,

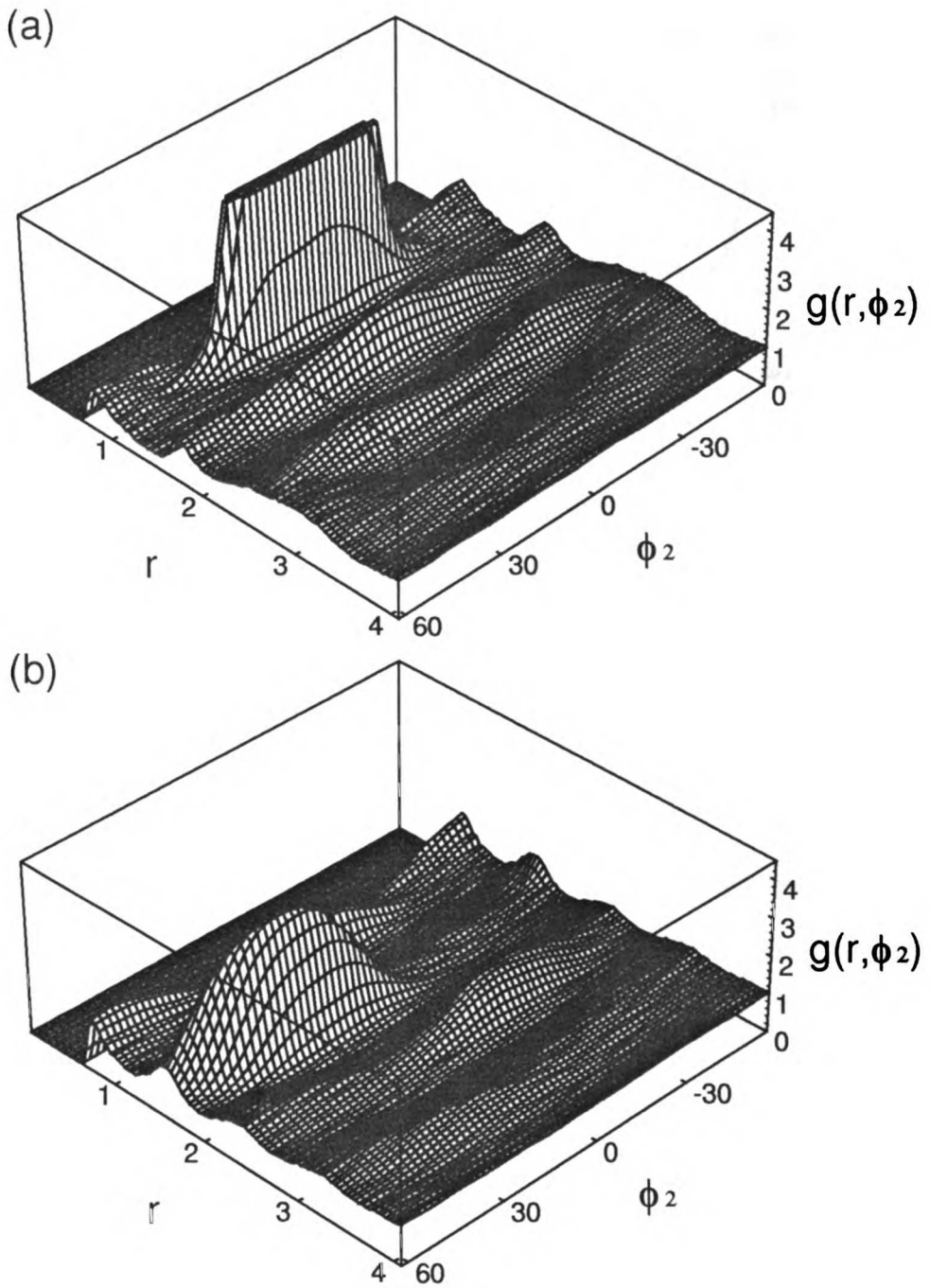

Figure 4.2: Two cross sections of the full water-water angular correlation curve $g_{WW}(r, \phi_1, \phi_2)$, where (a) $\phi_1 = 0°$ and (b) $\phi_1 = 30°$ for the phase point $T^* = 0.20$ and $\rho = 0.9$.

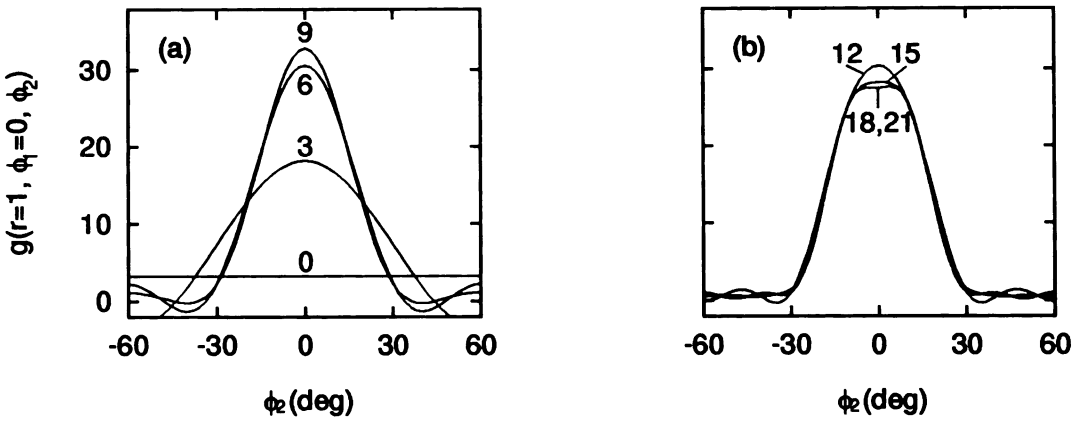

Figure 4.3: Convergence of the Fourier series estimate of $g^{(2)}_{WW}(r = 1.0, \phi_1 = 0°, \phi_2)$. (a) inclusion of all coefficients up to $m_1, m_2 = 0$ through ± 9 as indicated by the labels. (b) coefficients up to $m_1, m_2 = \pm 12$ through ± 21.

as shown by the largest peak.

The Fourier series used to expand the above correlation function converges with relatively few terms. In Figure 4.3 we show the progression of a portion of the correlation function, $g^{(2)}_{WW}(r = 1.0, \phi_1 = 0°, \phi_2)$, as higher order terms are added to the expansion. The 0th order term in Eq. 4.13 (i.e., $m_1, m_2 = 0$) has no angular dependence (see Figure 4.3). As more terms are added to the series, however, the peak at the angle which will align the arms quickly assumes its final shape.

The minimal contribution of higher order terms is more directly apparent in Figure 4.4. Here, we show the r-dependence of the real part of the coefficients themselves. The 0th order coefficient in Eq. 4.14 is the water-water pair correlation. Higher order coefficients make diminishing contributions which extend out to smaller radii.

The agreement between the direct histogram and series determinations of

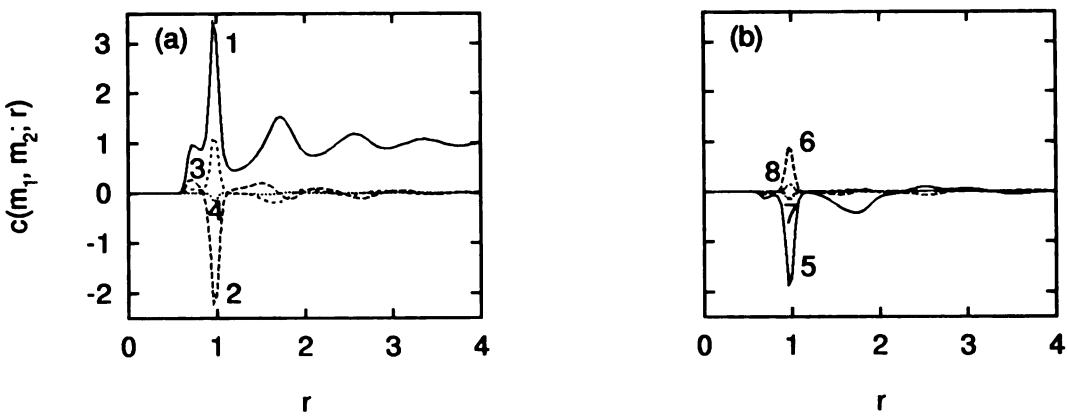

Figure 4.4: The real part of the coefficients (m_1, m_2) of the Fourier series estimate of $g^{(2)}_{WW}(r, \phi_1, \phi_2)$, as a function of r. (a) 1: (0,0), 2: (0,3), 3: (0,6), 4: (0,9) (b) 5: (3,3), 6: (3,6), 7: (3,9), 8: (3,12).

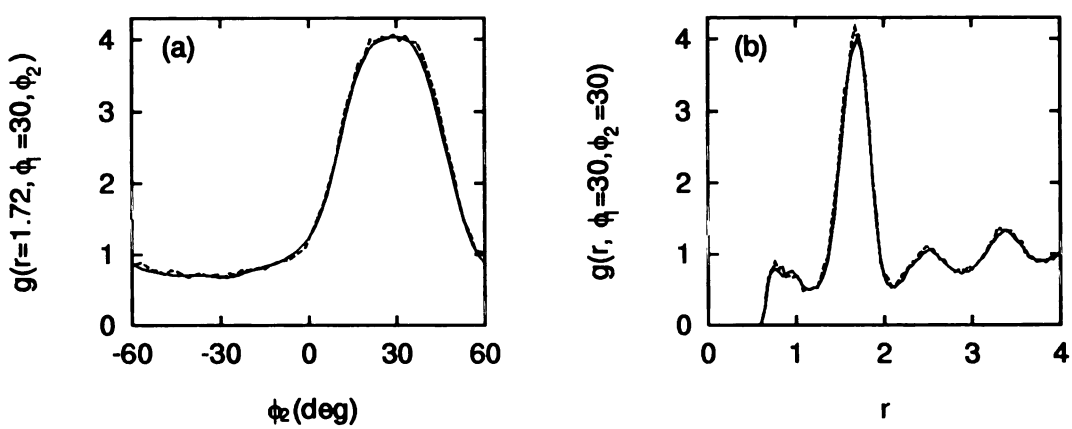

Figure 4.5: Comparison of the Fourier series (solid line) and histogram (dashed line) estimates for two cross sections of $g^{(2)}_{WW}(r, \phi_1, \phi_2)$: (a) as a function of ϕ_2 with r and ϕ_1 fixed at 1.72 and 30°, respectively. (b) as a function of r with ϕ_1 and ϕ_2 both fixed at 30°.

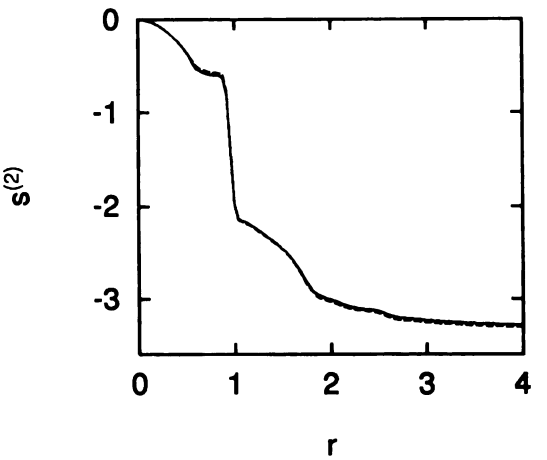

Figure 4.6: Comparison of the Fourier series (solid line) and histogram (dashed line) estimates for the 2-body entropy integral.

$g^{(2)}_{WW}(r, \phi_1, \phi_2)$ at a few chosen temperatures is excellent. Because of this fact, and the expense of accumulating histograms, correlation functions at all other temperatures were obtained only from the Fourier series method. Two separate one-dimensional cross sections of the function are plotted in Figure 4.5, comparing the two methods. Perhaps the most comprehensive measure of agreement is the two-body entropy expansion of Eq. 4.8. This integral is sensitive to all deviations from 1 in the correlation function. In Figure 4.6 we show the integral as a function of the radius for both the histogram- and Fourier-derived functions. From this figure, we see that (i) the integral converges at large r, and (ii) the histogram and series are in excellent agreement over the whole range of the correlation function.

The exact values for the excess entropy, computed separately using a constant-ρ and constant-T thermodynamic integration pathway were in excellent agreement with

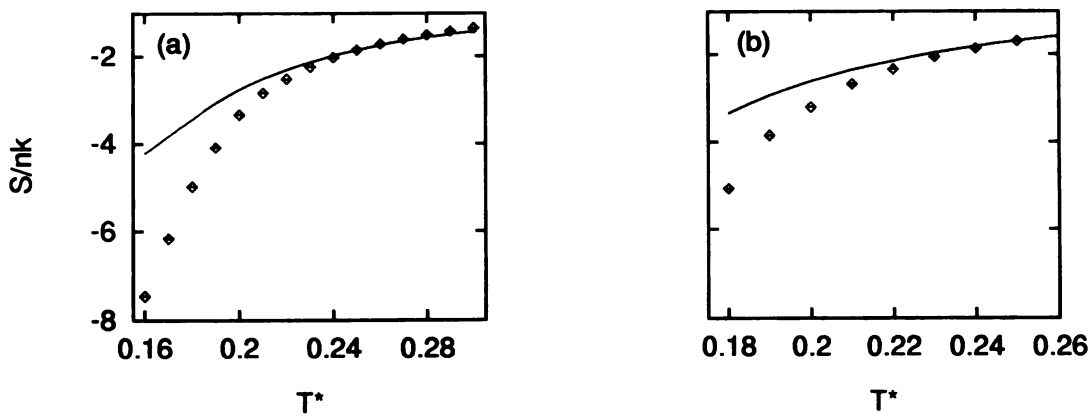

Figure 4.7: Comparison of the 2-body entropy term (diamonds) vs. the exact excess entropy (solid line, computed by thermodynamic integration) for the pure liquid. Trends are shown as a function of reduced temperature for two different densities: (a) $\rho = 0.9$, (b) $\rho = 0.7698$.

each other. For the phase point, $T^* = 0.20$, $\rho = 0.7698$, the two pathways yielded values of -2.63 and -2.64 respectively. Similarly, for the phase point $T^* = 0.20$, $\rho = 0.9$, the two values obtained were -2.78 and -2.82.

In Figure 4.7 we compare the 2-body entropy with the exact excess values for two densities over a range of temperatures. It is clear that at high temperatures, the 2-body term accounts for essentially all of the excess entropy (deviations are probably due to the finite size of the bins used in the numerical integration procedure). But at lower temperatures, the two-body approximation leads to a significant *overestimate* of the true model entropy. (The lowest temperatures shown are just above the freezing point of MB water at these densities.) This discrepancy at low temperature must be made up by 3- and higher-body terms. Note that the temperature dependence

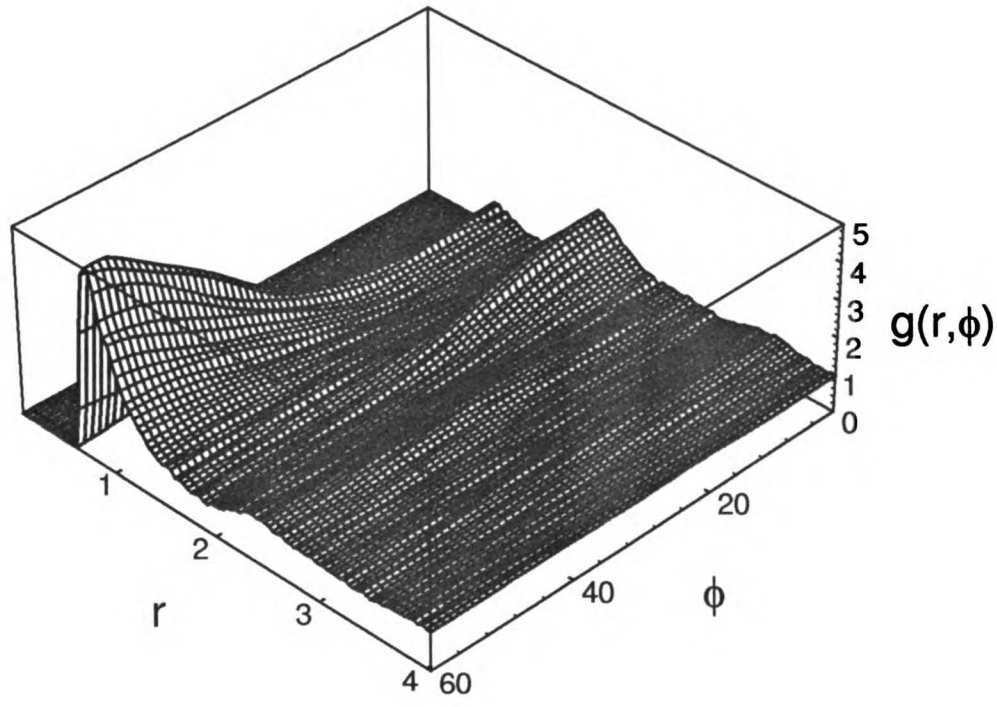

Figure 4.8: The full solute-water angular correlation curve $g_{SW}(r, \phi)$ for the phase point $T^* = 0.20$ and $\rho = 0.9$.

predicted by the two-body expression deviates significantly from the actual value.

4.5.2 Entropy for a Nonpolar Solute Molecule in Water

Figure 4.8 shows the full angular solute-water correlation curve, $g_{SW}(r, \phi)$. The first shell molecules prefer to straddle the solute (i.e., form a 60° angle), as we noted earlier [26]. Similarly second-shell waters show a preference to point their arms towards the first-shell molecules (and hence towards the solute) as well.

The Fourier cosine series used to expand this function requires only 3 terms for convergence. In Figure 4.9, we show the r-dependence of the coefficients and the

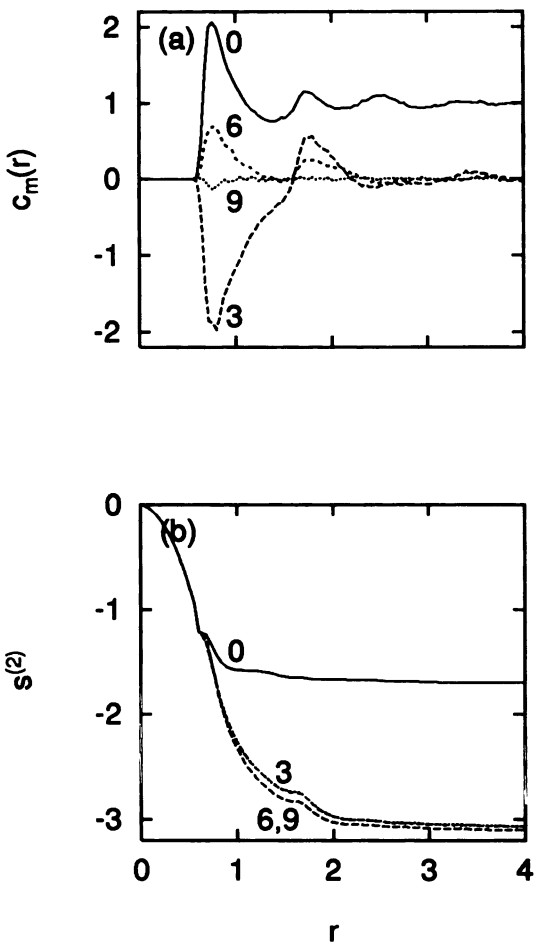

Figure 4.9: Convergence of the Fourier series expansion for the solution. (a) the coefficients ($m = 0 - 9$) themselves, as a function of r. (b) the corresponding entropy integral computed up to the order indicated by the labels.

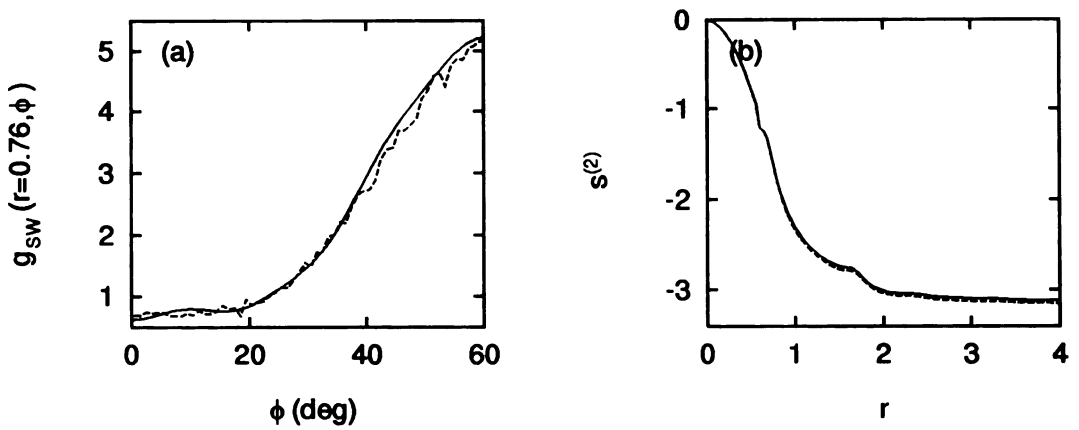

Figure 4.10: Comparison of the Fourier series (solid line) and histogram (dashed line) estimates for $g^{(2)}_{SW}(r,\phi)$. (a) a cross section of the correlation function as a function of ϕ with r fixed at 0.76. (b) the solute-water 2-body entropy integral.

entropy integral, which is computed from the correlation function truncated at each order. Since the 0th order term of Eq. 4.15 contains no angular information, the corresponding entropy integral corresponds simply to that which would be obtained by integrating only the centers-averaged pair correlation function. Figure 4.9 (b), shows that the angular contributions to the entropy are significant. In Figure 4.10 we compare the histogram and series estimates of the correlation function, using a cross section of the function itself, and the full entropy integral. Again, the agreement is excellent, with the series yielding better converged values.

In Figure 4.11 we compare the 2-body entropy term with the exact transfer entropy computed by the Widom fluctuation formula. Just as in the pure water case, the two curves are in excellent agreement at high temperature. Again, however, they deviate significantly at low temperature, where a similar overestimate of the entropic order

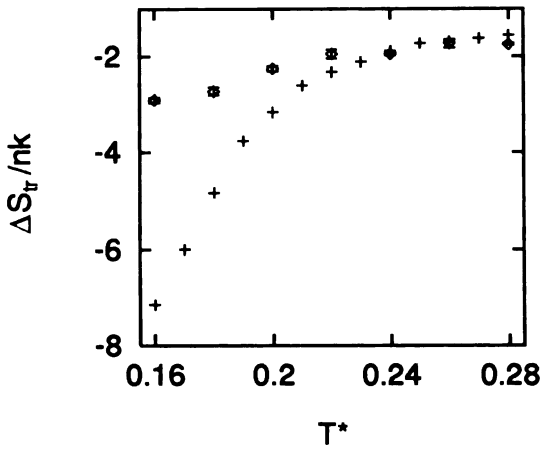

Figure 4.11: Comparison of the 2-body transfer entropy (+) vs. the corresponding exact value ($\diamond$, computed using the Widom particle insertion method) at $\rho = 0.9$. Trends are shown as a function of reduced temperature for the transfer of a simple inert Lennard-Jones solute with the same size as the solvent.

is observed relative to the corresponding exact values.

We have tested two approximations for the pair term which attempt to decouple translational and orientational components of the pair entropy of hydrophobic hydration. In view of the above results, such an approximate decoupling would be of practical value at the temperatures of interest if equally accurate and simple approximations where found for the higher order terms, and we know of no such approximations at present. In the approximation for the pair term, if it is assumed that (1) there are no orientational correlations (relative to the solute) beyond the first shell of waters, and (2) within a shell, water orientations have a homogeneous distribution, then the transfer entropy arising from solute-water correlations can be formally

separated into the following components [19, 21]:

$$\Delta s^{(2)} = \Delta s^{tr} + \Delta s^{or} \text{ , and} \tag{4.19}$$

$$\Delta s^{tr} = -\rho_W \int_0^\infty d\mathbf{r} \left[g_{SW}(\mathbf{r}) \ln g_{SW}(\mathbf{r}) - g_{SW}(\mathbf{r}) + 1 \right] . \tag{4.20}$$

The solute-water correlation function displayed here is merely a function of the center of mass positions of the two respective particles, and,

$$\Delta s^{or} = -\sum_{sh_i} \frac{N_{W,sh_i}}{\Omega} \int d\omega_W \left[p_{sh_i}(\omega_W) \ln p_{sh_i}(\omega_W) \right] , \tag{4.21}$$

where N_{W,sh_i} and $p_{sh_i}(\omega_W)$ are simply the coordination number and the orientational probability distributions, respectively, of the waters in the ith shell. The orientational probabilities are all normalized such that $\int d\omega_W p(\omega_W) = \Omega$.

As shown in Figure 4.12, at all temperatures, an extended version of this approximation (in which the orientations of waters in three shells, rather than simply the first one are included) does remarkably well at reproducing the full two-body angular entropy. More importantly, it is apparent in the second plot of Figure 4.12 that the orientational degrees of freedom of the water are far more temperature sensitive than the corresponding translational distributions.

4.6 Conclusions

We have used a multiparticle expansion of the entropy to calculate the two-body contribution for MB water, and a dilute hydrophobic solution. To do this, we calculate full angle-dependent pair correlation functions.

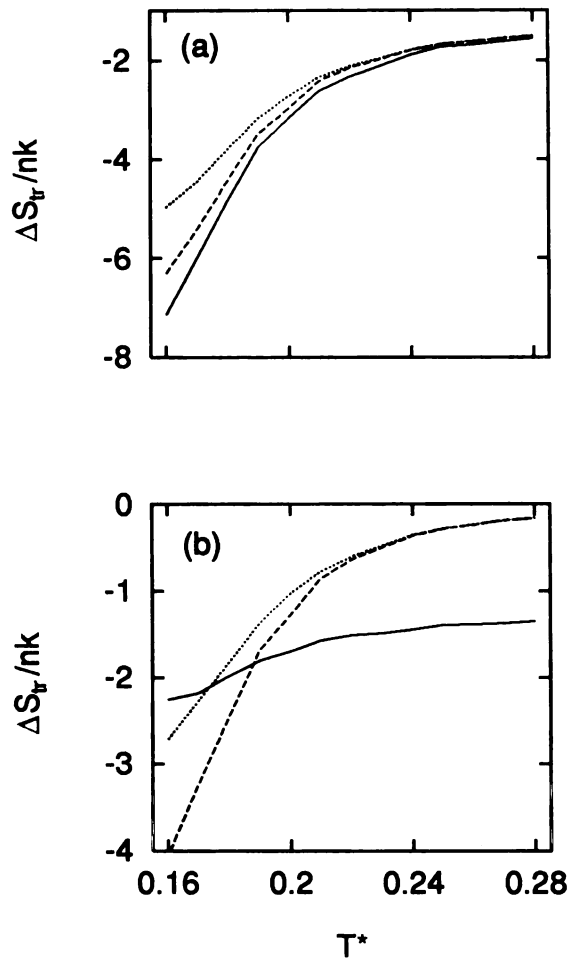

Figure 4.12: Decoupling of translational and orientational contributions to the entropy of transfer at $\rho = 0.9$. (a) Comparison of $\Delta s^{(2)}$ (solid line) with $\Delta s^{tr} + \Delta s^{or}$ (dotted line: orientations in the first shell included; dashed line: orientations in the first 3 shells included). (b) Temperature dependence of Δs^{tr} (solid line) and Δs^{or} (dotted line: fist shell; dashed line: first 3 shells).

We have determined that the two-body term overestimates the exact entropy at low temperatures for both the pure liquid and for simple nonpolar solute transfers. At high temperatures, the agreement is remarkably good.

We have tested the assumptions of Lazaridis and Paulaitis [19] in which the translational and orientation components of the transfer entropy for simple solutes are assumed to be independent. When the orientations of only a single shell are included, their approximation underestimates the two-body entropy term at low temperature. This underestimate, combined with the overestimate of the full two-body term, with respect to the total excess entropy, leads to a fortuitous cancellation between two unrelated errors as suggested by Smith *et al.* [28]. However, if the method of Lazaridis and Paulaitis is extended to multiple shells, then the agreement of their approximation with the full two-body term is reasonably good. Hence, the approximation appears to be a valid means to avoid calculating the full angular correlation function at the two-body level. In order to be of practical value, similar approximations of comparable accuracy will need to be made for the other terms that contribute to the full entropy.

Since it is clear that 2-body correlations alone fail to quantitatively account for entropy penalty incurred by solute transfer as well as the temperature dependence, the natural next step is to see if inclusion of 3-body terms is sufficient.

4.7 Acknowledgements

KATS greatfully acknowledges support under a U.S. National Science Foundation Graduate Research Fellowship and a UCSF Regent's Fellowship. In Australia, this research was supported by the Australian Research Council (ARC) (Grant No. A29530010), and SydCom, the USyd/UTS Distributed Computing Facility funded by an ARC infrastructure grant. In addition, KATS would like to thank Karen Tang for many pertinent and lengthy discussions.

Bibliography

[1] H. S. Ashbaugh and M. E. Paulaitis. Entropy of hydrophobic hydration: Extension to hydrophobic chains. *J. Phys. Chem.*, 100:1900–1913, 1996.

[2] A. Baranyai and D. J. Evans. Direct entropy calculation from computer simulation of liquids. *Phys. Rev. A*, 40:3817–3822, 1989.

[3] A. Ben-Naim. Statistical mechanics of 'waterlike' particles in two dimensions. I. Physical model and application of the Percus-Yevick equation. *J. Chem. Phys.*, 54(9):3682–3695, 1971.

[4] H. S. Frank and M. W. Evans. *J. Chem. Phys.*, 13:507, 1945.

[5] C. G. Gray and K. E. Gubbins. *Theory of molecular fluids.* Clarendon Press, Oxford, U.K., 1984.

[6] H. S. Green. *The Molecular Theory of Fluids.* North-Holland, Amsterdam, 1952.

[7] B. Guillot and Y. Guissani. A computer simulation study of the temperature dependence of the hydrophobic hydration. *J. Chem. Phys.*, 99(10):8075–8094, 1993.

[8] B. Guillot, Y. Guissani, and S. Bratos. A computer-simulation study of hydrophobic hydration of rare gases and of methane. I. Thermodynamic and structural properties. *J. Chem. Phys.*, 95(5):3643–3648, 1991.

[9] J.-P. Hansen and L. Verlet. Phase transitions of the Lennard-Jones system. *Phys. Rev.*, 184(1):151–161, 1969.

[10] A. D. J. Haymet, K. A. T. Silverstein, and K. A. Dill. Hydrophobicity reinterpreted as "minimization of the entropy penalty of solvation". *Faraday Discuss.*, 103:117–124, 1996.

[11] A. D. J. Haymet, K. A. T. Silverstein, and K. A. Dill. Hydrophobicity. In *International Symposium on Molecular Thermodynamics and Molecular Simulation*, pages 143–152, Tokyo, Japan, Jan 12-15 1997. Hosei University.

[12] J. A. Hernando. Thermodynamic potentials and distribution functions I. A general expression for the entropy. *Molecular Physics*, 69:319–326, 1990.

[13] J. A. Hernando. Thermodynamic potentials and distribution functions II. The HNC equation as an optimized superposition approximation. *Molecular Physics*, 69:327–336, 1990.

[14] J. G. Kirkwood. *J. Chem. Phys.*, 10:394, 1942.

[15] B. B. Laird and A. D. J. Haymet. Calculation of the entropy from multiparticle correlation functions. *Phys. Rev. A*, 45(8):5680–5689, 1992.

[16] B. B. Laird and A. D. J. Haymet. Calculation of the entropy of binary hard sphere mixtures from pair correlation functions. *J. Chem. Phys*, 97(1):2153–2155, 1992.

[17] B. B. Laird and A. D. J. Haymet. Entropy of electrolytes. *J. Chem. Phys.*, 100:3775–3779, 1994.

[18] B. B. Laird, J. Wang, and A. D. J. Haymet. Consistent integral equations for two- and three-body force models: Application to a model of silicon. *Phys. Rev. E*, 47:2491, 1993.

[19] T. Lazaridis and M. E. Paulaitis. Entropy of hydrophobic hydration: A new statistical mechanical formulation. *J. Phys. Chem.*, 96:3847–3855, 1992.

[20] T. Lazaridis and M. E. Paulaitis. Reply to the comment on 'entropy of hydrophobic hydration: A new statistical mechanical formulation'. *J. Phys. Chem.*, 97:5789–5790, 1993.

[21] T. Lazaridis and M. E. Paulaitis. Simulation studies of the hydration entropy of simple, hydrophobic solutes. *J. Phys. Chem.*, 98:635–642, 1994.

[22] L. Lee. Chemical potentials based on the molecular distance functions. *J. Chem. Phys.*, 97:8606, 1992.

[23] R. E. Nettleton and M. S. Green. *J. Chem. Phys.*, 29:1365, 1958.

[24] H. J. Raveché. Entropy and molecular correlation functions in open systems. I. Derivation. *J. Chem. Phys.*, 55:2242–2250, 1971.

[25] K. A. T. Silverstein, K. A. Dill, and A. D. J. Haymet. Hydrophobicity in a simple model of water: solvation and hydrogen bond energies. In *Thirteenth Symposium on Thermophysical properties*, Boulder, Colorado, June 22-27 1997. National Institute of Standards and Technology.

[26] K. A. T. Silverstein, A. D. J. Haymet, and K. A. Dill. A simple model of water and the hydrophobic effect. Submitted to the *Journal of the American Chemical Society*, 1997.

[27] K. A. T. Silverstein, A. D. J. Haymet, and K. A. Dill. A model of the hydrophobic effect. To be submitted to the *Proceedings of the National Academy of Sciences, USA*, Dec 1997.

[28] D. E. Smith, B. B. Laird, and A. D. J. Haymet. Comment on 'entropy of hydrophobic hydration: A new statistical mechanical formulation'. *J. Phys. Chem.*, 97:5788, 1993.

[29] W. B. Streett and D. J. Tildesley. Computer simulations of polyatomic molecules I. Monte Carlo studies of hard diatomics. *Proc. R. Soc. Lond. A.*, 348:485–510, 1976.

[30] D. C. Wallace. On the role of density fluctuations in the entropy of a fluid. *J. Chem. Phys.*, 87:2282–2285, 1987.

Chapter 5

Future Directions

With only a limited amount of computer time we have been able to conduct a varied and extensive study on a simple model of water and inert gas solutions. The scope of this MB model should not stop here. There are numerous fundamental problems which still remain unresolved, and are clearly within the domain of the model. In this chapter, I will briefly outline some of these problems for which today's computers are already sufficient using the MB model.

5.1 Convergence Temperatures

If the transfer entropies and enthalpies as a function of temperature are plotted for solutes of different size, an interesting observation is made: Each of the entropy curves (and separately the enthalpy curves) converge at a unique temperature[1, 13] (T_S^* and T_H^* for entropy and enthalpy, respectively). In other words, at some temperature T_S^*, the transfer entropy is independent of solute size, and a similar situation holds at a different temperature for the enthalpy. This curious behavior was explained *mathematically* by Lee[21]. He showed using basic algebra, that if (i) the enthalpy and entropy scale linearly with some property of the solute (e.g., the surface area or the number of hydrogens in the hydrocarbon) – which must hold since the free energy is also linearly dependent on that same property[6, 13, 15], and if (ii) the heat capacity change is independent of the temperature over the limited temperature range of interest, then the convergence temperatures must exist.

Using the Widom insertion method, we can quickly get an idea whether the convergence behavior occurs in the MB model. In Figure 5.1 we see that the enthalpies

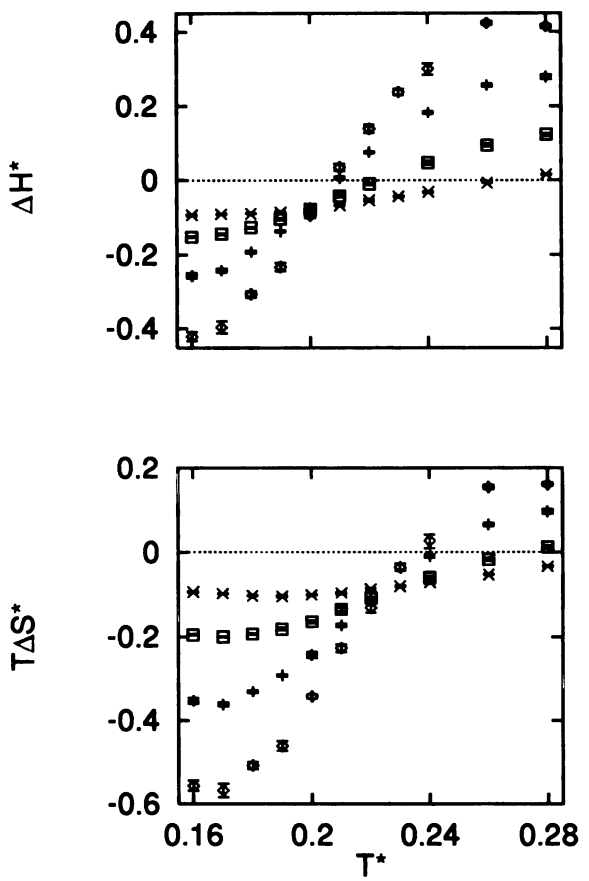

Figure 5.1: The (a) enthalpies and (b) entropies of transfer as a function of temperature for several solute diameters: (×), 0.1; (□), 0.3; (+), 0.5; (◇), 0.7.

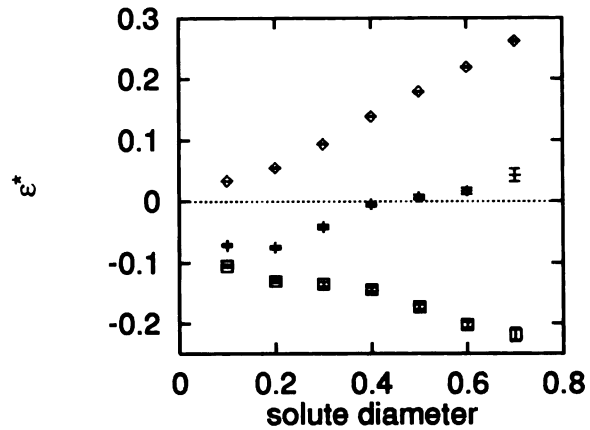

Figure 5.2: The (◇) free energy, (+) enthalpy, and (□) entropy of transfer as a function of solute diameter at $T^* = 0.21$.

and entropies of transfer do indeed converge at distinct temperatures in the model. Furthermore, Figure 5.2 demonstrates that the enthalpy, entropy and free energy all scale with solute diameter (which is proportional to the perimeter in 2D). Lee's assumption of constant heat capacity also holds over the range of temperatures encompassing both convergences, as shown in Figure 5.3.

All of this evidence is suggestive that the model has in it the proper physics. The difficult part is determining what the *physical* cause of the convergence is, regardless of the mathematical truism that implies its existence. Garde *et al.*[10] have suggested a link of the convergence temperatures to the relative temperature insensitivity of water's isothermal compressibility compared to simple liquids. They used an information theory model which tracks the fluctuations of void volumes in standard simulated water models. It would be interesting to investigate this and related microscopic factors which could lead to the solute-size-independent thermodynamics

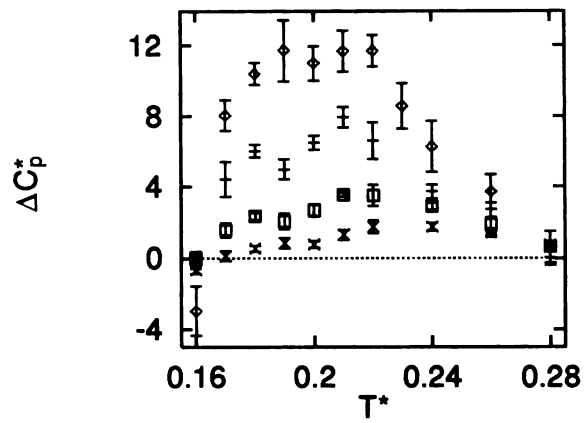

Figure 5.3: The heat capacity of transfer for several solute diameters: (×), 0.1; (□), 0.3; (+), 0.5; (◇), 0.7.

at the convergence temperatures in the MB model.

5.2 Other Problems

Numerous other issues can be addressed with today's computational power with the MB model. Below, I have itemized a list of some of those that are likely to bear fruit.

1. **Solute Size and Curvature Effects.** What are the effects of solute size, shape, and curvature on hydrophobicity? Throughout most of the literature, only a very small range of solute diameters have been systematically investigated (Ne-Xe, corresponding to diameters of 3.04 to 3.98 $\AA$). (One exception is the work of Wallqvist and Berne[36], who have looked at larger spheres and ellipses Due to computational time requirements, however, this study reported only free energy changes and shell coordination numbers. In principle, we can investigate

the full range of thermodynamic trends (including temperature dependence) as a function of solute size, shape, and curvature. Such a comprehensive study currently cannot be done with traditional water models. At some point, we will hit a limit beyond which clathration of waters around the solute will no longer be feasible. This must also hold in the 3-dimensional world. By systematically investigating different solute sizes and shapes we will determine (a) if certain shapes "fit" naturally into the surrounding solvent structure and (b) if there is a predictive rule of which do and don't. In such a study, we would expect to see a curvature dependence due to the incompatibility of solute structures and water geometry. Careful free energy determinations of the various shapes and curvatures may allow us to reconcile the factor of 3 difference in microscopic and macroscopic surface tension measurements [34].

2. **Role of Solvent Size.** What are the necessary ingredients for water's anomalous properties? Several researchers [20, 22, 31, 32] have argued that water's anomalous solvation properties are simply due to its unusually small size. This conclusion is in apparent conflict with much of the computational literature and the results obtained here, where hydrogen bonds play a key role. Much of the disagreement appears to arise from different definitions of hydrophobicity. Solvent size may indeed be a factor in determining the poor solubility of hydrophobic compounds in water. However we have shown that the marked temperature dependence is dependent on the unusual structural peculiarities of water (and it is likely that solvent-mediated effects *between* solutes are de-

pendent on the structuring as well). We believe this temperature dependence, as signified by the large heat capacity, and the structural features of water are crucial to the understanding of water's anomalous solvation behavior. Hence, we hope to clarify which thermodynamic properties arise from water's small size and also from the hydrogen bonds. To do this the current results should be compared to transfers in a simple LJ fluid with particles the same size as our current model water. Such a comparison, focusing on cavity distributions, has been conducted at a single phase point [32], however the LJ system in this study was under unphysical and inappropriate conditions (at a temperature and pressure that is near-critical, so that the LJ fluid would have a density comparable to water). It is possible, using a 2D model, to examine a far wider range of the solvation behavior (i.e. enthalpy, entropy, free energy, heat capacity, structure, etc.) in the reference LJ fluid *throughout the liquid range* to avoid the complication of an improper reference system.

3. **Const-p vs. Const-V Transfers.** Since the paper of Honig *et al.*[34], argument has surfaced over the difference of const-P vs. const-V transfers[2]. Matubayasi and Levy[28, 29] and Cann and Patey[5] have laid down some theoretical arguments for the differences in the two ensembles. While the difference between the two *at a single phase point* is merely a pV term (which is insignificant for real water), if you consider any dependence (e.g., temperature) of the transfer thermodynamics, they could be drastically different at const-P vs. const-V (because the pathways in phase space are very different). Our ability

to address this issue may be limited by the fact that the pV term in MB water is significant (due to our relatively high pressures).

4. **3-body Correlations.** Since we have shown that the two-body term overestimates the entropy, it is worth investigating whether the next term in the expansion is sufficient, or whether the series is non-convergent, as our exhaustive enumerations might suggest. Without question, the 3-body term can be calculated with current computer power in the MB model (and the full angular terms are impossible in 3D, since the necessary spherical harmonic expansion would require a prohibitive number of terms to converge[35]).

5. **Ring Entropy term.** As Laird and Haymet[19] have shown, Hernando's ring term[16, 17] (a summation of the 3- and higher-body closed-circuit configurations that merely requires the Fourier transform of a 2-body correlation function) recovers most of the excess entropy that is due to 3 and higher-body terms in the case of simple atomic fluids. A similar term may do the same for angle-dependent potentials such as MB water.

6. **Solutions of Model Methanol.** With simply the addition of a single, rotating arm on the solute, we can model methanol, and it's full temperature dependence with temperature. Since methanol is soluble in water, a lot of experimental data (including structural information from diffraction studies) is available for comparison.

7. **Comparisons of Model Water and Hydrazine.** The solubility of apolar compounds is anomalously low in hydrazine at room temperature[25]. Like water, this has been attributed[24] to the extensive H-bonding structure of the liquid. However, a large opposing entropy and compensating favorable enthalpy change accompanies the transfer of argon from hydrazine to water. This suggests there are great differences in the molecular details of the transfers in these two systems, which are masked by the comparatively small change in free energy. In our simple system, hydrazine can be modeled by joining 2 waters together at one of the "arms".

8. **Pressure effects.** Alkanes and alkanols have very different ΔV_{tr} values. With just the addition of a H-bonding group, alkanols have much smaller negative volumes of transfer (from pure phase to water) than their alkane counterparts[9, 27]. Also, Kauzmann was frustrated by the inconsistency of ΔV_{tr} for these model compounds with ΔV_{unf} for proteins[18]. Hence it would be valuable to gain a better understanding of the structural origins of the unusual pressure effects on pure water and solvation. In conventional MD studies, Billeter and van Gunsteren[3] have determined recently that, whereas energies and structural averages converge on the order of 10 ps, simulations on the order of 1 ns are needed to get converged values for $< p >$ or $< v >$ for systems of about 100 particles. Hence the need for fast computations, or a simple model such as ours, is evident.

9. **Additivity of functional groups.** In the literature, there are numerous assumptions of additivity of functional groups in solvation (e.g., alcohol or OH groups have a certain contribution, hydrophobic groups have a given contribution per unit surface, etc.) Typically the standard errors in these fits are 20-40%. A careful study could show structurally why such additivity assumptions may not be such a good thing.

10. **Non-additivity of Multiple Solutes.** So far we have not addressed hydrophobic *interactions.* While numerous studies have looked at the potential of mean force for 2 LJ solutes coming together in water, very few studies (only Palma's group[4]) have looked at the effects of the presence of a third fixed solute on the PMF of 2 solutes. Systematic studies should be done to approach bulk hydrophobic interactions.

11. **Long-range Surface Forces.** Several recent studies of solvent induced forces between apolar planar surfaces have suggested that forces may exist even up to 70-90 nm[7, 8]. (this would suggest that attractive forces are transmitted over distances corresponding to 300 interfacial water molecules!). Simulational studies have indicated that structuring away from such walls does not penetrate far into the medium[23, 26]. In 3D simulations, however, the walls are never really all that far apart because of the huge numbers of waters needed in between (a problem not present with the 2D MB model).

12. **Role of Bifurcated and Stretched H-bonds.** Bifurcated H-bonds have been observed spectroscopically in liquid water[11, 12]. Sciortino *et al.*[33] has argued

that bifurcated H-bonds are a major cause of hydrophobic effects. In bulk water, the presence of such bonds cause defects in the tetrahedral arrangements. This allows quick flipping to alternative structures. The presence of a solute, however, precludes such bifurcated H-bonds, due to excluded volume effects. Hence, the shell molecules slow down, and become trapped into fewer configurations. In our model, we can split the Gaussian width, σ_{HB}, into two parameters: one for the bond stretching term, and one for the H-bond bending term. By adjusting one or the other, thermodynamic comparisons can be made to systems with more/less allowed H-bond stretching and bending.

13. **Solvent-geometry Effects.** It appears that clathration plays an important role at low temperature in providing a few, low energy arrangements for the water around a solute. A comparison of 3-arm and 4-arm water may be interesting to show effects of the solvent geometry on the resulting structure and thermodynamics.

14. **Dielectric constant.** Currently our model has no dipole, and hence no dielectric constant. If we move to four arms, and allow 2 arms to attract the other two, then we will have a model of water that has polarity. Then we would be able to investigate dielectric behavior.

15. **Explicit Electrostatics.** Another variant of the model may be made (possibly necessary for charged ions) which has explicit charges on the arms. One could use a model similar to the four arm 2D model of Okazaki *et al.*[30].

16. **Ionic Solvation.** Helgeson *et al.* have suggested that the heat capacity of ions has a very different, though significant, heat capacity as a function of temperature[14]. We can try to model ionic solvation with the simple 4-arm dipolar liquid (no explicit charge). If it fails to look like experiments, then we can add explicit charges (and even polarization if necessary). Additionally, many of the studies described above for hydrophobic solutes can be extended to ionic species.

5.3 Concluding Remarks

The model potentially has a wide range of applications for which it shows promise. Its simple nature should make it easier to determine the essential ingredients of these problems. If the model fails to predict a property, it is much easier to test the addition of new features in a simple model, than it is to conjecture as to what went wrong in a model that was supposedly a realistic representation of water. Additionally, as we have seen, simple models often offer some fundamental surprises and insights into the physical nature of a system. For example, the current study has demonstrated (i) that one need not invoke long-range electrostatics to describe hydrophobic trends, nor to model many of water's anomalous properties; (ii) that a clear link of the molecular hydrogen-bond structuring to the thermodynamics of hydrophobic transfers exists; and (iii) that this structuring is marked by a strong many-body nature. We look forward to the future for more insights from the model.

Bibliography

[1] R. L. Baldwin. Temperature dependence of the hydrophobic interaction in protein folding. *Proc. Natl. Acad. Sci. USA*, 83:8069–8072, 1986.

[2] A. Ben-Naim and R. M. Mazo. Size dependence of the solvation free energies of large solutes. *J. Phys. Chem.*, 97:10829–10834, 1993.

[3] S. R. Billeter, P. M. King, and W. F. van Gunsteren. Can the density maximum of water be found by computer simulation? *J. Chem. Phys.*, 100(9):6692–6699, 1994.

[4] F. Bruge, S. L. Fornili, G. G. Malenkov, M. B. Palma-Vittorelli, and M. U. Palma. Solvent-induced forces on a molecular scale: Non-additivity, modulation, and causal relation to hydration. *Chem. Phys. Lett.*, 254:283–291, 1996.

[5] N. M. Cann and G. N. Patey. An investigation of the influence of solute size and insertion conditons on solvation thermodynamics. *J. Chem. Phys.*, 106(19):8165–8195, 1997.

[6] C. Chothia. *Nature*, 248:338–339, 1974.

[7] H. K. Christenson, P. M. Claesson, J. Berg, and P. C. Herder. Forces between fluorocarbon surfactant monolayers: salt effects on the hydrophobic interaction. *J. Phys. Chem.*, 93:1472–1478, 1989.

[8] P. M. Claesson and H. K. Christenson. Very long range attractive forces between uncharged hydrocarbon and fluorocarbon surfaces in water. *J. Phys. Chem.*, 92:1650–1655, 1988.

[9] M. E. Friedman and H. A. Scheraga. Volume changes in hydrocarbon-water systems. partial molal volumes of alcohol-water solutions. *J. Phys. Chem.*, 69(11):3795–3800, 1965.

[10] S. Garde, G. Hummer, A. E. García, M. E. Paulaitis, and L. R. Pratt. Origin of entropy convergence in hydrophobic hydration and protein folding. *Phys. Rev. Lett.*, 77:4966–4968, 1996.

[11] P. A. Giguere. Bifurcated hydrogen bonds in water. *Journal of Raman Spectroscopy*, 15(5):354–359, 1984.

[12] P. A. Giguere and M. Pigeon-Gosselin. The nature of free OH groups in water. *Journal of Raman Spectroscopy*, 17:341–344, 1986.

[13] S. J. Gill and I. Wadso. An equation of state describing hydrophobic interactions. *Proc. Natl. Acad. Sci. USA*, 73(9):2955–2958, 1976.

[14] H. C. Helgeson, D. H. Kirkham, and G. C. Flowers. Theoretical prediction of the thermodynamic behavior of aqueous electrolytes at high pressures and

temperatures. IV. Calculation of activity coefficients, osmotic coefficients, and apparent molal properties to 600 degrees C and 5 kb. *Am. J. Science*, 281:1249–1516, 1981.

[15] R. B. Hermann. *J. Phys. Chem.*, 79:163–169, 1975.

[16] J. A. Hernando. Thermodynamic potentials and distribution functions I. A general expression for the entropy. *Molecular Physics*, 69:319–326, 1990.

[17] J. A. Hernando. Thermodynamic potentials and distribution functions II. The HNC equation as an optimized superposition approximation. *Molecular Physics*, 69:327–336, 1990.

[18] W. Kauzmann. Thermodynamics of unfolding. *Nature*, 325:763–764, 1987.

[19] B. B. Laird and A. D. J. Haymet. Calculation of the entropy from multiparticle correlation functions. *Phys. Rev. A*, 45(8):5680–5689, 1992.

[20] B. Lee. The physical origin of the low solubility of nonpolar solutes in water. *Biopolymers*, 24:813–823, 1985.

[21] B. Lee. Isoenthalpic and isoentropic temperatures and the thermodynamics of protein denaturation. *Proc. Natl. Acad. Sci. USA*, 88:5154–5158, 1991.

[22] B. Lee. Solvent reogranization contribution to the transfer thermodynamics of small nonpolar molecules. *Biopolymers*, 31(8):993–1008, 1991.

[23] C. Y. Lee, J. A. McCammon, and P. J. Rossky. The structure of liquid water at an extended hydrophobic surface. *J. Chem. Phys.*, 80(9):4448–4455, 1984.

[24] R. Lumry. *Bioenergetics and thermodynamics. Model systems.* Reidel, Dordrecht, 1980.

[25] R. Lumry, E. Battistel, and C. Jolicoeur. Geometric relaxation in water: it's role in hydrophobic hydration. *Faraday Symp. Chem. Soc.*, 17:93–108, 1982.

[26] A. Luzar, D. Bratko, and L. Blum. Monte Carlo simulation of hydrophobic interaction. *J. Chem. Phys.*, 86(5):2955–2959, 1987.

[27] W. L. Masterson. Partial molal volumes of hydrocarbons in water solution. *J. Chem. Phys.*, 22(11):1830–1833, 1954.

[28] N. Matubayasi. Matching-mismatching of water geometry and hydrophobic hydration. *J. Am. Chem. Soc.*, 116:1450–1456, 1994.

[29] N. Matubayasi and R. M. Levy. Thermodynamics of the hydration shell. 2. Excess volume and compressibility of a hydrophobic solute. *J. Phys. Chem.*, 100:2681–2688, 1996.

[30] K. Okazaki, S. Nosé, Y. Kataoka, and T. Yamamoto. Study of liquid water by computer simulations. I. Static properties of a 2D model. *J. Chem. Phys.*, 75(12):5864–5874, 1981.

[31] A. Pohorille and L. R. Pratt. Cavities in molecular liquids and the theory of hydrophobic solubilities. *J. Am. Chem. Soc.*, 112:5066–5074, 1990.

[32] L. R. Pratt and A. Pohorille. Theory of hydrophobicity: Transient cavities in molecular liquids. *Proc. Natl. Acad. Sci. USA*, 89:2995–2999, April 1992.

[33] G. Sciortino, A. Geiger, and H. E. Stanley. Effect of defects on molecular mobility in liquid water. *Nature*, 354:218–221, 1991.

[34] K. A. Sharp, A. Nicholls, R. F. Fine, and B. Honig. Reconciling the magnitude of the microscopic and macroscopic hydrophobic effects. *Science*, 252:106–109, 1991.

[35] W. B. Streett and D. J. Tildesley. Computer simulations of polyatomic molecules I. Monte Carlo studies of hard diatomics. *Proc. R. Soc. Lond. A.*, 348:485–510, 1976.

[36] A. Wallqvist and B. J. Berne. Molecular dynamics study of the dependence of water solvation free energy on solute curvature and surface area. *J. Phys. Chem.*, 99:2885–2892, 1995.

Appendix A

Test-Particle equations

The main formula pertaining to the test-particle method for computing the transfer free energy is:

$$\Delta G_{tr} = -\ln < \exp(-\beta\mathcal{E}) >_N, \tag{A.1}$$

where $\mathcal{E}$ is the interaction energy of the ghost particle with the surrounding solvent, $\beta = 1/k_B T$, where k_B is Boltzmann's constant and T is the temperature, and the average is performed over the pure reference fluid. The transfer enthalpy is

$$\Delta H_{tr} = \frac{< H_{N+1} \exp(-\beta\mathcal{E}) >_N}{< \exp(-\beta\mathcal{E}) >_N} - < H_N >_N, \tag{A.2}$$

where H_N is the enthalpy of the pure solvent and $H_{N+1} = H_N + \mathcal{E}$. The corresponding entropy of transfer is therefore

$$T\Delta S_{tr} = \frac{< H_{N+1} \exp(-\beta\mathcal{E}) >_N}{< \exp(-\beta\mathcal{E}) >_N} - < H_N >_N + \ln < \exp(-\beta\mathcal{E}) >_N . \tag{A.3}$$

The molar volume of transfer and the heat capacity can be expressed as

$$\Delta V_{tr} = \frac{< V \exp(-\beta\mathcal{E}) >_N}{< \exp(-\beta\mathcal{E}) >_N} - < V >_N, \tag{A.4}$$

and

$$\Delta C_{p,tr} = \frac{< H_{N+1}^2 \exp(-\beta\mathcal{E}) >_N}{< \exp(-\beta\mathcal{E}) >_N} - \frac{< H_{N+1} \exp(-\beta\mathcal{E}) >_N^2}{< \exp(-\beta\mathcal{E}) >_N} - < H_N^2 >_N + < H_N >_N^2 \tag{A.5}$$

respectively.

Appendix B

Derivation of the Ideal-gas Entropy Term

We derive here a simple, but rigorous expression for the first term in the entropy expansion. This is done for the three-dimensional pure molecular fluid, but can straightforwardly be generalized to mixture in d dimensions. The nomenclature used is based upon that of Gray and Gubbins [2].

For a fluid of N rigid molecules in a volume V at temperature T, the classical expression for the canonical partition function is

$$Q_N = \frac{Z_N}{h^{\nu N} N! \sigma^N} \tag{B.1}$$

$$Z_N = \int_v d\mathbf{r}^N d\mathbf{p}^N d\omega^N d\mathbf{J}^N \exp(-\beta H_N) \tag{B.2}$$

where h is Planck's constant, ν is the number of degrees of freedom (5 for linear molecules, 6 for nonlinear molecules), σ is the symmetry number, $\beta = 1/kT$ is the inverse temperature with k denoting the Boltzmann constant, H_N is the Hamiltonian, $\mathbf{r}^N$ represents the Cartesian coordinates of the N molecules, and $\mathbf{p}^N$, ω^N, and $\mathbf{J}^N$ are the linear momenta, Euler angles, and angular momenta of those N molecules, respectively.

The probability of observing a given, *specific* subset of n of the total N particles in a given arrangement of positions, orientations, and momenta is

$$P_N^{(n)} = \frac{1}{Z} \int_v d\mathbf{r}^{N-n} d\mathbf{p}^{N-n} d\omega^{N-n} d\mathbf{J}^{N-n} \exp(-\beta H_N) \,. \tag{B.3}$$

It is often more useful, however, to know the probability of observing any n *indistinguishable* particles with the given arrangement in phase space, $(\mathbf{r}^n, \mathbf{p}^n, \omega^n, \mathbf{J}^n)$. This is the n-particle distribution function:

$$f_N^{(n)} = \frac{N!}{(N-n)!} \sigma^n P_N^{(n)} \,. \tag{B.4}$$

The one-particle distribution function is thus, from Eqs. B.3 and B.4:

$$f_N^{(1)} = \frac{N\sigma}{Z_N} \int_v d\mathbf{r}^{N-1} d\mathbf{p}^{N-1} d\omega^{N-1} d\mathbf{J}^{N-1} \exp(-\beta H_N) . \tag{B.5}$$

Noting that

$$H_N = H_{N-1} + \frac{\mathbf{p}_1^2}{2m} + \sum_{\alpha=X,Y,Z} \frac{\mathbf{J}_{1\alpha}^2}{2I_\alpha} + \psi , \tag{B.6}$$

where m is the molecular mass, I_α is the moment of inertia in the $\alpha = X, Y, Z$ dimension, and ψ is the potential of interaction between one molecule and the remaining $N-1$ molecules, we can obtain an explicit formula for the one particle distribution function. After substituting Eq. B.6 into Eq. B.5, separating the integrals, factoring the momenta integrals into products of like integrals, and dividing out like terms, we obtain an expression for the one-particle distribution function that is only dependent on one particle's momenta:

$$f_N^{(1)}(\mathbf{p}_1, \mathbf{J}_1) = \frac{\rho\sigma}{\Omega} \left(\frac{\beta}{2\pi m}\right)^{3/2} \left[\prod_{\alpha=X,Y,Z} \left(\frac{\beta}{2\pi I_\alpha}\right)^{1/2}\right] \exp\left(-\frac{\beta \mathbf{p}_1^2}{2m}\right) \exp\left(-\beta \sum_{\alpha=X,Y,Z} \frac{\mathbf{J}_{1\alpha}^2}{2I_\alpha}\right) , \tag{B.7}$$

where $\rho = N/V$ is the number density and Ω is the total angular volume of integration.

As Lazaridis and Paulaitis have shown [3], the canonical expression for the 1-particle term in the entropy expansion is

$$S_N^{(1)} = -\frac{kN\Omega}{\rho\sigma} \int_v d\mathbf{p} d\mathbf{J} \, f_N^{(1)}(\mathbf{p}, \mathbf{J}) \ln\left[h^\nu f_N^{(1)}(\mathbf{p}, \mathbf{J})\right] . \tag{B.8}$$

Substituting the expression of Eq. B.7 into this equation, and assigning the constants $a = \beta/2m$, $b_\alpha = \beta/2I_\alpha$, $c_1 = -Nk(a/\pi)^{3/2} \prod_{\alpha=X,Y,Z}(b_\alpha/\pi)^{1/2}$, and $c_2 =$

$-c_1 h^\nu \rho\sigma/(NkT)$ for mathematical simplicity, we have:

$$S_N^{(1)} = c_1 \int_v d\mathbf{p}d\mathbf{J} \left\{ \exp(-a\mathbf{p}^2) \exp(-\sum_{\alpha=X,Y,Z} b_\alpha \mathbf{J}_\alpha^2) \left[\ln c_2 - a\mathbf{p}^2 - \sum_{\alpha=X,Y,Z} b_\alpha \mathbf{J}_\alpha^2 \right] \right\} . \tag{B.9}$$

If the linear and angular momenta are assumed to be factorizable [2], then we obtain, after separating the integrals, and changing to spherical coordinates:

$$\begin{aligned} S_N^{(1)} = \; & 4\pi \; c_1 \{ \ln c_2 \int_0^{+\infty} dp \left[p^2 \exp(-ap^2) \right] \int_{-\infty}^{+\infty} d\mathbf{J} \exp\left(- \sum_{\alpha=X,Y,Z} b_\alpha \mathbf{J}_\alpha^2 \right) \\ & - a \int_0^{+\infty} dp \left[p^4 \exp(-ap^2) \right] \int_{-\infty}^{+\infty} d\mathbf{J} \exp\left(- \sum_{\alpha=X,Y,Z} b_\alpha \mathbf{J}_\alpha^2 \right) \\ & - \int_0^{+\infty} dp \left[p^2 \exp(-ap^2) \right] \sum_{\alpha=X,Y,Z} b_\alpha \int_{-\infty}^{+\infty} d\mathbf{J} \left[\mathbf{J}_\alpha^2 \exp\left(- \sum_{\alpha'=X,Y,Z} b_{\alpha'} \mathbf{J}_{\alpha'}^2 \right) \right] \} , \end{aligned} \tag{B.10}$$

which, after evaluating the linear momentum integrals from standard tables, and regrouping, we are left with

$$\begin{aligned} S_N^{(1)} = \; & \left(\tfrac{\pi}{a}\right)^{3/2} \; c_1 \{ (\ln c_2 - 3/2) \int_{-\infty}^{+\infty} d\mathbf{J} \exp\left(- \sum_{\alpha=X,Y,Z} b_\alpha \mathbf{J}_\alpha^2 \right) \\ & - \sum_{\alpha=X,Y,Z} b_\alpha \int_{-\infty}^{+\infty} d\mathbf{J} \left[\mathbf{J}_\alpha^2 \exp\left(- \sum_{\alpha'=X,Y,Z} b_{\alpha'} \mathbf{J}_{\alpha'}^2 \right) \right] \} . \end{aligned} \tag{B.11}$$

The two integrals in Eq. B.11 are evaluated to be

$$\int_{-\infty}^{+\infty} d\mathbf{J} \exp\left(- \sum_{\alpha=X,Y,Z} b_\alpha \mathbf{J}_\alpha^2 \right) = \prod_{\alpha=X,Y,Z} \left(\frac{\pi}{b_\alpha} \right)^{1/2} \tag{B.12}$$

and

$$\sum_{\alpha=X,Y,Z} b_\alpha \int_{-\infty}^{+\infty} d\mathbf{J} \left[\mathbf{J}_\alpha^2 \exp\left(- \sum_{\alpha'=X,Y,Z} b_{\alpha'} \mathbf{J}_{\alpha'}^2 \right) \right] = \frac{3}{2} \left[\prod_{\alpha=X,Y,Z} \left(\frac{\pi}{b_\alpha} \right)^{1/2} \right] , \tag{B.13}$$

respectively. After substituting these relationships back into Eq. B.11, replacing the constants c_1, c_2, a, and b_α as defined earlier, and collecting and canceling terms, we

obtain:

$$S_N^{(1)} = Nk\left[\frac{\nu}{2} - \ln\left(\rho\sigma\Lambda_t^3\Lambda_r\right)\right] , \tag{B.14}$$

where the translational and rotational thermal wavelengths are defined

$$\Lambda_t = \left(\frac{\beta h^2}{2\pi m}\right)^{1/2} \tag{B.15}$$

and

$$\Lambda_r = \begin{cases} \pi^{-1/2}\left(\frac{\beta h^2}{8\pi^2 I_X}\right)^{1/2}\left(\frac{\beta h^2}{8\pi^2 I_Y}\right)^{1/2}\left(\frac{\beta h^2}{8\pi^2 I_Z}\right)^{1/2} & \text{(non-linear)} \\ \frac{\beta h^2}{8\pi^2 I} & \text{(linear)} \end{cases} \tag{B.16}$$

respectively. Baranyai and Evans [1] have shown that the configurational contribution to the entropy of the ideal gas in the *canonical* ensemble is exactly 1. Hence, this value must be added to $S_N^{(1)}$ of Eq. B.14, to at last obtain the ideal-gas entropy:

$$s^{IG} = 1 + Nk\left[\frac{\nu}{2} - \ln\left(\rho\sigma\Lambda_t^3\Lambda_r\right)\right] . \tag{B.17}$$

Bibliography

[1] A. Baranyai and D. J. Evans. Direct entropy calculation from computer simulation of liquids. *Phys. Rev. A*, 40:3817–3822, 1989.

[2] C. G. Gray and K. E. Gubbins. *Theory of molecular fluids.* Clarendon Press, Oxford, U.K., 1984.

[3] T. Lazaridis and M. E. Paulaitis. Entropy of hydrophobic hydration: A new statistical mechanical formulation. *J. Phys. Chem.*, 96:3847–3855, 1992.

Appendix C

Fourier Series Expansion of the Angular Correlation Function

In this Appendix, we derive the formulae used in this work to express the water-water angular correlation function in terms of a Fourier series expansion. Additionally, some details which simplify the implementation are also discussed. The method by which the coefficients of this series are accumulated as ensemble averages is similar to that used by Streett and Tildesley [1] for the analogous case using spherical harmonics in three dimensions.

C.1 Derivation

We begin by assuming that the water-water angular pair correlation function, $g^{(2)}_{WW}(r, \phi_1, \phi_2)$, (which is a smooth, continuous function of ϕ_1 and ϕ_2 at any given r) can be expressed as a product of Fourier series of the form:

$$g^{(2)}_{WW}(r, \phi_1, \phi_2) = \sum\sum_{m_1, m_2 = -\infty}^{+\infty} c(m_1, m_2; r) e^{im_1\phi_1} e^{im_2\phi_2} \,. \tag{C.1}$$

The complex coefficients of this series, $c(m_1, m_2; r)$ have two integral indices, m_1 and m_2, and are themselves functions of r. The angles, ϕ_1 and ϕ_2 have the range $[0, 2\pi)$ and correspond[1] to those in Figure 4.1.

Now we have the task of obtaining usable expressions for the coefficients. We

[1] Actually, when this work was performed, ϕ_1 and ϕ_2 were both taken to be the angles relative to a fixed unit vector from molecule 1 to molecule 2 (i.e., ϕ_1 was the same, but ϕ_2' was related to ϕ_2 in Figure 4.1 by: $\phi_2' = \pi - \phi_2$). Then, the resulting curves were properly transformed to the angles of Figure 4.1 which are more intuitive given the model potential. In retrospect, the original, intuitive angles could have been used in the expansion, yielding the same results with less trouble. However, we make this note because the coefficients themselves, plotted in Figure 4.4 would have been different.

begin by multiplying both sides by the complex conjugate and integrating over all angular space to obtain:

$$\int_0^{2\pi}\int_0^{2\pi} d\phi_1 d\phi_2\, g^{(2)}_{WW}(r,\phi_1,\phi_2)\, e^{-im_1'\phi_1} e^{-im_2'\phi_2} = \tag{C.2}$$
$$\sum\sum_{m_1,m_2=-\infty}^{+\infty} c(m_1,m_2;r) \int_0^{2\pi} d\phi_1\, e^{-im_1'\phi_1} e^{im_1\phi_1} \int_0^{2\pi} d\phi_2\, e^{-im_2'\phi_2} e^{im_2\phi_2},$$

where m_1' and m_2' are any other arbitrary coefficients. Exchanging the right- and left-hand sides of the equation, and applying the orthogonality property

$$\int_0^{2\pi} d\phi \left(e^{im\phi}\right)^* e^{in\phi} = 2\pi\delta_{m,n} \tag{C.3}$$

we are left with

$$c(m_1,m_2;r) = \frac{1}{4\pi^2}\int_0^{2\pi}\int_0^{2\pi} d\phi_1 d\phi_2\, g^{(2)}_{WW}(r,\phi_1,\phi_2)\, e^{-im_1\phi_1} e^{-im_2\phi_2} \tag{C.4}$$

after the sums over m_1 and m_2 have been performed, and the dummy prime variables have been renamed. Though this is indeed a formula for the coefficients, it is not very practical, since the determination of the coefficients requires the computation of the angular correlation function itself – the very quantity we are trying to approximate!

To get around this obstacle, we use the definition, following the example of Streett and Tildesley, for the ensemble average of some quantity, $X(r,\phi_1,\phi_2)$, in a given shell of infinitesimal thickness about r:

$$\langle X\rangle_{r+\Delta r} = \frac{\int_0^{2\pi}\int_0^{2\pi} d\phi_1 d\phi_2\, X(r,\phi_1,\phi_2) f^{(2)}(r,\phi_1,\phi_2)}{\int_0^{2\pi}\int_0^{2\pi} d\phi_1 d\phi_2\, f^{(2)}(r,\phi_1,\phi_2)} \tag{C.5}$$

where

$$f^{(2)}(r,\phi_1,\phi_2) \equiv \frac{\rho^2\sigma^2}{\Omega^2} g^{(2)}_{WW}(r,\phi_1,\phi_2) \tag{C.6}$$

is the 2-particle distribution function, and ρ, σ, and $\Omega \equiv \int_0^{2\pi} d\phi = 2\pi$ refer to the water density, symmetry number (3 for MB water), and total volume of integration, respectively.

Noting that, from Equation C.4,

$$c(0,0;r) = g^{(2)}_{WW}(r) = \frac{1}{\Omega^2}\int_0^{2\pi}\int_0^{2\pi} d\phi_1 d\phi_2\, g^{(2)}_{WW}(r,\phi_1,\phi_2) \tag{C.7}$$

it follows from Eqs. C.5 and C.6 that

$$\int_0^{2\pi}\int_0^{2\pi} d\phi_1 d\phi_2\, X(r,\phi_1,\phi_2) g^{(2)}_{WW}(r,\phi_1,\phi_2) = 4\pi^2 g^{(2)}_{WW}(r)\,\langle X\rangle_{r+\Delta r} \tag{C.8}$$

Finally, using Eq. C.4 to interpret the product of Fourier terms as the quantity X, we obtain a useful equation for the coefficients:

$$c(m_1,m_2;r) = g^{(2)}_{WW}(r)\left\langle e^{-im_1\phi_1}e^{-im_2\phi_2}\right\rangle_{r+\Delta r}. \tag{C.9}$$

C.2 Simplifications for Implementation

The Fourier series expansion derived in the previous section may be simplified by exploiting additional properties of the angular correlation function. The first of these simplifications uses the $2\pi/3$ symmetry of the MB molecule to obtain a condition on the indices m_1 and m_2 which eliminates 2/3 of the needed coefficients. The second takes note of the fact that the correlation function is always real, and results in a further 50% reduction in the number of coefficients that must be accumulated.

Due to the symmetry of the MB water molecule, the following condition holds:

$$g^{(2)}_{WW}(r,\phi_1,\phi_2) = g^{(2)}_{WW}(r,\phi_1+\frac{2\pi}{3},\phi_2)\,. \tag{C.10}$$

This implies that, after expanding the right hand side in the Fourier series of Eq. C.1,

$$g^{(2)}_{WW}(r,\phi_1,\phi_2) = \sum\sum_{m_1,m_2=-\infty}^{+\infty} c(m_1,m_2;r)e^{im_1\phi_1}e^{im_2\phi_2}e^{im_1\frac{2\pi}{3}} \,. \tag{C.11}$$

Since this expansion must be equivalent to the original expression of Eq. C.1, the coefficients must be zero whenever the last term is not 1 (i.e., whenever m_1 is not a multiple of 3). Hence, the coefficients are only non-zero for $m_1 = 0, \pm 3, \pm 6, \ldots$. In an analogous fashion, the condition $g^{(2)}_{WW}(r,\phi_1,\phi_2) = g^{(2)}_{WW}(r,\phi_1,\phi_2 + 2\pi/3)$ requires that $m_2 = 0, \pm 3, \pm 6, \ldots$ as well.

The requirement that the correlation function be real can be expressed as:

$$g^{(2)}_{WW}(r,\phi_1,\phi_2) = g^{(2)*}_{WW}(r,\phi_1,\phi_2) \,, \tag{C.12}$$

where the asterisk denotes the complex conjugate. Substituting the Fourier expansion for both sides, we have

$$\sum\sum_{m_1,m_2=-\infty}^{+\infty} c(m_1,m_2;r)e^{im_1\phi_1}e^{im_2\phi_2} = \sum\sum_{m_1,m_2=-\infty}^{+\infty} c^*(m_1,m_2;r)e^{-im_1\phi_1}e^{-im_2\phi_2} \tag{C.13}$$

After multiplying both sides by the complex conjugate of an arbitrary rank, integrating over all angular space, using the orthogonality property of Eq. C.3, and performing the sums over m_1 and m_2, we obtain the equality:

$$c(m_1,m_2;r) = c^*(-m_1,-m_2;r) \,. \tag{C.14}$$

This relationship allows us to re-express the series expansion the form:

$$\begin{aligned} g^{(2)}_{WW}(r,\phi_1,\phi_2) = \sum\sum_{m_1,m_2=0}^{+\infty} \Big[& c(m_1,m_2;r)e^{im_1\phi_1}e^{im_2\phi_2} + c^*(m_1,m_2;r)e^{-im_1\phi_1}e^{-im_2\phi_2} \\ & + c(m_1,-m_2;r)e^{im_1\phi_1}e^{-im_2\phi_2} + c^*(m_1,-m_2;r)e^{-im_1\phi_1}e^{im_2\phi_2} \Big] \,. \end{aligned} \tag{C.15}$$

The advantage of this form, which we use in practice, is that only the positive-positive and positive-negative coefficients need to be determined from simulations. The remaining coefficients can then simply be obtained by taking the appropriate complex conjugates, hence reducing the direct computational requirements by half.

Bibliography

[1] W. B. Streett and D. J. Tildesley. Computer simulations of polyatomic molecules I. Monte Carlo studies of hard diatomics. *Proc. R. Soc. Lond. A.*, 348:485–510, 1976.